Radon transport in autoclaved aerated concrete

Radon Transport in Autoclaved Aerated Concrete

PROEFSCHRIFT

ter verkrijging van de graad van doctor aan de Technische Universiteit Eindhoven, op gezag van Rector Magnificus, prof.dr. R.A. van Santen, voor een commissie aangewezen door het College voor Promoties in het openbaar te verdedigen op woensdag 7 januari 2004 om 16.00 uur

door

Michel van der Pal

geboren te Hoorn

Dit proefschrift is goedgekeurd door de promotoren:

prof.ir. N.A. Hendriks
en
prof.dr. R.J. de Meijer

Copromotor:
dr.ir. W.H. van der Spoel

ISBN: 90-386-1586-8
NUR: 971

Radon Transport in Autoclaved Aerated Concrete / by Michel van der Pal – Eindhoven : Technische Universiteit Eindhoven 2003

Cover design by Ton van Gennip

Published as issue 75 of the Bouwstenen series of the Faculty of Architecture, Building and Planning

Printed by University Press, Eindhoven University of Technology, Eindhoven, The Netherlands

Stellingen

1. Een breed opgeleide ingenieur *(TU/e faculteit Bouwkunde, Opleidingsgids 2002-2003)* heeft weinig diepgang.

2. De invloed van het vochtgehalte op de exhalatie van radon uit bouwmaterialen dient te worden meegenomen bij de bepaling van de bijdrage van bouwmaterialen aan de radonconcentratie in Nederlandse woningen *(dit proefschrift)*.

3. Het zou de kwaliteit van een gebouw ten goede komen wanneer, analoog aan de vroegere praktijk waarbij de zoon van de architect werd gedood wanneer bij het instorten van de woning de zoon van de opdrachtgever was omgekomen, een architect kan worden verplicht om in een door hem/haar ontworpen gebouw te wonen of te werken.

4. Je kunt je beter niet verzekeren bij een pensioenfonds dat ervan uitgaat dat je oud wordt, aangezien deze aanname leidt tot een hogere pensioenpremie en/of een lager pensioen.

5. Poreuze bouwmaterialen dienen niet als een homogeen maar als een heterogeen medium te worden beschouwd, zeker wanneer het het transport van radon betreft *(dit proefschrift)*.

6. De slogan “Er gaat niets boven Groningen” getuigt van een beperkte geografische kennis.

7. Het terugdringen van de radonconcentraties kan efficiënter en effectiever dan de voorgestelde Stralingsprestatienorm door van elke nieuwe woning de radonconcentratie te meten en bij overschrijding van de norm maatregelen te treffen *(Nederlandse norm, NEN 7181, Stralingsprestatie van een woonfunctie - Bepalingsmethode, 2001)*.

8. Meten is niet weten maar maakt onderdeel uit van een groter proces om de hoofdvraag te beantwoorden *(Haselager N., Basisboek Milieumetingen, 2001)*.

9. Onderzoek doen is als reizen: hoe goed je je ook voorbereidt, je wordt iedere keer toch weer verrast.

10. Radon vormt geen zwaarwegend probleem.

11. Een regering die bezuinigt in tijden van recessie, heeft de lessen op de middelbare school niet begrepen *(Blaas J.P.M., Samengevat / VWO Economie, 2003)*.

12. Het is onmogelijk het risico van langdurige blootstelling aan de radonconcentratie van een gemiddelde Nederlandse woning nauwkeurig te bepalen.

1 Introduction

2 Modelling of radon transport

3 Materials and methodology

4 Emanation and adsorption of radon

5 Radon transport measurements

6 General discussion and conclusions

1

Introduction

1.1 An introduction to radon

This thesis deals with the quantitative analysis of the radon concentration in an experimental set-up containing a cylinder of autoclaved aerated concrete (AAC). The results show that the description of radon transport is much more complicated than expected from earlier measurements. A good description of the generation and transport of radon in a porous medium is an important step in developing measures to reduce the radon concentrations in Dutch dwellings.

What is radon?

Radon, ^{222}Rn, is an odourless, radioactive noble gas, which originates from the decay of radium (^{226}Ra) and has a decay time of 3.8 days. Radon and radium are part of the uranium (^{238}U) decay series. An overview of the uranium decay series is given in Figure 1.1. Together with the thorium (^{232}Th), actinium (^{235}U) and potassium (^{40}K) decay series, it forms the natural decay series.

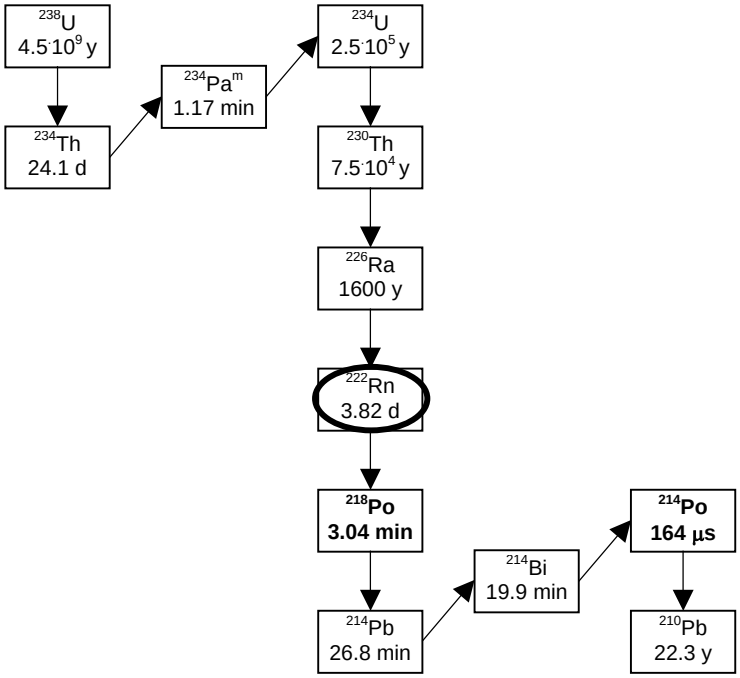

*Figure 1.1 Part of the decay series of ^{238}U. Radon is encircled and its short-lived, alpha emitting progeny are printed **bold**. The time under the element is its decay time.*

Radon transport phenomena in dwellings can be divided in the generation and transport of radon in the underlying soil and porous building materials, and the distribution of radon inside a dwelling via airflows. The Department of the Physical Aspects of the Built Environment (FAGO) at the Eindhoven University of Technology

(TU/e), where this project has been conducted, has been investigating the transport of matter in porous media and buildings. Pel [11] developed a set-up for non-destructive measurement of the moisture transport in porous building materials using Nuclear Magnetic Resonance (NMR). This technique has been used by Brocken [4] to develop and verify a model description for the moisture transport in masonry. Despite the advanced techniques, good agreement between model calculations and measurements could not be obtained. This underlines the complexity involved in the transport of matter in porous media. Carmeliet [5] used multi-scale modelling to obtain a better description of the transport of moisture in porous media. These results can help to understand the transport of radon in porous media. Reversely, knowledge on transport of radon may strengthen the understanding of moisture transport.

Another aspect that determines the amount of radon in dwellings is the airflow. The complexity of the airflows in a dwelling is illustrated in *Figure 1.2*. Air can enter and leave the dwelling via various routes such as openings in the facade, pores and cracks in building materials and crawl space / soil. The ventilation depends on pressure gradients induced by temperature gradients and wind pressures, which are time-dependent.

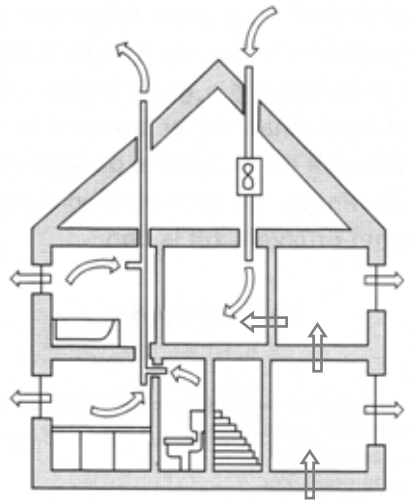

Figure 1.2 A schematic overview of a dwelling and the airflows in it.

At FAGO, several research projects have been conducted to gain insight into the time-dependent transport of air in buildings. Loomans [9] measured airflows in a test office space and compared them with Computational Fluid Dynamics (CFD) model calculations. Although a good relation between measurements and calculations was found, it was also shown that this approach required detailed input parameters, something that is often not available for regular office spaces. Another example is a study on the combined moisture and heat transport in churches by Schellen [15]. This research showed that it is possible to describe airflows in churches and to estimate the results on the relative humidity using CFD modelling. Both projects showed that

simulating airflows in buildings is complex and requires detailed information of various parameters.

By focussing on only a single room and identifying the airflows in it, the complexity is reduced. *Figure 1.3* shows a hypothetical living room where air can enter this compartment via various routes. Both the route and the flow rate determine how the air in the room is refreshed with outdoor air (either directly or indirectly via other compartments), how much energy is needed to keep the room at a comfortable temperature and whether the airflow is considered (un)comfortable. It may be clear that also the transport of radon is influenced by these flows. Provided the transport of radon out of building materials is understood, radon might, due to its non-reactive behaviour as a noble gas and its low concentrations, prove to be a useful tracer to determine changes in the condition of a building.

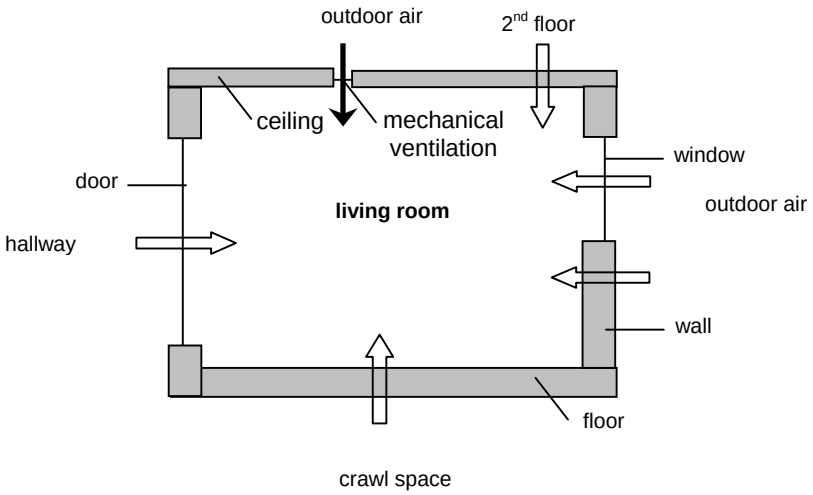

Figure 1.3 Possible entry routes for air in a living room are shown by the arrows.

Health risks of radon

Exposure to high concentrations of radon and its progeny in air leads to increased chance of lung cancer. The latest report of the World Health Organisation (WHO) on the biological effects of alpha radiation, Bear VI, estimates the radiation dose due to the exposure to radon to be 0.025 mSv per year per Bq m^{-3}. This is equivalent to a chance of lung cancer of approximately $2 \cdot 10^{-6}$ per Bq m^{-3} per year per person. To reduce the exposure to radon, the WHO recommended setting an action level for radon of 200 Bq m^{-3}. Action to reduce indoor air radon concentrations should be taken when radon concentrations exceed this level. The Dutch government uses a different approach and addresses the risk of individuals, assuming a linear extrapolation of the risks to low doses. In this approach, a maximum risk level of $1 \cdot 10^{-6}$ deaths per year per person is set for a single source (e.g. radon). This implies a radon concentration of 0.5 Bq m^{-3}, considerably lower than the average outdoor air radon concentration. The Dutch radon policy will be presented in the next text-box.

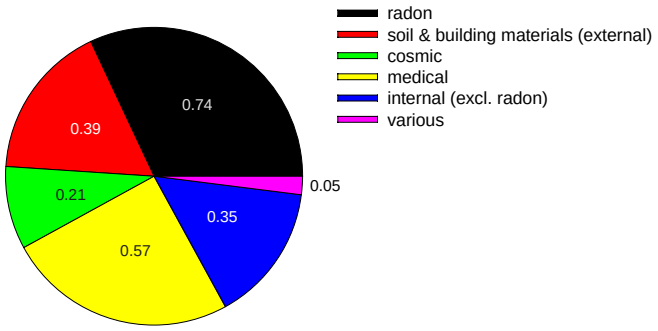

Figure 1.4. Contribution of the various sources to the average radiation dose (in mSv per year per person) in The Netherlands [3].

1.2 Radon generation and transport

1.2.1 Radon generation

Radon is being produced in soil as a result of the presence of trace amounts of ^{238}U. Depending on the properties of the soil such as porosity, tortuosity, permeability, presence of cracks and the conditions such as moisture content, rate of saturation and pressure gradients, radon can be transported through the soil and building materials and enter the dwelling. The amount of radon from the soil entering the indoor air can range several orders of magnitude due to (changes in) these properties.

Although the outdoor air does not produce radon, it is considered to be a source of radon. The continuous release of radon by the soil results in an increased outdoor radon concentration. This radon enters the dwelling via air exchange. Due to the

necessity to ventilate a dwelling, the outdoor radon concentration is the lowest level of indoor air radon concentration that can be reached in a dwelling (provided radon is not removed from the incoming ventilation air). The contribution of the outdoor air to the total radon concentration in a dwelling is often relatively small.

Most building materials also generate radon, caused by the uranium and/or radium containing natural minerals in its components. The radon generation depends on the age of the building material [13], the relative humidity [19] and of course on the sort and the amount of building material. However, also between similar building material samples, the amount of generated radon can differ by an order of magnitude [6]. This makes comparison of radon concentrations between “identical” dwellings more difficult.

1.2.2 Radon transport in porous media

It is assumed that two mechanisms play a role in the transport of radon:

a) Radon can be transported due to differences in radon concentration (see *Figure 1.5*), called diffusive transport. Diffusive transport is considered to be one of the main process for exhalation of radon from building materials [14] and is also considered to play a role in the transport of radon from the soil to the crawl space [1].

b) Radon can be transported by the flow of air, advective transport, which is not limited to exchange of air between open spaces but can also be flow through porous materials such as soil and building materials (see *Figure 1.5*). As a result, porous media act as sources of advective radon. Advective transport is considered to be the most important mechanism for entry of radon from the soil to the crawl space and further to the living space.

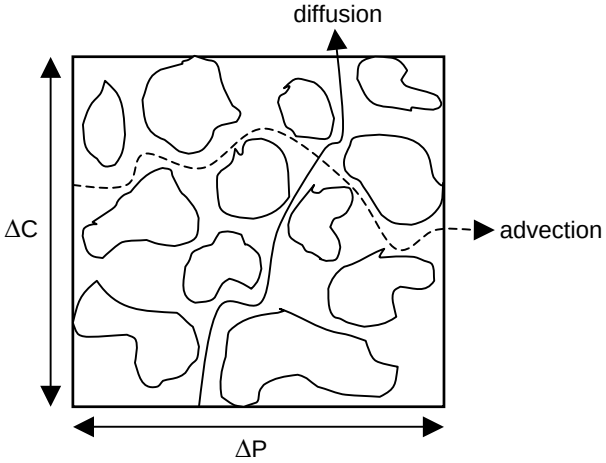

Figure 1.5 Schematic representation of advective and diffusive transport of radon due to pressure and concentration gradients, respectively, in porous media.

Several studies have been conducted to determine the radon concentration in dwellings and their origin. The trend observed in these studies is that where the indoor air radon concentrations exceed the action levels of the WHO, this is caused by the entry of radon from the soil into the dwelling. This entry could be reduced by preventing transport of air from the soil or crawl space into the living room. An exception is the high levels of radon found in Swedish dwellings build of aerated concrete based on alum shale [20]. The radon concentrations in these dwellings exceed the WHO action level as a result of the additives in the aerated concrete. Further investigations into the relation between the soil and the high radon concentrations showed that the geological history of the soil plays an important role. Therefore, it is possible to use geological data to identify areas with potentially high (and low) radon concentrations: so-called radon risk mapping. The radon policy of most countries focuses on the determination of the areas with high radon potential and to prevent in these areas the entry of radon from the soil into the indoor air via ventilation of the crawl space or by building dwellings on a layer of (ventilated) gravel.

1.3 Radon surveys in The Netherlands

To determine the radon concentrations in Dutch dwellings, their sources and potential areas with enhanced radon entry from the soil, two national radon surveys have been carried out. The first national survey [12], 1980 - 1984, was part of the Dutch National Research Program SAWORA. It showed that in Dutch dwellings the average radon concentration was 22 Bq m^{-3}, a relatively low concentration compared to other countries. Also, the range of radon concentrations was small compared to other countries and only a few dwellings were found that exceeded the WHO recommended action levels. Based on simplified assumptions, the results of the survey were interpreted such that the contribution of the soil and building materials had to be 70% and 15%, respectively. Neither the contribution of the building materials nor that of the soil was measured. However, based on radon-exhalation rates of building materials taken from laboratory measurements and ventilation rates in dwellings reported in the literature, it was concluded that at maximum, 15% of the indoor radon could arise from the building materials. With a contribution of 15% from the outdoor air, it was deduced that the remaining amount (70%) had to come from the soil.

To gain insight into the sources and transport of radon in dwellings, a study of the KVI was conducted from 1989 to 1994 on a test house in Roden [1]. Under various ventilation regimes, where both the magnitude and the direction of the airflow was controlled, pressure differences and radon concentrations were measured. The main conclusion of this study was that calculating the radon concentration from independently measured radon-exhalation rates of soil and building materials and the measured ventilation rates did not match the measured radon concentration. A large reduction in radon concentration was found when the test house was pressurised at the same ventilation rate as under depressurised conditions. The question, however, remained whether the results of this test house were representative for the average Dutch dwelling. This led to the second national survey, which was carried out in 1996.

The second national radon survey [18] focused on dwellings built in the period 1985-1993 and on the relation between ventilation and radon concentrations. For this purpose, the ventilation rate of the living room and the crawl space and the air exchange between living room and the crawl space were measured using passive tracer gases. The survey showed increased levels of radon for more recently built dwellings. This trend was similar to the trend found in the first radon survey. Based on the measurements, the contribution of the soil was 15 - 25%, which is a factor 3 to 5 smaller than estimated of the first survey. This time, the remaining amount had to come from the building materials. As a result, the contribution of the building materials was estimated at 60 - 70%.

Triggered by this relatively large contribution of the building materials, the Dutch government decided to develop a model to calculate the radiation dose in dwellings, the so-called Radiation Performance Index (RPI) [2]. This approach differs from other countries where indoor air radon concentrations are measured rather than calculated. Furthermore, the foreign radon policies focus on the contribution of the soil to the indoor radon concentration rather than on the contribution of the building materials and on the high radon concentrations only.

The Dutch radon policy
As the risk of the average radon concentration in Dutch dwellings exceeds the limit set by the Dutch government, remedial action on radon is required. Before the second survey showed the contribution of the building materials, the policy was mainly focused on reducing entry of radon from the soil via the crawl space. After the second survey, the policy of the Dutch government shifted towards reducing the contribution of building materials to indoor radon. To reduce the exposure of the public to high radiation doses in dwellings, the Dutch government developed a model called the Radiation Performance Index (RPI). The RPI calculates the risk of a dwelling for its inhabitants due to both the exposure to radon in the indoor air and the exposure to external gamma radiation. The RPI is foreseen to come into effect in 2004.

1.4 Modelling of radon transport in dwellings

In principle, it is possible to calculate the indoor radon concentration provided the radon sources and airflows in a dwelling are precisely known. In practice, this is impossible due to the many time-dependent and unknown parameters and location specific conditions. Consequently, many assumptions are made to simplify the description.

Although various model calculations exist to estimate radon concentrations in dwellings, only two models will be discussed here that are applicable to the Dutch situation, where building materials play an important role in the indoor radon concentration. The first model (section 1.4.1) that will be discussed is the radiation performance index (RPI) [2], whose results will be compared with the results of the

second national radon survey. The second model (section 1.4.2) is the Roden-model. This model was used to describe the radon entry in a test house in Roden, The Netherlands, where extensive measurements were carried out on radon concentrations and airflows. A comparison between measurements and modelling results will also be made here.

1.4.1 Radiation Performance Index

The goal of the RPI is to estimate the radiation dose in a Dutch dwelling based on the building plans rather than actual measurements. This way, the building plans can be adjusted to meet radiation dose requirements prior to building the dwelling. In the RPI, the radiation dose in a dwelling is considered to be the sum of the contribution of the gamma radiation and the contribution of the alpha radiation from radon and its progeny.

The model is a steady-state model and the radiation performance is the sum of the effective dose rate resulting from the external radiation and the effective dose rate resulting from the exposure to radiation from radon and its progeny:

$$RP_i = \Delta C_{\mathrm{Rn};i} \cdot c_{\mathrm{dc}} + E_{\mathrm{ext};i}\,, \tag{1.1}$$

where:

RP_i radiation performance (Sv year^{-1});
$\Delta C_{\mathrm{Rn};i}$ the average difference in radon concentration between compartment *i* and the outdoor air (Bq m^{-3});
c_{dc} dose conversion factor for radon (Sv year^{-1} Bq^{-1}m^3);
$E_{\mathrm{ext};i}$ the effective dose rate resulting from external radiation of building materials in compartment *i* (Sv year^{-1}).

The average difference in radon concentration between compartment *i* and the outdoor air is calculated using the following equation:

$$\Delta C_{\mathrm{Rn};i} = \frac{S_i + \frac{A_i}{\sum_{i=1}^{r} A_i} \cdot S_{\mathrm{or}}}{0.5 \cdot Q_{\mathrm{vg};i}}\,, \tag{1.2}$$

where:

S_i total radon exhalation in compartment *i* (Bq s^{-1});
S_{or} radon production in all other rooms (Bq s^{-1});
A_i total floor surface area of compartment *i* (m^2);
r the number of compartments;
$Q_{\mathrm{vg};i}$ the average airflow in room *i* (m^3 s^{-1}).

The first term on the right-hand side, S_i, is calculated from the diffusive radon exhalation rates, measured under well-controlled conditions in a laboratory, and the mass of the applied building materials. The second term describes the entry of radon

from the other compartments. $Q_{vg;i}$ describes the loss of radon due to the airflow in the compartment *i* and includes a factor that compensates for the occupants behaviour. The factor 0.5 results from the rule that the air flowing into a compartment may consist of up to 50% of air from other compartments.

Although the model compensates for entry of radon from other compartments, limited entry of fresh air (50%) and occupants behaviour, it does not include the effects of (time-dependent) changes in moisture content, temperature, pressure gradients, ventilation rates and age of the building materials. These factors can influence the radon exhalation rates considerably. An evaluation of the model by van der Spoel and van der Graaf [17] indicates that the RPI-model underestimates the contribution of radon production of the building materials.

This underestimation can be observed when applying this model to the results of the second Dutch survey using the measured ventilation rates rather than the ones estimated in the building plans. This approach yields a contribution of the building materials to the indoor radon concentration of 12 Bq m^{-3} [8]. This is considerably lower than the estimated contribution of 21 Bq m^{-3} from the second national survey. This difference can be the result of a too low estimate of the radon-exhalation rate. On the other hand, the difference could be the result of a systematic overestimation of the measured ventilation rate. However, if that would be correct, the contribution from the soil will be larger and the contribution of building materials to the indoor radon concentration will be less than the assumed 60 to 70%. In other words: the model calculations do not comply with the measured radon concentrations and the measured ventilation rates.

1.4.2 Test house in Roden

Stoop and Aldenkamp have conducted measurements and model calculations on a test house in Roden [1]. Here, an overview of their work is given.

From 1980 to 1994, measurements were conducted on a test house in Roden, The Netherlands. These measurements included measurement of the radon concentrations, radon-exhalation rates and ventilation characteristics. A simplified conceptual model was used to calculate the indoor radon concentrations. According to this model the indoor radon concentration is the result of (i) airflows, from one compartment to another, transporting a radon flux equal to the concentration in the air of the compartment of origin multiplied by the airflow and (ii) radon source strengths present in each compartment. Indoor radon concentrations can, therefore, be calculated using a radon balance model. For the test house, a multi-compartment model was used. The model assumes well-mixed compartments. The radon source strengths were calculated using the measured time-averaged ^{222}Rn concentrations and the ventilation rates measured. This yielded 2.5 and 1.0 kBq h^{-1} for the crawl space and the dwelling, respectively. Radon-exhalation rate measurements conducted on the surfaces of the building materials and the soil yielded source strengths of 1.1 and 0.7 kBq h^{-1} for the dwelling and crawl space respectively. This means a discrepancy of a factor 4 for the radon source strength in the crawl space

between measurements and model calculations. Stoop and Aldenkamp gave two possible explanations for this discrepancy. First, the radon source strength can have an advective term that is not measured with the exhalation meter, as this device is placed airtight on exhaling material. Measurements on the Roden test house showed significant decrease in radon concentration when the house was pressurised and a considerable increase under reduced pressure conditions. Secondly, the static model may be too simple. Airflows have a dynamic character due to wind and differences in temperature between indoor and outdoor. Because of this, the radon concentration will fluctuate as a function of time. Additional measurements by Aldenkamp and Stoop suggest that the effect of advective transport is the most important.

1.4.3 Hypotheses

From the attempts described above, it can be concluded that for the Dutch situation, where building materials contribute significantly to the indoor air concentration, no model is yet available for an accurate description of the transport of radon in a dwelling.

Two hypotheses to explain the differences between measurements of indoor air radon concentrations and model calculations are described below:

1) Incorrect model parameter values

Incorrect parameter values can explain the differences between model calculations and measurements of the indoor air concentration. For the RPI, for example, incorrect parameters of the used model parameters would imply that either the measurements of the second Dutch survey are incorrect or the used radon-exhalation rates are incorrect. It seems unlikely that the results of the second survey are incorrect as the used techniques for measuring the radon concentration and the ventilation rate have been thoroughly validated. However, the laboratory radon-exhalation rates measurement on building materials have also been validated. Measurements conducted by various laboratories using several techniques yielded similar results. Therefore, a large deviation from the reported radon-exhalation rates in Dutch building materials is not expected. Nevertheless, there may be other causes that cannot be ruled out. The first is a difference in size of the samples of which the radon-exhalation rates have been measured and the actual size of building materials. Concrete slabs, for example, contain more cracks than the test cubes from the same batch. Secondly, the (varying) conditions that building materials in dwellings are exposed to, such as variations in relative humidity, temperature and pressure gradients can influence the radon-exhalation rate. Such effects are not dealt with in the measurements under laboratory conditions.

2) Incomplete model description

The model is, by definition, a simplified representation of reality. The assumptions made to come to a model can have a large effect on the model results. Already mentioned is the fact that the model is static and thus not time-dependent. This, however, can only explain part of the differences as the time-dependent processes have only a limited effect on the (average) radon

concentration. Extreme variations in time-dependent parameters such as ventilation rates and relative humidity levels are required to completely compensate for the found differences. Another aspect is that the main transport processes, diffusive and pressure driven, advective transport, are not explicitly included in the presented models. Instead, a static radon-exhalation rate is used. Flows of air through porous building materials can take radon-rich air form the building material into the indoor air. Because the advective transport is not included in the radon-exhalation rate measurement, the actual contribution of advective transport might be important in the contribution of building materials to the radon concentration in the indoor air. This hypothesis is strengthened by measurements on the radon test house that show that, under some circumstances, advective transport plays a more important role than expected [1].

To better understand the transport of radon in dwellings, it is required to test both hypotheses. In this thesis, we will focus on the second hypothesis. Therefore, measurements are required that are conducted under well-defined and well-controlled conditions. Because these conditions are hard to achieve in a dwelling, this thesis deals with laboratory measurements and model calculations of the radon generation and transport in a single building material.

1.5 Modelling of radon transport in porous media

The transport of radon in sand has been extensively measured and modelled. Van der Spoel [16] compared measurements of radon transport in a column of sand with time-dependent model calculations. The model was a macroscopic model using the laws of Fick and Darcy for the diffusive and advective transport, respectively. It was concluded that this model is sufficient to describe the transport of radon in sand with an uncertainty of 10% for (well-defined) dry sand and a 15 to 40% uncertainty for (partly) wetted sand. The radon transport in sand can be described provided the transport parameters are accurately known. Such a validated model for building materials would mean a step forward in describing the contribution for building materials to the radon concentration in dwellings.

Studies on transport of radon in building materials, where measurements are compared with model calculations, are limited. Most studies on building materials are limited to measuring the static radon-exhalation rate. However, there are some studies focussing on the transport mechanisms of radon in building materials. Nam and Renken [10] studied the effect of osmotic electric pulsing on the diffusive transport of radon through concrete slabs. This study showed a significant decrease in the diffusion coefficient as a result of the osmotic electric pulsing. The explanation of this effect, the movement of water inside the concrete, was, however, not well founded. Another attempt was made by Cozmuta [7], who used a model to calculate the structure of concrete as a function of time. The results of this model were used to calculate the transport of radon. These results were compared with static radon-exhalation rate measurements on cubic samples of concrete. A fair correlation

between measurements and model calculations was found. However, both studies restrict themselves to diffusive transport of radon in building materials only.

1.6 Goal and outline of this thesis

The goal of this thesis is to gain insight into the mechanisms and processes that play a role in the generation and transport of radon in building materials. To reach this goal, model calculations are compared with measurements of combined diffusive and advective transport of radon in a cylinder of autoclaved aerated concrete (AAC).

The choice for AAC was based on, among others, the requirements of the set-up, and its radon transport properties. An overview of the requirements can be found in chapter 3, where a description of the building material and the experimental set-up for measuring the advective and diffusive transport is given. Among the most important requirements are the possibility to create a cylinder with an outer diameter of 0.8 m, the building material to be isotropic and homogeneous, to exhale measurable amounts of radon and have no or little change in structure and/or radon-exhalation rates in time. These requirements disqualified many common building materials such as concrete, which changes significantly fast in time, and brick, which produces too little radon.

The model calculations are based on the model that was successfully validated for sand. This model is a macroscopic model describing the advective and diffusive transport using the laws of Darcy and Fick, respectively. A description of the model can be found in chapter 2. This chapter also discusses the limitations of the macroscopic model and the possible effects of (micro) inhomogeneity in the AAC.

The model parameters were determined by independent measurements as much as possible. These measurements included determination of the emanation coefficient and the adsorption coefficient, which is described in chapter 4. The measurement of the diffusion coefficient is discussed in chapter 5. This chapter also presents the results of the combined diffusive and advective transport measurements and compares them with the model calculations.

The last chapter gives an overview of the results, general conclusions and an outlook on and recommendations for further research on radon transport in porous building materials and dwellings.

References

[1] Aldenkamp F.J., Stoop P., Sources and Transport of indoor radon, Ph.D. thesis, University of Groningen, The Netherlands, 1994.

[2] Anonymous, NEN7181: Radiation performance of a residential function: determination function, NEN, The Netherlands, 2001 (in Dutch).

[3] Blaauboer R., Blootstelling van de Nederlandse bevolking aan externe straling vanuit de omgeving, *NVS Nieuws*, 26(3): 29-33, 2001 (in Dutch).

[4] Brocken H.J.P., Moisture transport in brick masonry: the grey area between bricks, Ph.D. thesis, Eindhoven University of Technology, The Netherlands, 1998.

[5] Carmeliet J., A multiscale network model for simulating moisture transfer properties of porous media, *Transport in porous media*, 35(1):67-88, 1999.

[6] Cozmuta I., van der Graaf E.R., Radon release of concrete and its components, KVI-report R-116, KVI, The Netherlands, 1999.

[7] Cozmuta I., Radon generation and transport - a journey through matter, Ph.D. thesis, University of Groningen, The Netherlands, 2001.

[8] van der Graaf E.R., Schaap L.E.J.J., Bosmans G., Radiation performance index for Dutch dwellings: consequences for some typical situations, KVI-report R-106, KVI, The Netherlands, 1999.

[9] Loomans M.G.L.C., The measurement and simulation of indoor air flow, Ph.D. thesis, Eindhoven University of Technology, The Netherlands, 1998.

[10] Nam Y.S., Renken K.J., Laboratory measurements of electro-osmotic pulsing technology in reducing radon soil gas diffusion through a concrete slab, Radon in the Living Environment conference, Greece, 157, 1999.

[11] Pel L., Moisture transport in porous building materials, Ph.D. thesis, Eindhoven University of Technology, The Netherlands, 1995.

[12] Put L.W., de Meijer R.J., Hogeweg B., Survey of radon concentrations in Dutch dwellings, *Sci. Tot. Environ.*, 45:441-448, 1985.

[13] Roelofs L.M.M., Scholten L.C., The effect of aging, humidity and fly-ash additive on the radon exhalation from concrete, *Health Physics*, 67(3):266-271, 1994.

[14] Rogers V.C., Nielson K.K., Multiphase radon generation and transport in porous materials, *Health Physics*, 60(6):807-815, 1991.

[15] Schellen H.L., Heating monumental churches: indoor climate and preservation of cultural heritage, Ph.D. thesis, Eindhoven University of Technology, The Netherlands (2002).

[16] van der Spoel W.H., Radon transport in sand: a laboratory study, Ph.D. thesis, Eindhoven University of Technology, The Netherlands, 1998.

[17] van der Spoel W.H., van der Graaf E.R., Enkele kanttekeningen bij de stralingsprestatienormering, *Bouwfysica*, 15(4):8-12, 2002.

[18] Stoop P., Glastra P., Hiemstra Y., de Vries L., Lembrechts J., Results of the second national survey on radon in dwellings, RIVM report: 610058006, RIVM, The Netherlands, 1998.

[19] Stranden E., Kolstad E., Lind B., The influence of moisture and temperature on radon exhalation, *Rad. Prot. Dos.*, 7(1-4):55-58, 1984.

[20] Swedjemark G.A., Mjönes L., Radon and radon daughter concentrations in Swedish homes, *Radiation Protection Dosimetry*, 7(1-4):341-345, 1994.

2

Modelling of radon transport

2.1 Introduction

This chapter deals with a mathematical description of generation and transport of radon in autoclaved aerated concrete (AAC). The description of transport includes diffusive and advective transport, similar to the examined measurement conditions. For this type of transport of radon in sand, a model has already been developed [23,21,18,3], based on a macroscopic approach, which allows the use of macroscopic properties of sand as input parameters. This model describes the diffusive and advective transport of radon with Fick's law and Darcy's law, respectively. Model calculations have shown a good correlation with measurements on sand under well-defined and well-controlled conditions [23]. The equations for the transport of radon in AAC will be derived in analogy with the model for sand. Special attention will be paid to the differences between the two materials.

The next section describes the concepts of the macroscopic approach. In section 2.3, the macroscopic approach is applied to describe the generation and transport of radon in a porous medium. The following sections will examine the described processes in more detail. Section 2.4 discusses the mechanisms involved in the flow of air that cause advective transport. Section 2.5 discusses the effects and mechanisms that can occur in combined advective and diffusive transport in porous media. The last section discusses how these effects apply to AAC and what other effects may occur and how to deal with them.

2.2 Macroscopic approach

The section deals with the concepts of the macroscopic approach which includes the translation of the microscopic structure to macroscopic parameters.

2.2.1 From microscopic to macroscopic approach

When observing both sand and AAC, one notices that part of the material is occupied by a solid, persistent phase which we will call the solid matrix, and a part, between the solid phase, the void space. The latter is, depending on the conditions, occupied by dry air and/or water in the vapour, liquid and/or solid phase. When in a material both a solid matrix and a void space is present, it is called a porous medium according to the definition of Bear [8]. This means that both sand and AAC are porous media.

In principle, it is possible to define transport equations for the transport of a substance, i.e. radon, present in a porous medium by using a microscopic description of the structure of the material and solve these equations for certain boundary and initial conditions. This is the microscopic approach. However, the complexity of the configuration, if at all known, renders hopeless any attempt to solve the equations. The complexity of AAC can be seen from *Figure 2.1* that shows the various pore types in AAC. And even if it would be possible to calculate the transport, no means would be available to compare the results with measurements of radon transport at the microscopic level. To overcome this problem, a description is required that:

1) circumvents the need to know the exact configuration of the inter phase boundaries and the material structure at a microscopic level;
2) enables the description of the transport in terms of measurable quantities.

This description is given in a continuum or macroscopic approach. This approach states that the heterogeneous, discontinuous structure of the material can be replaced by a hypothetical substance to which kinematic and thermodynamic properties can be assigned that are continuous and differentiable functions in space and time [7]. Using this approach, the detailed information at microscopic level is lost, however the ability to formulate processes in porous media as well as posed boundary conditions in terms of measurable quantities is gained. This can be made clear with an example: the function describing the porosity of a material at microscopic level is discontinuous: for any given point in space it yields either a value of 0 when the solid matrix is present at that point, or a value of 1 for a void space. The porosity of a porous medium at macroscopic scale is a continuous function.

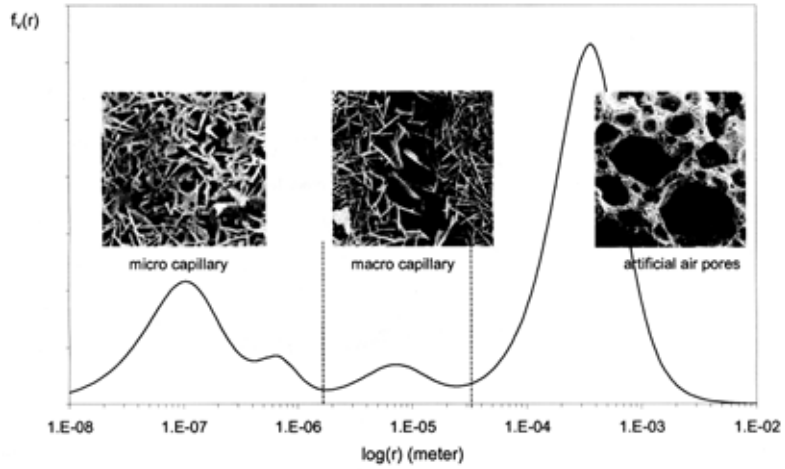

Figure 2.1 Pore volume distribution of AAC based on the main wetting curve. Picture taken from [20].

2.2.2 Concept of the Representative Elementary Volume (REV)

The first step in translating microscopic properties of a porous medium to a macroscopic scale is the definition of a representative elementary volume (REV) and a representative elementary area (REA). A REV is a hypothetical volume that replaces a real volume by averaging the (discontinuous) microscopic details to a macroscopic (continuous) function.

The size of a REV must be chosen such that no matter where it is placed in a porous medium domain, it always contains both a persistent solid phase and a void space. Similarly, a planar REA can be determined such that, no matter where it is placed within a porous medium domain, it will always contain both a persistent solid phase and a void space. The size of a REV and a REA is chosen such that the parameters

that represent the distributions of the void space and of the solid phase within it are statistically meaningful [8]. This means that, no matter where a REV (or REA) is placed in a porous medium domain, the value of the considered parameter does not vary significantly. The value for the porosity as a function of the chosen REV-size is shown schematically in *Figure 2.2*. For the porosity of sand, this condition is met when a REV contains approximately 100 to 1000 grains. For AAC it is more difficult to determine the required REV size. This is due to the large range of pore sizes present in AAC. As artificial air pores, being the largest pores in the AAC, have the largest influence on the porosity per pore, a REV for AAC should contain at least 100 artificial air pores, which is equal to a volume of >100 mm^3.

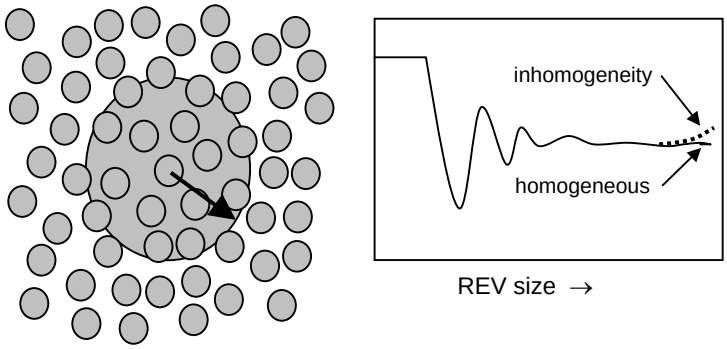

Figure 2.2 On the left a schematic representation of a porous medium is shown where the light grey area and the arrow show the size of a REV. The graph on the right shows the porosity as function of the size of the chosen REV.

Using a REV and REA, a material can be described using macroscopic properties. However, these properties can vary within a material. To deal with this, domains are used. A domain is chosen so that a REV has the same value for any given parameter (such as porosity, diffusion coefficient, permeability and porosity) wherever it is placed in the domain. By definition, a homogeneous material is described by one domain whereas an inhomogeneous material is described by several domains.

2.2.3 Processes and boundary conditions

After defining a material in terms of domains with their macroscopic properties, processes must be expressed in terms of these macroscopic parameters. When the correct initial and boundary conditions are applied to these descriptions, a set of (coupled) equations is created that can be solved using either analytical or numerical calculations.

2.3 Macroscopic description for porous media

2.3.1 REV and fluxes

To describe radon transport in porous media using a macroscopic approach, we have to define a REV. The REV, denoted as δV (m^3), is defined as the sum of the volumes of the solid phase, δV_s, the water phase, δV_w, the air phase, δV_a, and isolated pores, δV_{ip}, respectively:

$$\delta V = \delta V_s + \delta V_w + \delta V_a + \delta V_{ip} . \tag{2.1}$$

From these volumes, a macroscopic parameter, porosity can be defined according to the ratio of the various volumes. The following definitions are used for the total porosity, ε_t, the air-filled porosity, ε_a, and the water-filled porosity, ε_w:

$$\varepsilon_t = \frac{\delta V_a + \delta V_{ip} + \delta V_w}{\delta V}, \tag{2.2}$$

$$\varepsilon_a = \frac{\delta V_a}{\delta V}, \tag{2.3}$$

$$\varepsilon_w = \frac{\delta V_w}{\delta V}. \tag{2.4}$$

To describe the time-dependent, combined diffusive and advective transport of radon in the REV, the equation of continuity (mass conservation) for gas in a porous medium is applied to the radon concentration in the air phase:

$$\varepsilon_a \frac{\partial C_a}{\partial t} = -\nabla \bullet \left(\vec{j}_{d,a} + \vec{j}_{a,a} \right), \tag{2.5}$$

where:

t	time;
C_a	radon concentration in the air phase (Bq m^{-3});
$\vec{j}_{d,a}$	diffusive flux of radon in the air phase (Bq $m^{-2}s^{-1}$);
$\vec{j}_{a,a}$	advective flux of radon in the air phase (Bq $m^{-2}s^{-1}$).

$\vec{j}_{d,a}$ describes the flux of radon in the air phase due to diffusion. The derivation and definition of this flux can be found in section 2.3.3. The second term, $\vec{j}_{a,a}$, is the flux of radon in the air phase due to movement of the carrier gas. The definition of this advective flux is given in section 2.3.4.

In addition to – and independent of – these two transport processes, the rate of change of the radon concentrations in the air phase is also determined by radon decay and radon generation:

$$\varepsilon_a \frac{\partial C_a}{\partial t} = -\nabla \bullet \left(\vec{j}_{d,a} + \vec{j}_{a,a} \right) + j_s - j_d \,, \tag{2.6}$$

where:

j_s generation of radon (Bq $m^{-3}s^{-1}$);
j_d decay of radon (Bq $m^{-3}s^{-1}$).

A description for the generation and decay of radon can be found in section 2.3.2.

So far, we have only considered radon in the air-phase. However, from the literature [21] it is known that in porous media, radon is not only present in the air phase but it is also adsorbed to pore walls and dissolved in water present in a porous medium. Assuming the exchange of radon between the three phases is rapid compared to the other processes, the total rate of change in the air-filled pore-space can be written as:

$$\beta \frac{\partial C_a}{\partial t} = -\nabla \bullet \left(\vec{j}_{d,a} + \vec{j}_{a,a} \right) + j_s - j_d \,, \tag{2.7}$$

with:

$$\beta = \varepsilon_a + L\varepsilon_w + \rho_b k_a \,, \tag{2.8}$$

where:

L Ostwald coefficient (0.26 $m^3\,m^{-3}$ at 298K);
k_a adsorption coefficient ($m^3\,kg^{-1}$).

Note that the fluxes of 2.8 now also include the generation and decay of radon that is adsorbed and dissolved in the water. β is called the partition-corrected porosity, a term suggested by Andersen [3] and represents an apparent volume available for radon that differs from the air-filled porosity due to adsorption of radon to pore walls and dissolving of radon in water-filled pores. The Ostwald coefficient is the dimensionless form of the Henry's constant and gives the ratio between the radon concentrations in water and air phase in equilibrium. The adsorption coefficient, k_a, is an empirical parameter that has to be determined for every porous material and also depends on the moisture content and the temperature.

With the descriptions for the generation, decay and advective and diffusive transport together with the initial and boundary conditions, the radon transport in a homogeneous, porous medium can be described at a macroscopic level. This approach has proven to able to describe the generation and transport of radon in sand with an uncertainty of 10% for dry sand and 15 - 40% for (partly) wetted sand [23].

2.3.2 Radon generation and decay

Radon, ^{222}Rn, is formed in the decay of its parent: radium (^{226}Ra). The rate of generation of radon is therefore proportional to the amount of radium. As radium concentrations are generally considerably higher in the solid matrix than in the pore space, it is reasonable to assume that all radon is produced in the solid phase. Part of the generated radon remains in the solid matrix of the porous material and is (thus)

not available for transport. The other fraction is present in the water-phase and/or air-phase of the porous material and is available for transport. The ratio between the amount of radon that becomes available for transport and the total amount of radon generated is called the emanation coefficient and is denoted by η.

$$\eta = \frac{\text{amount of radon available for transport}}{\text{total amount of radon generated}} . \tag{2.9}$$

The presence of radon in any other phase than the solid matrix (which contains the radium) is due to the kinetic energy that radon gained, the so-called recoil energy. The recoil energy, due to the conservation of energy and momentum in the decay process, allows a radon atom to travel a certain distance in a porous material. The typical distance travelled is called the recoil-distance and depends on the material (phase) it travels through. This distance is about 0.02 - 0.07 μm in common minerals, 0.1 μm in water, and 63 μm in air [17]. The smaller recoil-distance for water compared to air is assumed to cause the regularly observed increase in emanation coefficient with increasing moisture content [13,24,25]. Model studies have shown similar trends [19,11].

The rate of decay of radon is proportional to the number of radon atoms. The total rate of change of the number of radon atoms per unit of time due to generation and decay is described by:

$$\frac{dN_{Rn}}{dt} = -\lambda_{Rn} N_{Rn} + \eta \lambda_{Ra} N_{Ra} , \tag{2.10}$$

where:

N_{Ra} number of radium atoms;
N_{Rn} number of radon atoms;
λ_{Ra} radium decay constant ($3.6 \cdot 10^{-12}$ s^{-1});
λ_{Rn} radon decay constant ($2.1 \cdot 10^{-6}$ s^{-1}).

The first term on the right hand side describes the loss of radon due to decay and the term second term describes the amount of radon atoms gained by generation of radon. However, often the radio-activity is not expressed in the number of atoms but in the number of atoms disintegrating per second. This is called the activity and can be calculated from the number of atoms and the decay constant, λ. For radium and radon this respectively yields:

$$A_{Ra} = \lambda_{Ra} N_{Ra} , \tag{2.11}$$

$$A_{Rn} = \lambda_{Rn} N_{Rn} , \tag{2.12}$$

where:

A_{Ra} radium activity (Bq);
A_{Rn} radon activity (Bq).

The radon activity concentration, C, is often expressed as the activity of radon per unit of volume, where the radium activity concentration is expressed as the activity per unit of mass:

$$C = \frac{A_{Rn}}{V}, \tag{2.13}$$

$$C_{Ra} = \frac{A_{Ra}}{m_s}, \tag{2.14}$$

where:

C radon activity concentration (Bq m^{-3});
C_{Ra} radium activity concentration (Bq kg^{-1});
V volume (m^3);
m_s mass of sample (kg).

Note that the activity in activity concentration is *not* the chemical activity but the radioactivity expressed in disintegrations per second. The rate of change in radon activity concentration can be written as:

$$\frac{dC}{dt} = -\lambda_{Rn} C + \eta \lambda_{Rn} \rho_b C_{Ra}, \tag{2.15}$$

where:

ρ_b bulk density (kg m^{-3}).

The decay constant of radium is not explicitly present in equation 2.15 as it is included in the radium activity concentration. For the effective transport equation 2.7, this yields the following expressions for the decay and the generation of radon:

$$j_s = \eta \lambda_{Rn} \rho_b C_{Ra}, \tag{2.16}$$

$$j_d = \beta \lambda_{Rn} C_a. \tag{2.17}$$

The partition corrected porosity, β, appears in equation 2.17, because not only radon in the air phase decays but also the radon adsorbed to pore walls and dissolved in the water phase. Radon that is generated in water and adsorbed to pore walls is included in the definition of the emanation coefficient.

Equations 2.16 and 2.17 show that the radium concentration, the partition corrected porosity, the emanation coefficient and the density of a porous medium are the material properties required to describe the generation of radon in a porous medium. The methods used to determine these parameters and the measurement results can be found in chapters 3 and 4.

2.3.3 Diffusive transport

This subsection deals with the transport of radon due to diffusion. Although diffusion of radon takes place in all three phases, the transport rate for radon in air dominates the process, provided water does not completely block the pathways through the porous media. To describe the diffusive transport in a porous medium, we will first focus on diffusive transport of radon in air.

Transport of component A (i.e. radon) through a binary mixture of components A and B (i.e. radon and air), is described by Fick's law of diffusion:

$$\vec{j} = -D_m \nabla C_a , \tag{2.18}$$

where:

$\vec{j}$ flux (Bq m^{-2} s^{-1});

D_m molecular diffusion coefficient ($m^2 s^{-1}$);

∇C_a (radon) concentration gradient (Bq m^{-4}).

The left hand term of the equation describes the amount of radon that is transported per surface area per unit of time, and the right hand term of the equation gives the driving force, ∇C_a and the effect of that driving force on the flux, the molecular diffusion coefficient D_m. Note that this equation assumes a mixture of ideal gases and very low radon concentration. The latter assumption can be considered correct as a radon concentration of $1 \cdot 10^3$ Bq m^{-3} equals a molar concentration of approximately $2 \cdot 10^{-15}$ mol m^{-3}.

Let us now consider diffusion in a porous medium. A porous medium contains, by definition, void space and a persistent solid phase. We assume diffusive transport takes place via the air-filled pores (i.e. void space) only and thus diffusion of radon along pore walls, in the water-filled pores and in the solid phase are ignored. Furthermore, it is assumed that effects of collisions with the pore walls are negligible (i.e. no Knudsen diffusion). When assuming that all pores are oriented in the same direction as the applied concentration gradient, the bulk flux of radon through a porous medium with an air-filled porosity, ε_a, is given by:

$$\vec{j}_{d,a} = -D_b \nabla C_a = -\varepsilon_a D_m \nabla C_a , \tag{2.19}$$

where:

$\vec{j}_{d,a}$ flux of radon as result of diffusion in the air-phase (Bq m^{-2} s^{-1});

D_b bulk diffusion coefficient of porous medium (m^2 s^{-1});

ε_a air-filled porosity.

It is clear that for this situation a bulk diffusion coefficient can easily be deduced from the molecular diffusion coefficient for radon in air. However, in an isotropic material the pores will be oriented in random directions. As a result, radon will have to travel a longer distance than the thickness of the sample, which results in a reduction of the flux. To compensate for this effect and others (such as dead-end pores and varying

pore-radii), a tortuosity factor is introduced to relate the bulk diffusion coefficient to the molecular diffusion coefficient:

$$D_b = D_m \varepsilon_a \tau_a , \tag{2.20}$$

where:

τ_a tortuosity of the air-filled pores.

In the definition of the tortuosity that is used here, the value of the tortuosity ranges from 0 to 1. Note that sometimes in the literature the tortuosity is defined as $\tau_a{}^{-1}$.

Another term that often leads to confusion is the effective diffusion coefficient. In some papers, the term effective diffusion coefficient is used for what is called here the bulk diffusion coefficient. In this thesis, however, the more common definition of the effective diffusion coefficient, D_e, is used:

$$D_e = \frac{D_b}{\varepsilon_a} . \tag{2.21}$$

In this definition, the effective diffusion coefficient describes the actual transport rate for radon in the air-filled pore space rather than the bulk transport. The effective diffusion coefficient can, for example, be used to compare diffusion rates in materials with similar pore structure but different porosity. The flux of radon activity in the air-filled pore space can then be rewritten by substituting equation 2.20 in 2.18:

$$\vec{j}_{d,a} = -D_b \nabla C_a . \tag{2.22}$$

2.3.4 Advective transport

In addition to diffusive transport, radon can be transported via bulk movement of a carrier gas. Radon transport due to movement of gas (e.g. air) is called advective transport. The flux of radon in the air-phase due to advection is given by:

$$\vec{j}_{a,a} = C_a \vec{q} , \tag{2.23}$$

where:

$\vec{j}_{a,a}$ flux of radon in the air-phase as a result of advection (Bq $m^{-2}s^{-1}$);

C_a radon concentration in the air-phase (Bq m^3);

$\vec{q}$ flow rate of air (m s^{-1}).

Although this movement can be caused by various processes, we will limit our description to the movement due to air pressure differences.

2.4 Flow of gas

To understand the macroscopic description for the transport of gas through an isothermal medium, it is necessary to describe the transport on a microscopic level.

2.4.1 Mass balance equations

Consider a fixed volume *V* that is surrounded by a permeable surface area *A*. The mass within this volume equals:

$$\iiint_V \rho \, dV \,, \tag{2.24}$$

where:

ρ density (kg m^{-3}).

The change in mass per unit of time is given by:

$$\frac{\partial}{\partial t} \iiint_V \rho \, dV \,. \tag{2.25}$$

The mass flux (out of the volume) through surface area *dS* is given by:

$$\rho \vec{v}_n dS = \rho \left(\vec{v} \bullet \vec{n} \right) dS \,, \tag{2.26}$$

where:

$\vec{n}$ vector perpendicular to the surface area *dS*;

$\vec{v}$ local velocity (m s^{-1});

$\vec{v}_n$ local velocity in the direction perpendicular to the surface area *dS* (m s^{-1}).

The total mass flowing out of the volume per unit of time is then given by:

$$\iint_S \rho \left(\vec{v} \bullet \vec{n} \right) dS \,. \tag{2.27}$$

According to the conservation of mass in the volume, this means that:

$$\frac{\partial}{\partial t} \iiint_V \rho \, dV = - \iint_S \rho \left(\vec{v} \bullet \vec{n} \right) dS \,. \tag{2.28}$$

Using the Gauss theorem, equation 2.28 can be rewritten as:

$$\iiint_V \left[\frac{\partial \rho}{\partial t} + \nabla \bullet \left(\rho \vec{v} \right) \right] dV = 0 \,. \tag{2.29}$$

As *V* can be chosen arbitrarily, this implies:

$$\frac{\partial \rho}{\partial t} + \nabla \bullet \left(\rho \vec{v} \right) = 0 \,. \tag{2.30}$$

This equation is often called the differential form of the continuity equation.

2.4.2 Momentum balance equations

The momentum of a system can, similar to the continuity equation, be written in a differential form [16]:

$$\rho \frac{\partial \vec{v}}{\partial t} + \rho \left(\vec{v} \cdot \nabla \right) \vec{v} = -\nabla P + \nabla \bullet \overline{\overline{\tau}} + \rho \vec{g} \,. \tag{2.31}$$

where:

$\overline{\overline{\tau}}$ viscous forces (Pa);
ΔP pressure gradient (Pa m^{-1})
$\vec{g}$ acceleration of gravity (m s^{-2}).

The term on the left hand side is often written as *Dv/Dt*. The terms on the right hand side describe respectively the effects of pressure, viscous forces and gravity on the change in momentum. For incompressible, Newtonian fluids the viscous forces are described by (*i* = x,y,z):

$$\overline{\overline{\tau}}_{ij} = \mu \left(\frac{\partial v_i}{\partial j} + \frac{\partial v_j}{\partial i} \right) , \tag{2.32}$$

where:

μ dynamic viscosity (Pa s).

The contribution of the viscous forces to the change of momentum is than described by:

$$\nabla \bullet \overline{\overline{\tau}} = \mu \nabla^2 \vec{v} \,. \tag{2.33}$$

Substituting equation 2.33 into 2.31 yields the Navier-Stokes equation:

$$\rho \frac{\partial \vec{v}}{\partial t} + \rho \left(\vec{v} \bullet \nabla \right) \vec{v} = -\nabla P + \mu \nabla^2 \vec{v} + \rho \vec{g} \,. \tag{2.34}$$

2.4.3 From a microscopic to a macroscopic description

Equation 2.34 can be used to describe transport of air in a porous medium on a macroscopic scale. If a porous medium can be represented by two smooth, parallel walls that are separated by distance *h* on the z-axis and we assume transport along the x-axis only, ignore the effect of gravity and the term of inertia, the Navier-Stokes equation has an exact solution (Poiseuille flow) for the steady state. Furthermore, the influence of gravity component, $\rho\vec{g}$, is assumed negligible. The velocity is then given by [27]:

$$v_x = \frac{1}{2\mu}\frac{dP}{dx}\left[z^2 - \left(\frac{h}{2}\right)^2\right], \quad v_z = 0. \tag{2.35}$$

If we integrate the full cross-section, we obtain for the average velocity, $\langle v_x \rangle$:

$$\langle v_x \rangle = \frac{1}{h}\int_0^h \left(\frac{1}{2\mu}\frac{dP}{dx}\left[z^2 - \left(\frac{h}{2}\right)^2\right]\right)dz = \frac{1}{2\mu}\frac{dP}{dx}\frac{1}{12}h^2. \tag{2.36}$$

This relation is of the same form as Darcy's law [10] and can be used to relate the permeability to the an effective pore height:

$$\vec{q} = -\frac{K}{\mu}\nabla P, \tag{2.37}$$

with:

$$K = \frac{1}{24}h^2, \tag{2.38}$$

where:

K	permeability (m^2);
μ	dynamic viscosity (for air at 293K: $1.83 \cdot 10^{-5}$ Pa s);
$\vec{q}$	flow velocity (m s^{-1});
∇P	pressure gradient (Pa m^{-1}).

Darcy's law is often sufficient to describe the relation between applied pressure (difference) over a porous medium (like soil and building materials) and the resulting flow. For flows that are not dominated by viscous forces the relation has to be extended with additional parameters. One of those extensions is the Darcy-Forchheimer equation:

$$\frac{\mu\vec{q}}{K} + \phi\rho_a\vec{q}\left|\vec{q}\right| = -\nabla P, \tag{2.39}$$

where:

ϕ	Forchheimer coefficient [12].

The Forchheimer coefficient corrects for the inertia term of the Navier-Stokes equation. Its value depends on the pore structure of the material and the applied pressure gradient. To determine whether or not a flow is dominated by viscous forces, the Reynolds number can be used. For a flow, with a characteristic velocity *v*, around an object with characteristic size or pore radius, *a*, the Reynolds number, *Re* is calculated as:

$$Re = \frac{\rho_a v_{pore} a}{\mu}, \tag{2.40}$$

with:

$$v_{pore} = \frac{Q}{\varepsilon_a A}, \tag{2.41}$$

where:

ρ_a density of the flowing gas (e.g. air) (kg m^{-3});
v_{pore} characteristic effective flow velocity in the pores (m s^{-1});
a characteristic size or pore radius (m);
μ dynamic viscosity of air ($1.83 \cdot 10^{-5}$ Pa s, at T=293 K);
Q mass flow ($m^3 s^{-1}$);
A surface area perpendicular to the flow (m^2).

For *Re* « 1, the flow is dominated by viscous forces. The flow is then called viscous flow or 'creeping flow'. For *Re* » 1, the contribution of the viscous forces is negligible compared to the inertia terms and the flow is then called quasi-non viscous flow [16]. For Reynolds numbers larger than approximately 2000, the flows become turbulent. The effects described by the Darcy-Forchheimer equation can become noticeable for Reynolds numbers of the order of unity.

2.4.4 Relation pressure gradient and flows in AAC

Using the experimental conditions applied to AAC in the combined diffusive and advective transport measurement (see chapter 5) and the dimensions of the set-up (see chapter 3), an estimate can be made of the Reynolds number for the flow of air through the AAC. Assuming a typical flow velocity of $1 \cdot 10^{-4}$ m s^{-1} and a pore size of $1 \cdot 10^{-3}$ m, a value of *Re* = 0.01 is found. For this value, the flow will be laminar and dominated by viscous forces, i.e. the relation between the pressure and the flow will be described using Darcy's law. However, a variation in pore sizes can locally lead to an increase in the airflow velocity and thereby in an increase of the Reynolds number. Depending on the variation, the Darcy-Forchheimer equation can be required to describe the relation between the pressure gradient and the flow velocity.

2.5 Combined diffusive and advective transport

In this section we will look into the effect of combined diffusive and advective transport of radon. First we will show how the dominant process is determined, secondly we will look into the possible mixing effects of advective flow.

2.5.1 Characterising the dominant process

For an ideal solution with relatively low flow rates, a radon flux due to combined diffusive and advective transport is the sum of two fluxes (see equation 2.18 and 2.23). For this situation, it is possible to determine whether the flow is dominated by diffusive or advective transport using the Peclet number, *Pe* :

$$Pe = \frac{v_{\text{pore}} \cdot l}{D_{\text{e}}}, \tag{2.42}$$

where:

D_{e} effective diffusivity (m^2s^{-1});

l characteristic length of system (m).

Pe » 1 indicates transport dominated by the advective flow where *Pe* « 1 indicates transport dominated by diffusion. For the experimental set-up, the thickness of the cylinder of AAC was chosen as the characteristic length. For the combined advective and diffusive transport measurements presented in this thesis, the Peclet number is approximately 1.

2.5.2 Dispersion

When a gas containing various components (e.g. radon and air) flows through a medium, additional mixing can occur. This effect is called dispersion. Dispersion is defined in this thesis as the mixing of radon occurring in an advective flow through a porous medium due to other processes than molecular diffusion. Note that in the literature, various (other) definitions of dispersion are used.

The main mechanisms causing dispersion are often divided in hydrodynamic dispersion (dispersion caused by variations in flow rate) and mechanical dispersion (dispersion caused by the pore structure of the material). Other effects that can contribute to dispersion of gases in porous media are turbulence, adsorption and desorption of gases to and from the pore surface and differences in viscosity and density of the gases. A previous study [15] concluded that these effects can be considered negligible.

2.5.3 Hydrodynamic dispersion

A description of hydrodynamic dispersion in a circular capillary was given in 1953 by Taylor [26]. This type of dispersion is called Taylor-dispersion and occurs when two fluids or gases, flowing in a capillary, are divided by a plane perpendicular to the capillary. By applying a driving force (e.g. pressure difference), a flow is created. Due

to friction, the velocity of the gases will be largest in the centre of the capillary and smallest near the walls. Therefore, the plane between the two gases will change shape, resulting in an apparent increase in diffusive transport. This process is schematically shown in *Figure 2.3*.

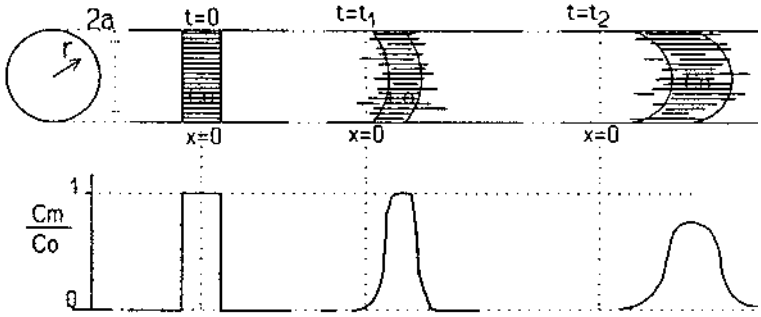

Figure 2.3 Taylor-dispersion: extra mixing occurs due to differences in flow-rate at the centre and the walls of the capillary. The upper row shows the cross-section of a capillary containing two gases presented by the white and grey surfaces moving with time, the lower row shows the average concentration of the "grey" gas.

Aris [5] added an effect of diffusive transport perpendicular to the capillary. For a circular capillary with radius *a*, the effect of Taylor-Aris dispersion on the diffusion coefficient in the direction of the flow, the longitudinal diffusion coefficient, K_L is described by:

$$K_L = D_m + \frac{a^2 v_{pore}^{\ 2}}{48 \cdot D_m}, \tag{2.43}$$

where:

K_L longitudinal diffusion coefficient ($m^2 s^{-1}$).

The factor 1/48 results from the (circular) shape of the capillary. Hydrodynamic dispersion in oval (and other shapes) capillaries is described by Ananthakrishan [2]. Note that the effect of Taylor-Aris dispersion increases for larger capillary radii and larger flow velocities. For flow rates applied in the measurements presented in this thesis, where *Pe* seems smaller than 1, the Taylor-Aris dispersion seems negligible. However, without precise knowledge of the structure of AAC, it is difficult to give a good estimate of the Peclet number.

2.5.4 Mechanical dispersion

Particles moving through a porous medium will use different paths with different lengths and at different flow velocities. Because of these differences, the time needed for particles of two gases to pass a medium will be different, resulting in mixing of particles entering the medium at an earlier or a later moment. This effect is called

mechanical dispersion and is schematically shown in *Figure 2.4.* Saffman [22] included mechanical dispersion in his random walk model. This model represents the porous medium as a static, isotropic network of straight tubes with length *l* and radius *a*. Although this model is a very simplified representation of a porous medium, model calculations and measurements on granular beds show, after some corrections, a good correlation. Mechanical dispersion may play a role in the transport of air through AAC as the structure of AAC will allow various flow paths and velocities. However, it is difficult to give a reliable estimate of this effect without having more information on the structure of the AAC and the paths the air flows through.

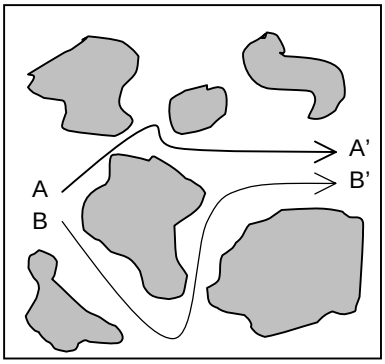

Figure 2.4 Mechanical dispersion: particles may follow a number of flow-paths (A and B). Due to differences in velocity and path length, this results in additional mixing.

2.6 Radon transport in AAC

To apply a macroscopic approach as described in section 2.3, it is required that AAC can be represented as a homogeneous medium. A representation of AAC as a homogeneous material is probably correct for large REV-sizes, provided no cracks are present. A possible problem can arise from the large range of pore sizes in AAC as their connectivity can influence transport. This section examines how these and other inhomogeneities on a microscopic level can influence the macroscopic description.

2.6.1 Pore configuration

Pore size distribution measurements on AAC [20] have shown three types of pores with their own distinct sizes:

- artificial air pores (AAP) with a radius between approximately 10^{-3} and 10^{-4} m. These pores are formed by hydrogen gas and/or surface active agents during the manufacturing of the AAC and make up for about half of the pore volume.
- macro-capillary pores (MCP) with a radius between 10^{-4} and 10^{-6} m. These pores make up about one fifth of the pore volume but play an important role in the moisture transport in AAC [20].

- micro-capillary pores (mCP) with a radius smaller than 10^{-6} m. Under normal conditions, part of these pores are filled with water.

Assuming the artificial air pores and macro-capillary pores are the main contributors to the transport, the characteristic pore size can be anywhere between 10^{-3} and 10^{-6} m. This assumption seems reasonable because these pores make up about 70% of the porosity . These pores can be connected in many configurations of which the parallel connected and serial connected pores are the two most extreme (see *Figure 2.5*).

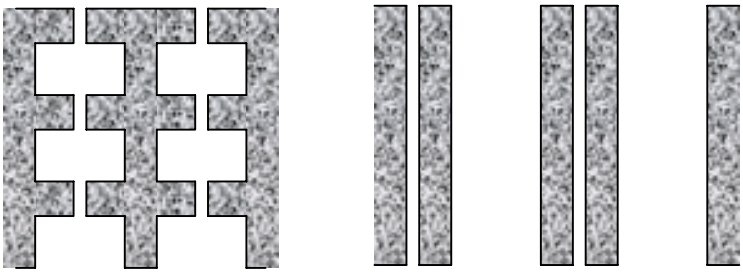

Figure 2.5 Left: serial pore configuration, right: parallel pore configuration.

Poiseuille's law, which is given by:

$$Q = \frac{\pi r^4}{8\mu}\frac{dP}{dx}. \tag{2.44}$$

where Q is the mass flow (m^3s^{-1}) and x the pore radius (m), implies that if the parallel pore configuration is a correct representation, the flow velocity will be largest in the largest pores. As the Reynolds number increases with larger pore radii and flow velocities, a larger Reynolds number can be expected for this configuration. Let us now consider the serial configuration: according to the laws of mass conservation, the amount of air (Q) flowing through the large pores must be equal to the amount flowing through the small pores under steady state conditions. If the large pores have a radius of r_1 and the small pores a radius r_2, the flow velocities in the pores must be related according to:

$$v_1 r_1^2 = v_2 r_2^2 \ , \tag{2.45}$$

where:

v_1, v_2 average airflow velocity in pore with radius r_1 and r_2 respectively (m s^{-1}).

If this relation is entered in the equation 2.40, it yields:

$$Re(r_2) = \frac{r_1}{r_2} Re(r_1). \tag{2.46}$$

This means that in a serial configuration, the Reynolds number in the small pores increases with a factor R_1/R_2 in comparison with the Reynolds number for a

homogeneous medium (*Re* = 0.01). This means that the Reynolds number for an airflow through either of the configurations discussed here is larger than expected for a homogeneous material. When these configurations are present in AAC, this means the actual Reynolds number is larger than the calculated value assuming a homogeneous material. A larger Reynolds number results in increased dispersion (see equations 2.40 and 2.43).

2.6.2 Effects of (micro)cracks

In addition, consolidated porous building materials often contain (micro)cracks that can form preferential flow paths. These features can either be implicitly or explicitly be accounted for. Discrete (fracture) network models, that explicitly account for cracks, can be used when the size, position and number of the cracks is known. The double porosity model accounts for fractures implicitly [6]. Typically, in the double porosity model, the matrix blocks have a high porosity for storage while the cracks have a high permeability. Note that in the (original) double porosity models, no flow is assumed in the matrix blocks. When this is allowed, the model should be called a double porosity/double permeability model. Other aspects that can influence the transport of radon in AAC include dead-end pores, ratio between path lengths and the effective travelled distance and varying cross-sections. These aspects are (partly) included in the tortuosity of the material.

2.7 Model extensions

It has been shown that the advective and diffusive transport of radon depend strongly on the material microstructure. For the combined advective and diffusive transport of radon in sand, a good correlation was found when neglecting dispersion effects. As measurement conditions are comparable, this model for sand will be our starting point for modelling the measurements presented in this thesis. This will give insight in the magnitude of the effects described and help to understand the transport of radon in AAC. The more complex pore structure of AAC, however, might require a model that includes dispersion effects and/or inhomogeneity. The latter can be done with a *parallel-media model*, where the inhomogeneity of the material is represented by two media with different permeability, volume and/or diffusion coefficient (see *Figure 2.6*). A more detailed description of these two models can be found in chapter 5.

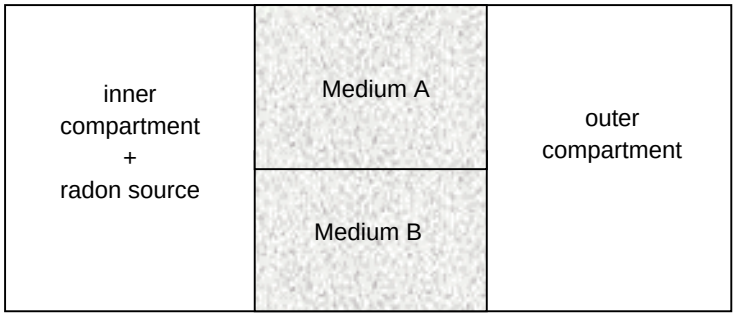

Figure 2.6 Schematic representation of the parallel-media model.

References

[1] Aldenkamp F.J., Stoop P., Sources and Transport of Indoor Radon – Measurements and Mechanisms, Ph.D. thesis, University of Groningen, The Netherlands, 1994.

[2] Ananthakrishan V., Gill W.N., Barduhn A.J., Laminar Dispersion in Capillaries, *A.I.Ch.E. Journal*, 11:1063-1072, 1965.

[3] Andersen C.E., Entry of Soil Gas and Radon into Houses, Ph.D. thesis, Risø National Laboratory, Denmark, 1992.

[4] Anonymous, NEN7181: Radiation performance of dwellings and residential buildings – Determination method, NEN, The Netherlands, 2001.

[5] Aris R., On the dispersion of a solute in a fluid flowing through a tube, *Proc. Roy. Soc. (London)*, A235:67-77, 1956.

[6] Barenblatt G.I., Zheltov Y.P., Kochina I.N., Basic concepts in the theory of seepage of homogeneous liquids in fissured rocks, *J. Appl. Math. Mech.*, 24:1286-1303, 1960.

[7] Bear J., Corapcioglu M.Y., Fundamentals of Transport Phenomena in Porous Media, NATO ASI series, E82, 1984.

[8] Bear J., Bachmat Y., Introduction to Modelling of Transport Phenomena in Porous Media, Kluwer Academic Publishers, 1990.

[9] Cozmuta I., Radon Generation and Transport: a journey through matter, Ph.D. thesis, University of Groningen, The Netherlands, 2001.

[10] Darcy H.P.G., Les Fontaines Publiques de la Ville de Dijon, Librarie de Corps Imperiaux des Ponts et Chausses et de Mines, Paris, 1856.

[11] Edwards J.C., Bates R.C., Theoretical evaluation of radon emanation under a variety of conditions, *Health Physics*, 39:263-274, 1980.

[12] Forchheimer P., Wasserbewegung durch Bodem, *Zeit. Ver. Deut. Ing.*, 45:1781-1788, 1901.

[13] Goh T.B., Oscarson D.W., Cheslock M., Shaykewich C., Fluence rate of radon from soil: effect of sorption barriers, moisture content, and temperature, *Health Physics*, 61:359-365, 1991.

[14] van der Graaf E.R., Cozmuta I., van der Pal M., Calibration of the NGD-KVI porosimeter and results of initial experiments on aerated concrete samples from TUE, KVI-report S-75, KVI, The Netherlands, 1996 (in Dutch).

[15] de Groot E.H., Menging van Helium en Stikstof door Diffusie en Dispersie in een Zandkolom, report VDF/NK 94-20, Eindhoven University of Technology, The Netherlands, 1994 (in Dutch).

[16] van Heijst G.J.F., van de Vosse F.N., Stroming en Diffusie, College Aantekeningen 3D030, Eindhoven University of Technology, The Netherlands, 2002.

[17] Nazaroff W.W., Moed B.A., Sextro R.G., Soil as a Source of Indoor Radon: Generation, Migration, and Entry. In: Nazaroff W.W., Nero A.V., editors, Radon and its Decay Products in Indoor Air, John Wiley & Sons, 1988.

[18] Nielson K.K., Rogers V.C., Rogers V., Holt R.B., Raetrad Model Extensions for Radon Entry into Multi-level Buildings with Basements or Crawl Spaces, *Health Phys*ics, 73:668-679, 1997.

[19] Plantinga S.D., Radon emanation: its dependence on moisture content and grain size, KVI-report R-94, KVI, The Netherlands, 1996.

[20] Roels S., Sermijn J., Carmeliet J., Modelling unsaturated moisture transport in autoclaved aerated concrete: a microstructural approach, proceedings of the 6th Nordic Symposium Building Physics, 167-174, 2002.

[21] Rogers V.C., Nielson K.K., Multiphase radon generation and transport in porous materials, *Health Physics*, 60:807-815, 1991.

[22] Saffman P.G., On the effect of the molecular diffusivity in turbulent diffusion, *Fluid Mech.*, 8:273-283, 1960.

[23] van der Spoel W.H., Radon transport in sand: a laboratory study, Ph.D. thesis, Eindhoven University of Technology, The Netherlands, 1998.

[24] Stranden E., Kolstad A.K., Lind B., The influence of moisture and temperature on radon exhalation, *Rad. Prot. Dosim.*, 7:55-58, 1984.

[25] Strong K.P., Levins D.M., Effect of moisture content on radon emanation from uranium ore and tailings, *Health Physics*, 42:27-32, 1982.

[26] Taylor G.I., Dispersion of soluble matter in solvent flowing slowly through a tube, *Proc. Roy. Soc. (London)*, A219:186-203, 1953.

[27] Zimmerman R.W., Fluid Flow in Rock Fractures: From the Navier-Stokes Equations to the Cubic Law, In: Dynamics of Fluids in Fractured Rock, Geophysical Monograph 122, 2000.

List of Symbols

symbol	description
β	partition corrected porosity
δV	representative elementary volume (REV) (m^3)
δV_{ip}	volume of isolated pores (m^3)
δV_p	volume occupied by air-phase (m^3)
δV_s	volume occupied by solid-phase (m^3)
δV_w	volume occupied by water-phase (m^3)
ε_a	air-filled porosity
ε_t	total porosity
ε_w	water-filled porosity
ϕ	Forchheimer coefficient
η	emanation coefficient
λ_{Ra}	radium decay constant (s^{-1})
λ_{Rn}	radon decay constant (s^{-1})
μ	dynamic viscosity of air ($1.83 \cdot 10^{-5}$ Pa s, at T = 293 K)
ρ	density (kg m^{-3})
ρ_a	density of air (kg m^{-3})
ρ_b	bulk density (kg m^{-3})
$\bar{\bar{\tau}}$	viscous forces (Pa)
τ_a	tortuosity of the air-filled pores
A_{Ra}	radium activity (Bq)
A_{Rn}	radon activity (Bq)
A	surface area (m^2)

List of symbols (continued)

symbol	description
C	radon concentration (Bq m^{-3})
C_a	radon concentration in the air-phase (Bq m^{-3})
C_{Ra}	radium concentration (Bq m^{-3})
D_b	bulk diffusion coefficient (m^2s^{-1})
D_e	effective diffusion coefficient m^2s^{-1})
D_m	molecular diffusion coefficient (m^2s^{-1})
K	permeability (m^2)
K_L	apparent longitudinal diffusion coefficient (m^2s^{-1})
L	Ostwald coefficient
N_{Ra}	number of radium atoms
N_{Rn}	number of radon atoms
P	pressure (Pa)
Pe	Peclet number
Q	mass flow (m^3s^{-1})
Re	Reynolds number
S	surface area (m^2)
V	volume (m^3)
a	characteristic pore-radius (m)
$\vec{g}$	acceleration of gravity (m s^{-2})
h	distance on the z-axis (m)
j_d	decay of radon (Bq $m^{-3}s^{-1}$)
j_s	generation of radon (Bq $m^{-3}s^{-1}$)
$\vec{j}_{a,a}$	flux of radon in the air-phase due to advection (Bq $m^{-2}s^{-1}$)
$\vec{j}_{d,a}$	flux of radon in the air-phase due to diffusion (Bq $m^{-2}s^{-1}$)
k_a	adsorption coefficient (m^3kg^{-1})
m_s	mass of sample (kg)
$\vec{n}$	vector normal to the surface area dS
$\vec{q}$	bulk flow rate (m s^{-1})
r	pore radius (m)
t	time (s)
v_{pore}	characteristic effective flow velocity in the pores (m s^{-1})
v_x	velocity on the x-axis (m s^{-1})
v_n	velocity normal to surface area dS (m s^{-1})

3

Materials and methodology

3.1 Introduction

To investigate the influence of various parameters on the generation and transport of radon in porous building materials, measurements under well-defined and well-controlled conditions were conducted. For this purpose, a set-up was built of which the core is a cylindrical stainless-steel vessel. The vessel contains a hollow cylindrical sample of autoclaved aerated concrete (AAC), which is sealed at top and bottom. In this way, the set-up comprises two compartments separated by AAC. The main reason for using a cylindrical geometry rather than a rectangular shape are the difficulties encountered at the KVI when sealing cubic concrete samples [6]. AAC was chosen as sample material for its homogeneity, relatively short curing period and the possibility to produce and carve large samples.

The conditions in the set-up are measured, set and controlled by a series of devices. The set-up and the devices measuring and controlling the various parameters are described in the next section. Besides the conditions in both compartments, the radon concentration in the vessel is determined by the properties of the AAC cylinder. The fabrication of the AAC cylinder and the measurement of its properties are described in section 3.3. Special attention was paid to the avoidance of uncontrolled leakage of air and radon from the set-up. The measurements carried out for this purpose are described in section 3.4.

3.2 Experimental set-up

3.2.1 General description

During the design of the set-up, three factors have played an important role: minimal leakage of radon and air, values of the measured and controlled quantities should be above the detection limit of the devices, and conditions in the set-up should mimic a regular dwelling. The latter meant that the relative humidity, pressure and pressure-difference, temperature, ventilation rate, thickness of building material and ratio of surface building material to compartment volumes should be close or similar to those of a regular dwelling. Main reason for this requirement is the mismatch between radon exhalation rates of (relative) small samples of building materials and their contribution to radon in dwellings [10]. By choosing set-up (and sample) dimensions close to those of a real dwelling, uncertainties introduced by the scaling from sample to dwelling-size are reduced. A limit to the scaling is set by the detection limit of the radon meters because with increasing volume to surface ratio, the radon concentration in the set-up will decrease. These requirements are reflected in the dimensions of the set-up (see *Table 3.1*). Probability of leakage of air and radon was reduced by using a cylindrical symmetry. This allows relative easy sealing of steel to steel connections with O-shaped rubber rings placed in U-shaped profiles.

A general overview of the set-up is given in *Figure 3.1*. The set-up consists of a cylindrical stainless-steel vessel with an inner diameter of 1.00 m and a height of 1.16 m. The vessel is closed at the upper side by a lid with a diameter of 1.11 m and

thickness of 0.03 m. In the centre of the vessel, a hollow cylinder of AAC with an inner radius of 0.303 m, an outer radius of 0.399 m and a height of 0.743 m is placed. The dimensions for the volumes of the inner and outer compartment and the AAC cylinder are given in *Table 3.1*. The uncertainties are calculated from repeated measurements and do not include systematic errors such as variations in symmetry. The magnitude of these errors is estimated to be less than 1% of the volumes of the compartments and AAC cylinder. Note that the sum of the volumes of the inner and outer compartment and AAC cylinder is not equal to the total volume as the latter also includes the volume of the rings and lid present in the vessel.

Table 3.1 Dimensions of the vessel and the AAC cylinder

property	value
volume vessel	0.887 ± 0.005 m^3
volume inner compartment	0.224 ± 0.003 m^3
volume outer compartment	0.483 ± 0.006 m^3
height aerated concrete cylinder	0.743 ± 0.002 m
inner diameter AAC cylinder	0.606 ± 0.002 m
outer diameter AAC cylinder	0.798 ± 0.002 m
volume AAC cylinder	0.157 ± 0.003 m^3

Figure 3.2 shows the AAC cylinder sealed in the vessel. The AAC cylinder is sealed at top and bottom to two stainless-steel rings with a 4 mm thick layer of polyurethane-based adhesive compound[1]. The bottom ring is placed on the bottom plate of the vessel. The ring on top of the AAC cylinder is sealed with a stainless-steel lid inside the cylinder called the inner lid. To optimise sealing, the metal rings are cleaned with ethanol to remove organic contaminants prior to sealing. The dust in the pores on the outside of the AAC cylinder has been removed using compressed air. The adhesive compound is then applied to the AAC cylinder and the AAC cylinder is placed on the lower ring. The stainless-steel outer lid has been placed on top of the AAC cylinder to press the AAC and the ring together for better adhesion. 72 hours after the AAC cylinder has been placed on the lower ring, the upper ring is sealed to the AAC cylinder following a similar procedure. Three U-shaped profiles are used to assure airtight sealing of the rings. The air in the middle profile is evacuated using a vacuum pump whereas the two other profiles contain a rubber O-shaped ring. By monitoring the pressure in the middle profile, leakage of air through one of the rubber O-shaped rings can be detected. Six rods, placed on the outside of the AAC cylinder, are applied to press the inner lid down to obtain airtight sealing of the O-shaped rings.

By sealing the AAC cylinder, two separate air volumes are created in the set-up. The air volume inside the hollow cylinder of AAC is called the *Inner Compartment*. The air volume outside the AAC cylinder is called the *Outer Compartment*. The conditions in these two compartments are measured and controlled using a series of devices.

[1] Sikaflex, type 260

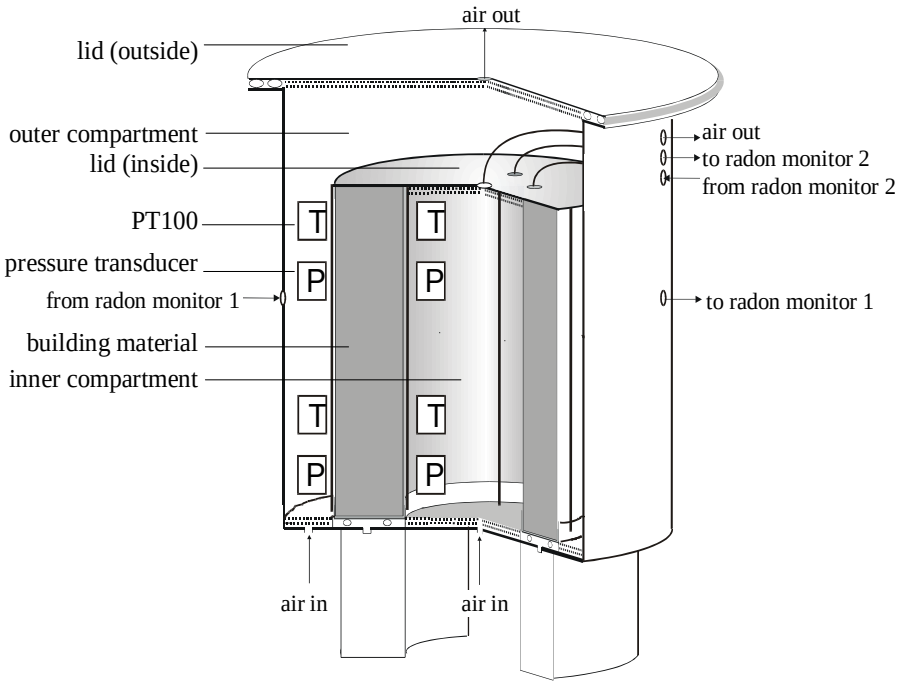

Figure 3.1 Schematic overview of the experimental set-up for measuring radon generation in and transport through rigid porous materials.

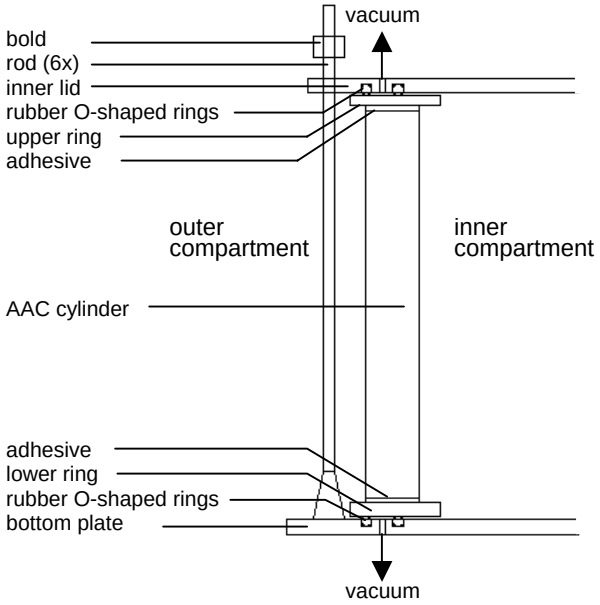

Figure 3.2 Detailed view of the sealing of the AAC cylinder. It is sealed on top and bottom with an adhesive connection to a stainless-steel ring. This ring is sealed to the bottom and lid via O-shaped rings.

3.2.2 Devices

A series of devices is used to measure and control the conditions in the set-up. An overview of the airflow through the set-up and the devices measuring and/or controlling the conditions in the vessel is given in *Figure 3.3*. A description of the measured and controlled parameters and devices is given below:

- The temperature in the vessel is measured with four thermometers[1] with a range from 0 ^{o}C to 100 ^{o}C and an uncertainty of 0.1 ^{o}C. Two are placed in the inner compartment and two in the outer compartment. Two (one in each compartment) are located at 0.25 m from the bottom of the vessel; the other two are located 0.25 m from the top of the vessel. The set-up is placed in a temperature-controlled room.
- The pressure in the outer compartment is measured with a pressure gauge[2] suitable for the range 800 hPa to 1100 hPa with an uncertainty of 0.2% full scale + 0.8% of reading. The pressure in the compartments is controlled by opening the control valve connected to the outer compartment for a decrease in pressure (or closing for an increase in pressure). This valve is part of one of the two mass-flow controllers[3] for the outgoing air as shown in *Figure 3.3*. Measurements show that the pressure can be controlled within 0.5 hPa.
- The atmospheric pressure is measured with a pressure gauge[4] for a range of 800 – 1100 hPa with an uncertainty of 0.05% full scale.
- The pressure difference between the inner and outer compartment is measured with two differential pressure-sensors[5] for values from 0 Pa to 100 Pa with an uncertainty of 0.2 Pa. The pressure difference is controlled by increasing (decreasing) the out-flowing air of one of the compartments while decreasing (increasing) the airflow into the other.
- A mass-flow controller[6] measures the flow rate for each compartment with a range of 0-20 L_n N_2 min^{-1} and an uncertainty of 0.2% full scale + 0.8% of reading. L_n equals a volume of 1 litre at 293.15 K at 1 bar. The flow rate can be set for each compartment with two mass-flow controllers (MFC's)[7]. These MFC's have a range of 0 – 10 L_n N_2 min^{-1} each and an accuracy of 0.5% full scale.
- Four sensors[8] measure the relative humidity in a range from 0 to 100% with an uncertainty of 2% full scale. The relative humidity can be set by adjusting the ratio between the one MFC connected to an air-humidifier producing nearly 100% humid air and one MFC supplying dry air.
- The radon concentration is measured with two α-counting quasi-continuous radon meters, designed according to Aldenkamp and Stoop [1]. The radon

[1] Kelatron K431 4-wire PT100 thermometer
[2] Setra type 276 barometric pressure gauge
[3] Bronkhorst type F-004AC-LU-22-V
[4] Setra type 270 barometric pressure gauge
[5] Setra type 264 differential pressure gauge
[6] Bronkhorst type F-102D-FA-22-V mass flow controller
[7] Bronkhorst type F-201C-FA-22-V mass flow controller
[8] Rense type HT-773-M-06 relative humidity sensor

meters measure radon concentration in an air volume of 3 litres each with a detection efficiency of approximately 0.3 for α-decay of ^{222}Rn to ^{218}Po. Together with a background count rate of less than 2 counts per minute, this results in a detection limit for each radon meter of 10 Bq m^{-3} for a measuring interval of 30 minutes.

A Pentium-166MHz computer with a Keithley DAS1802HC data-acquisition board, a Keithley PD-ISO8 relays switchboard and a Keithley CTM05/A Counter/Timer board was used to collect the data and to control the set conditions. Software was developed to automate the set-up. The software included the collection of data at regular intervals and control of parameters such as pressure and mass-flows according to a pre-set program. A description of the software was made by Berentsen [4].

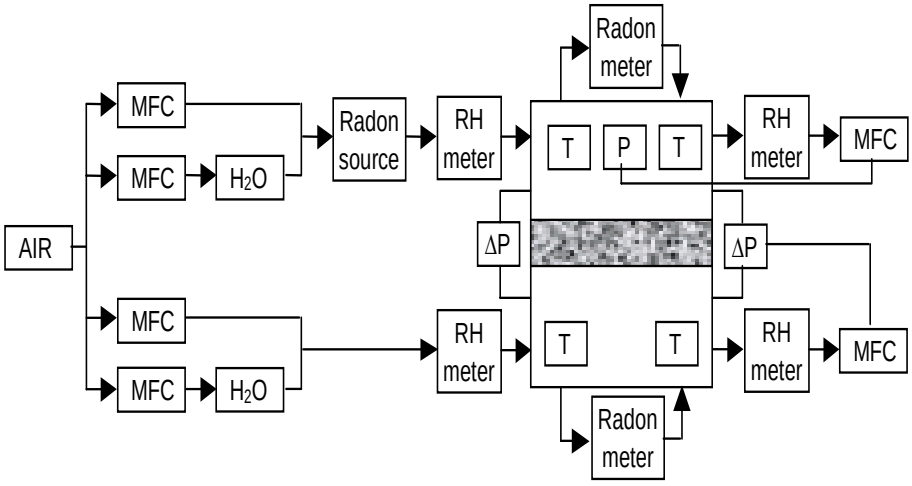

Figure 3.3: Diagram showing the airflow through the set-up where relative humidity (RH-meter), pressure (P), pressure difference (ΔP), temperature (T) and Mass Flow (MFC) are controlled and/or measured. The large block represents the inner and outer compartment of the stainless-steel vessel and the AAC cylinder.

3.3 Characteristics of AAC

This section introduces Autoclaved Aerated Concrete (AAC) as porous building material. It gives a description of the production process and the milling of the AAC cylinder. In addition, a description is given of the properties of the AAC and accompanying measuring methods.

3.3.1 Composition, production and fabrication

AAC is a lightweight, porous building material. Although many compositions of AAC are applied, a mixture of (quartz) sand, cement and lime is used for the work in this thesis. Of these components, it is likely that the cement [6] will contribute most to the radon exhalation of AAC. The formation of AAC starts with a chemical reaction

between water and lime. This reaction is initiated when water and a catalyst (e.g. aluminium powder) are added to the mixture. The heat generated by this reaction causes the slurry to set and the alkaline conditions combined with the catalyst generate hydrogen gas bubbles, which cause the blocks to rise. The blocks are then heated in an autoclave, which promotes reactions between calcium and silicates in the sand and cures the mixture, giving it its final honeycombed shape. Except for the release of water present in AAC, its physical properties hardly change in time, especially when compared to (curing of) concrete.

To make the cylinder, a block of 1.2 by 1.2 m was cut from the slurry before it was heated in an autoclave at Ytong[1]. Several holes were drilled in the middle of this block to let the steam escape more easily. In total, four blocks of 1.2 x 1.2 x 0.8 m each were made. Note that Ytong produces mainly building blocks and planks (with a thickness of less than 0.2 m). Therefore, the properties of AAC described in this thesis are not necessarily the same as for the commercial AAC products from Ytong. The cylindrical shape was obtained by milling at the workshop of the Buildings Physics group of the Eindhoven University of Technology. This technique was chosen for its possibility to create the desired shape with high precision considering symmetry and dimensions. *Figures 3.4* and *3.5* show the various stages of the milling process.

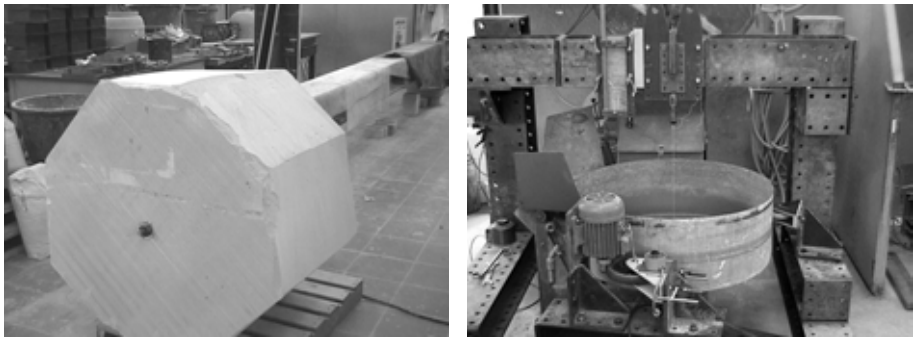

Figure 3.4 The corners of the AAC block were removed prior to milling (shown on the left) so it would fit in the milling set-up (shown on the right)

[1] Ytong Nederland, Meppel, The Netherlands

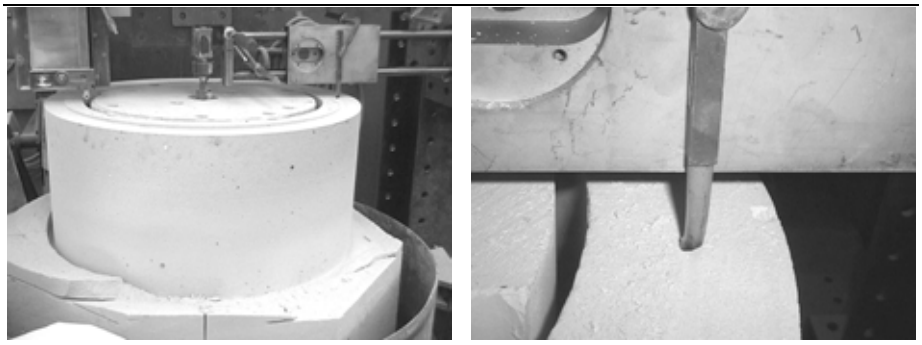

Figure 3.5 First the upper outer part was milled, followed by the upper inner part (shown on the left), after flattening the surface of cylinder (shown on the right), the cylinder was rotated 180^o and the remaining outer and inner part were milled and the surface flattened.

3.3.2 Porosity

A gas-displacement method [8] was used to determine the air-filled porosity, ε_a. The basic concept of the gas-displacement method is to determine the volume of a certain enclosure by pressurising a gas in this volume and then expand the pressurised gas in another enclosure of which the volume is accurately known. The unknown volume is deduced from a measurement of the pressures in both enclosures prior and after expanding. This principle is depicted schematically in *Figure 3.6*.

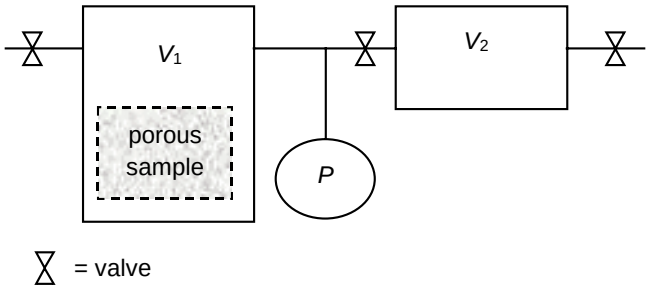

Figure 3.6 Schematical overview of the gas-displacement set-up, P represents the pressure transducer, V_1 is the enclosure containing the sample, and V_2 is the enclosure with a well-known volume.

Volume V_1 is pressurised to a certain pressure P_1 and subsequently the gas is expanded in the volume V_2 with initial (barometric) pressure P_2 and the resulting equilibrium pressure P_{eq} is measured. Assuming ideal-gas behaviour and constant temperature during the measurement, the volume V_1 follows from equation 3.1:

$$P_1V_1 + P_2V_2 = P_{eq}\left(V_1 + V_2\right), \tag{3.1}$$

where:

P_1 pressure in enclosure 1 at the start of the experiment (Pa);

V_1 volume available for air in enclosure 1 (m^3);
P_2 pressure in enclosure 2 at the start of the experiment (Pa);
V_2 volume available for air in enclosure 2 (m^3);
P_{eq} pressure in both enclosures at the end of the experiment (Pa).

The volume of enclosure V_1 is measured with and without a sample with bulk volume V_{AAC} present. Because the difference between the two measured volumes V_1 (without sample) and V_1' (with sample) is caused by the volume of the sample inaccessible for air, the air-filled porosity, ε_a, can be calculated:

$$V_1 - V_1' = (1 - \varepsilon_a) V_{AAC}, \tag{3.2}$$

or

$$\varepsilon_a = 1 - \frac{V_1 - V_1'}{V_{AAC}}, \tag{3.3}$$

where:

ε_a air-filled porosity (m^3m^{-3});
V_1' volume of enclosure 1 with AAC sample present (m^3);
V_{AAC} bulk volume of AAC sample (m^3).

To optimise the measurement method, the sensitivity for the dimensions of the enclosures was assessed. The procedure and results of this sensitivity analysis and the results of the calibration of the set-up are described in Appendix A.

Four AAC blocks of 0.2 x 0.2 x 0.2 m^3 were used to determine the air-filled porosity of AAC. Two samples were dried in an oven at 60 ^oC for more than 24 hours; the two other samples were stored at a relative humidity (*RH*) of 50% and a temperature of 20 ^oC. To determine the effect of large pressure (changes) on the air-filled porosity, the porosity is subsequently measured with a relatively low pressurisation of 0.15 MPa and at 0.5 MPa. *Table 3.2* shows the results of the porosity measurements. The results show no significant difference between the air-filled porosity measured before and after the pressurisation to 0.5 MPa. This means that the volume of dead-end pores opened during the pressurisation to 0.5 MPa can be ignored. Therefore it was concluded that the effect of the pressurisation on the pore-structure is limited. Furthermore, the porosity of the oven-dried samples is higher than the porosity of the samples stored at 50% *RH*. This is expected as part of the air-filled pores are filled with water. The weighted mean porosity of oven-dried AAC is 0.780 ± 0.009.

Table 3.2 Porosity determined with the gas-displacement method at different pressures on oven dried and at 50% relative humidity (RH) conditioned samples

Sample	Oven dried	50% *RH*
0.15 MPa (before)	0.786 ± 0.008	0.765 ± 0.006
0.50 MPa	0.780 ± 0.009	0.755 ± 0.005
0.15 MPa (after)	0.793 ± 0.007	0.768 ± 0.006

In addition, the total porosity was determined by the following procedure; The mass, height and diameter of a cylinder of AAC were measured using a balance[1], ruler and sliding callipers, respectively. From the length and diameter, the volume of the cylinder was calculated. Subsequently, the cylinder was grinded, transferred to a calibrated flask and filled with water to the calibrated volume and weighted. Also, the weight of the flask with the water only was determined. From this measurement, the total porosity was calculated at 0.80 ± 0.03. This value is the same, within the uncertainties, as the air-filled porosity. This indicates there is no evident that pores in the AAC sample are closed off from air. For the model calculations the porosity measured at 0.50 MPa will be used because the set-up was optimised and calibrated for this pressurisation and therefore more reliable.

3.3.3 Sorption isotherm

The relation between relative humidity (*RH*) and moisture content was determined using the following procedure: 12 AAC samples with a diameter of 100 mm and a height of 30 mm were dried in an oven at 105 ^{o}C and their mass determined in 48 hour intervals. The samples were considered dry when the change in mass between two intervals was within the precision of the balance. This dry mass is used as reference to determine the amount of moisture present in AAC. Subsequently, the samples were placed in containers containing a saturated salt solution. In equilibrium the relative humidity in the container is determined by the type of dissolved salt. Salt solutions with equilibrium relative humidity levels of 6, 33, 63 and 86% were used. After a period of four weeks, the samples were weighed again. By subtracting the dry mass from this value, the fraction of the water-filled pores was obtained. In a similar procedure the desorption curve of the sorption isotherm was determined. The samples were placed in a container with demineralised water and subsequently the air in the container was evacuated using a vacuum pump. After measuring the mass of the wetted samples, the samples were stored at the various saturated salt solutions for 4 weeks after which they were weighed.

Figure 3.7 shows the moisture content in AAC as a function of the relative humidity. A sharp increase in moisture content is found between 86% and 97% *RH*. The results are comparable with results presented in literature [2]. The increase in mass between 0% and 50% *RH* is slightly smaller than calculated from the difference in air-filled porosity of oven-dried samples and samples at 50% *RH*. Calculations by Van der Graaf [7] show that under dry conditions, adsorption of nitrogen to dry pore-surface can occur at pressures of 0.5 MPa can occur. This would result in an apparently increased porosity at high pressure.

1 Mettler balance type AT460

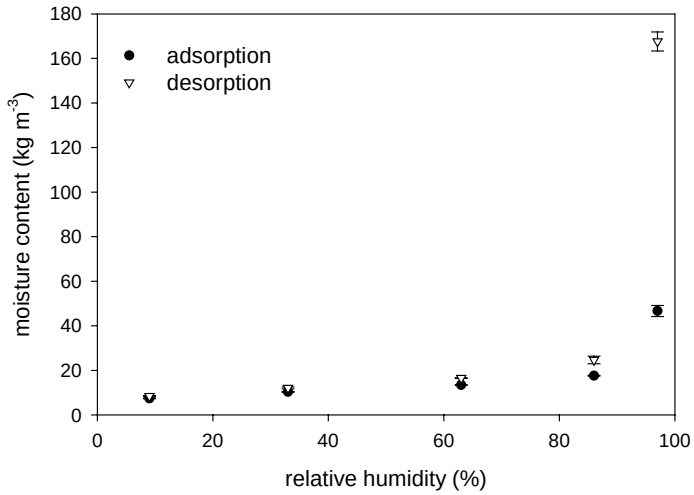

Figure 3.7 The moisture content as a function of the adsorption (lower line) and desorption (upper line) of moisture from AAC samples placed in air with a constant relative humidity.

3.3.4 Radium content

The radium content (^{226}Ra) of AAC was determined by means of semiconductor gamma-spectrometry in a Marinelli beaker geometry at the Nuclear Geophysics Division of the KVI[1]. The gamma-spectrometer was calibrated for this geometry using nuclide cocktails with certified activities. Corrections for self-absorption and background radiation have been applied.

The sample was made by filling a Marinelli beaker with powdered AAC. Subsequently, the sample was sealed radon-tight for a period of three weeks to reach secular equilibrium between radon and its daughters. After this period, the gamma-ray spectrum of the sample was measured on a 6 cm diameter and 8 cm thick HPGe-detector in a low-background set-up (lead shielding of 10 cm) at the KVI.. The activity concentrations for ^{232}Th, ^{226}Ra and ^{40}K were determined from the gamma-ray spectra for the energies between 120 keV and 2700 keV. The activity of ^{226}Ra was determined from the decay of ^{214}Pb (295 keV and 352 keV gamma-rays) and ^{214}Bi (609 keV, 1120 keV and 1764 keV gamma-rays). The ^{232}Th-activity was determined using gamma ray from the decay products ^{208}Tl, ^{212}Pb, ^{212}Bi and ^{228}Ac. For the ^{40}K activity, the 1461 keV gamma-ray was used. *Table 3.3* shows the measured activity concentrations and the range of activity concentrations for AAC used in The Netherlands [5]. The measured activities are within the range of activities for AAC used in The Netherlands. From the table we may conclude the AAC used in this thesis is similar to common AAC.

[1] Kernfysisch Versneller Instituut, Rijksuniversiteit Groningen, The Netherlands.

Table 3.3 Activity concentrations for the AAC used in this thesis and the range of activity concentration for AAC used in The Netherlands [5].

source	^{226}Ra (Bq kg^{-1})	^{232}Th (Bq kg^{-1})	^{40}K (Bq kg^{-1})
AAC sample (this study)	11.5 ± 0.4	7.4 ± 0.3	198 ± 12
AAC The Netherlands	9 - 13	7 - 8	110 – 230

3.3.5 Radon-release rate

The radon-release rate of AAC was determined at the KVI with the radon-release rate set-up that is shown in *Figure 3.8*, and conform the procedures of the Dutch pre-normative protocol NVN 5699 [3]. Note that the radon-release rate is not the same as the emanation coefficient because it does not correct for radon that is available for transport but decays before escaping the sample. The set-up consists of an 80-litre stainless-steel box that contains the AAC sample. A set nitrogen flow of 0.400 L min^{-1} with a relative humidity (*RH*) of 50% flows through this box. Radon in the flow leaving the set-up is absorbed onto active charcoal placed at liquid nitrogen temperature. After absorbing radon for 24 hours, the charcoal is placed in a standard calibrated geometry of a low-background, HPGe spectrometer for gamma-ray measurement. During a time-interval, t_m, the count rate from the sample is measured.

The relation between the count rate from radon released by the building material, N_{bm}, and the time after adsorption is given by:

$$N(t) = N_{bm} e^{-\lambda_{Rn} t} , \tag{3.4}$$

where:
λ_{Rn} decay constant of ^{222}Rn (s^{-1});
N_{bm} count rate due to radon release of the building material (s^{-1}).

The total number of counts collected on the HPGe spectrometer in the measurement interval from t_w to (t_w + t_m) is given by:

$$N_{tot} t_m = N_{bg} t_m + \int_{t_w}^{t_w + t_m} N(t) dt , \tag{3.5}$$

where:
N_{tot} total count rate in the energy range between 52 keV and 680 keV (s^{-1});
N_{bg} background count rate (s^{-1});
t_m measuring time for gamma-ray spectrum (s);
t_w waiting time before measurement (s).

The count rate due to radon release of the building material can thus be calculated from the total count rate using:

$$N_{bm} = \left(N_{tot} - N_{bg} \right) \frac{\lambda_{Rn} t_m e^{\lambda_{Rn} t_w}}{1 - e^{-\lambda_{Rn} t_m}} . \tag{3.6}$$

The change in N_{bm} during the adsorption phase as a function of time is the sum of the adsorption rate of radon and the decay of the adsorbed radon:

$$\frac{dN_{bm}}{dt} = \alpha C V \lambda_v - N_{bm}\lambda_{Rn}, \tag{3.7}$$

with:

$$C = \frac{R_{bm} + R_{setup}}{(\lambda_v + \lambda_{Rn})V}, \tag{3.8}$$

where:

λ_v ventilation rate of the set-up (defined as the ratio between the air flow and the volume of the box) (s^{-1});

α efficiency of the method, the product of the fraction of radon adsorbed on the charcoal and the efficiency of the gamma-ray detection system;

R_{setup} contribution of components of the set-up (such as silica gel in the pre-dryer).

N_{bm} as function of time is then given by:

$$N_{bm} = \frac{\alpha\lambda_v (R_{bm} + R_{setup})}{\lambda_{Rn}(\lambda_v + \lambda_{Rn})}\left(1 - e^{-\lambda_{Rn}t}\right). \tag{3.9}$$

For an adsorption time t_a, the radon-release rate of the building material, R_{bm} (Bq s^{-1}), is given by:

$$R_{bm} = \frac{N_{bm}\lambda_{Rn}(\lambda_v + \lambda_{Rn})}{\alpha\lambda_v\left(1 - e^{-\lambda_{Rn}t_a}\right)} - R_{setup}, \tag{3.10}$$

where:

t_a adsorption time (s).

The results of this measurement, which was conducted three times, are shown in *Table 3.4*. If we assume all emanated radon is exhaled during the radon-release measurement, i.e. radon decay in the sample due to adsorption and low diffusion rates are negligible, the emanation coefficient, η, can be calculated from the measured mass radon exhalation rate, E_m, and the radium activity concentration, A_{Ra}:

$$\eta = \frac{E_m}{\lambda_{Rn} A_{Ra}}, \tag{3.11}$$

where:

η emanation coefficient;

E_m mass radon exhalation rate (Bq $kg^{-1}s^{-1}$);

A_{Ra} radium activity concentration (Bq kg^{-1}).

This yields an emanation coefficient of 0.083 ± 0.005 for the examined AAC samples. This value is comparable with emanation coefficients measured for other porous (building) materials [9].

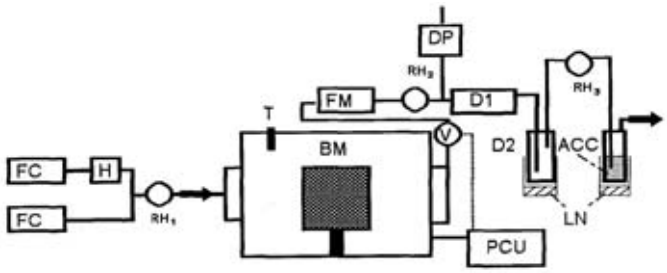

Figure 3.8 The KVI-NGD set-up for measuring the radon-release rate of building materials. The released radon is adsorbed on charcoal and subsequently the adsorbed amount is measured using a gamma-ray spectrometer.

Table 3.4 Radon-release rates, R, and mass-exhalation rates, E_m, of three AAC samples measured with the radon-release rate set-up at KVI-NGD.

Measurement	R_{bm} (10^{-5} Bq s^{-1})	E_m (10^{-5} Bq $kg^{-1}s^{-1}$)
#1	1.88 ± 0.09	2.01 ± 0.10
#2	1.83 ± 0.08	1.95 ± 0.09
#3	1.97 ± 0.11	2.11 ± 0.12
weighted mean	1.88 ± 0.05	2.01 ± 0.06

3.4 Leakage tests

To assure well functioning of the set-up, including the control of the various parameters, several tests were conducted. The most relevant tests are described in this section.

3.4.1 Air-leakage testing

The ventilation rate and the advective flow through the AAC cylinder have great influence on the radon concentrations in both compartments. Therefore, it is necessary to assure a leak-tight set-up. During the design of the set-up, it was screened for spots that are prone to leakage. These spots include the metal-rubber-metal connections that seal the outer lid, the inner lid and bottom plate of the set-up, the several air in- and outlets, temperature-probe connections and the various devices measuring and controlling the conditions in the set-up.

To test the sealing of metal-rubber-metal connections, the U-profiles between the two O-shaped rings were evacuated and the pressure in the profiles monitored. Since the pressure remained (near) zero for more than 72 hours, it was concluded that no relevant leakage of air via the rubber O-shaped rings occurred.

The various temperature-probe connections, air feed throughs and the attached devices were tested for leakage by increasing the pressure in the entire set-up to an overpressure of 60 hPa with respect to the barometric pressure and subsequently monitoring the pressure and temperature in the set-up. Using the ideal-gas law, the

amount of gas in the set-up was calculated from the measured pressure and temperature as function of time. The change in amount of gas showed good correlation to the pressure-difference between the set-up and the outside. This test showed a leakage of air of 0.005 ± 0.002 L $h^{-1}hPa^{-1}$. Under regular working conditions, where a pressure-difference of approximately 60 hPa is maintained, the loss of radon due to airflow is 5% in comparison with the loss of radon due to decay. Similar pressurisation measurements were conducted on the various devices and connections in the set-up separately to identify the location of the leakage. The quasi-continuous radon meters appeared to be the main source of the air leakage. Several improvements were made to (the design of) these radon meters and later tests showed reduced leakage. Although fully leak-tight measurements could not be accomplished with the quasi-continuous radon meters, the leakage of air from the radon meters was negligible compared to the changes in radon concentration due to the processes studied in the measurements.

3.4.2 Radon-leakage testing

Next to pressure-driven air-leakage tests, radon-leakage was measured because airtight does not necessarily imply radon-tight [7]. The radon leakage was derived from measuring the ingrowth of radon produced by the AAC cylinder in the inner and outer compartment and by measuring the decay of a high radon concentration. Before the measurement, the set-up and the AAC cylinder were flushed with radon-free air for at least 24 hours at a rate of at least 10 L min^{-1} corresponding to a ventilation rate of more than 0.7 h^{-1}. The results of the measurement are shown in *Figure 3.9*. The curves were fitted with a least-squares method using:

$$C(t) = C_0 e^{-(\lambda_{Rn}+\lambda_L)t} + C_{eq}\left(1 - e^{-(\lambda_{Rn}+\lambda_L)t}\right) , \qquad (3.12)$$

where:

$C(t)$	radon concentration at time t (Bq m^{-3}) ;
C_0	radon concentration at time t = 0 (Bq m^{-3}) ;
C_{eq}	equilibrium radon concentration (at t = ∞) (Bq m^{-3});
t	time (s);
λ_{Rn}	decay constant for radon ($2.1 \cdot 10^{-6}$ s^{-1});
λ_L	leakage constant defined as the ratio between the air flow out of the set-up and the volume of the set-up (s^{-1}).

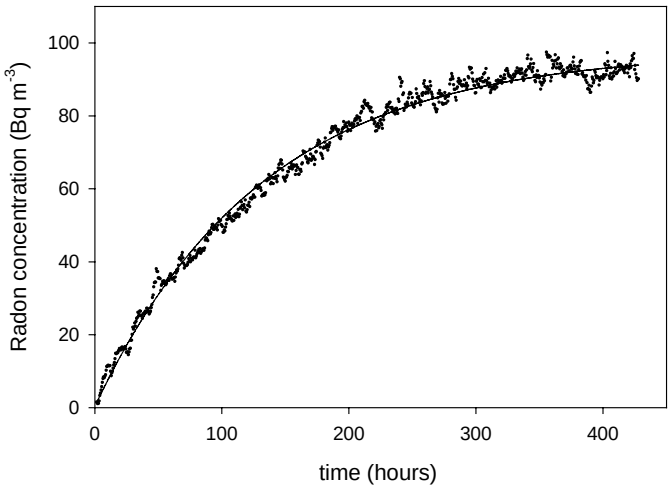

Figure 3.9 Measurement (dots) and least-square fit (line) of the ingrowth of radon in the inner compartment produced by the AAC cylinder in the set-up.

Table 3.5 Fit parameters of the ingrowth measurement

	C_0 (Bq m^{-3})	C_{eq} (Bq m^{-3})	λ_L (10^{-6}s^{-1})
radon meter 1	0.5 ± 1.6	97 ± 2	-0.04 ± 0.08
radon meter 2	-0.3 ± 1.8	98 ± 2	-0.05 ± 0.07
weighted mean		97.6 ± 1.7	

The results of the least-squares fit are presented in *Table 3.5*. Because a negative value of λ_L is physically impossible, and the fitted values do not differ significantly from 0, the quantity λ_L was set to zero. The fit yielded a χ^2_{red} of 1.19 and 1.16 for radon meter 1 and radon meter 2, respectively. This indicates that the model fits the data correctly. Both the fitted initial concentration as the leakage parameter do not differ significantly from zero. Therefore, it was concluded that leakage of radon from the set-up is negligible under these circumstances. Using the equilibrium radon concentration and the volume of the set-up, the emanation coefficient was calculated:

$$\eta = \frac{\left(V_{setup} - \left(1-\varepsilon_a\right)V_{AAC}\right)C_{eq}}{V_{AAC}\rho C_{Ra}} \cdot \frac{\left(\lambda_{Rn} + \lambda_L\right)}{\lambda_{Rn}}, \qquad (3.13)$$

where:

ρ density of AAC (560 ± 6 kg m^{-3}).

This yielded a value of 0.082 ± 0.005 for the emanation coefficient. This value is accordance with the value of 0.083 ± 0.005 measured with the radon-release rate set-up and comparable to values reported in literature [9].

In addition, radon-decay measurements were conducted. A large amount of radon was released in the set-up and its decay monitored with the quasi-continuous radon

meters for a period of 5 days. The results of this measurement are shown in *Figure 3.10*. The radon concentrations were calculated using equation 3.12 with λ_L and C_0 as free parameters. For C_{eq} the equilibrium radon concentration found in the radon-ingrowth measurement (thus due to the production of radon by the AAC cylinder) has been used.

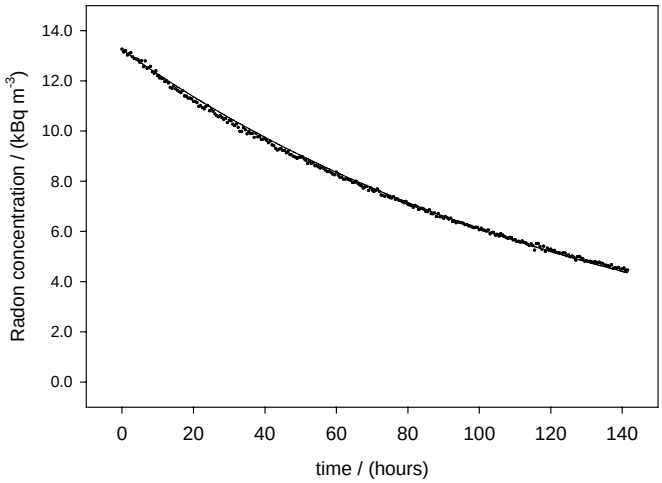

Figure 3.10 Measurement (dots) and least-square fit (line) of radon decay in the set-up without ventilation.

Also for this measurement, the fit-parameter λ_L does not significantly differ from zero. Therefore it was concluded that leakage of radon out of the set-up is not relevant to our measurements. Together with the measurements of the airflow from the U-profiles that show no leakage of air through the various rubber O-shaped rings, it can be concluded that leakage of radon and air out of / into the set-up is negligible and that transport between inner and outer compartment is essentially due to transport through either the AAC or the sealed connection between the AAC and the metal ring at top and bottom of the cylinder.

3.4.3 Adhesive compound

Several parameters of the adhesive have been tested to assure the adhesive and adhesive-connections have little to no influence on the radon transport properties of AAC. These properties include the radium content, radon exhalation rate, radon adsorption and leakage of radon and air through the adhesive and adhesive-connections.

To determine the radon adsorption and the radium content of the adhesive, a pillow box with a diameter of 50 mm was filled with a 20 mm thick layer of adhesive. After drying, the adhesive was placed for a period of three weeks in a closed container together with a radon source to create a high radon concentration (>50 kBq m^{-3}). At the end of this period, equilibrium between the production and decay of (adsorbed)

radon was reached. Subsequently, the gamma-ray spectrum of the sample was measured on a 6 cm diameter and 8 cm thick HPGe-detector as described in section 3.3.4. From the spectrum, the radium activity concentration and the radon-decay products were determined. These results are shown in *Table* 3.*6*. The radium content of the adhesives (in Bq kg^{-1}) are similar to the radium content of AAC. However, the contribution of the adhesive to the total radon production is considered negligible because the mass of the adhesive is more than a factor 100 smaller than the mass of the AAC cylinder. The activity concentrations of the radon decay-products do not exceed the activity concentration of radium ^{226}Ra in the adhesives. Because adsorption of radon would have lead to increased activities in radon decay-products, it was concluded that adsorption is negligible for all adhesives. Of the examined adhesives, Sikaflex 260 has been used for sealing of the AAC cylinder. This choice was based on the positive experiences of the general workshop of the Eindhoven University of Technology concerning its flexibility and adhesive power.

Table 3.*6 Radium content and radon decay products of various adhesives measured with a low background HPGe-detector. The values shown in Italic are below the detection limit of the HPGe-detector.*

	Mass	Radionuclide-concentration (Bq kg^{-1})			
	(g)	^{226}Ra	^{214}Pb	^{214}Bi	^{210}Pb
Araldite 2020	12.5	*10.6*	*0.80*	*3.25*	*3.8*
Bison Acrylate	20.5	*17.6*	9.60 ± 0.14	5.9 ± 1.4	*4.3*
Bison Bytylene	34.0	*8.9*	5.6 ± 0.4	4.0 ± 0.5	*1.7*
Bison Silicones	16.1	*13.2*	*4.64*	*4.64*	*6.1*
Sikaflex 260	24.2	*24.2*	*3.23*	5.2 ± 1.4	*5.4*

The next step is to determine the possible leakage through and along the adhesive. Therefore, measurements were conducted on three configurations with different sealings (see *Figure 3.11*). In the first configuration, the inner compartment is separated from the outer compartment by the adhesive and metal, in the second configuration the compartment are separated by both the metal, the adhesive and an AAC sample. The third configuration is equal to the second, except that an extra layer of adhesive is added to increase the number of adhesive - AAC connections. Because of relatively rapid transport of radon through AAC, the outer compartment in the second and third configuration is ventilated at a ventilation rate of more than 1 h^{-1}. In all configurations a high radon concentration is created in the inner compartment using a radon source (S ≈ 100 Bq) and the radon concentration monitored in the inner and outer compartment.

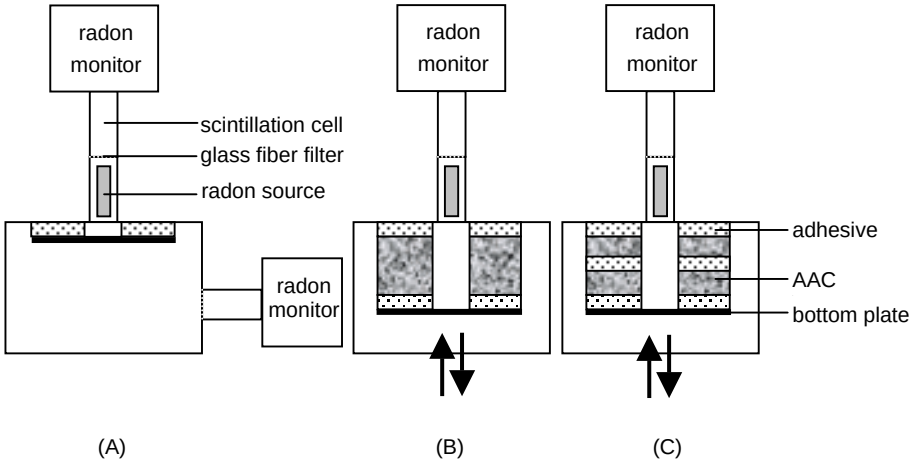

Figure 3.11 Three configurations required for determining the transport of radon through the adhesive and along the adhesive to AAC and the adhesive to metal connections; (A): adhesive attached to metal only, (B): AAC attached to metal with adhesive, (C): AAC attached to metal, with an additional layer of adhesive. The arrows at (B) and (C) indicate ventilation of the outer compartment.

.

The first configuration is used to detect transport of radon through the adhesive and along the adhesive - metal connection. Such transport would result in the ingrowth of radon in the outer compartment. The second and third configuration were used to detect leakage of radon along the adhesive - AAC connection. Such leakage would result in a lower radon equilibrium concentration in the inner compartment of the third configuration.

The radon concentration measured in the first configuration did not exceed the detection limit. It was therefore concluded that transport of radon through the adhesive and/or the adhesive-metal connection is negligible. The measurements on the second and third configuration showed no significant difference in the radon equilibrium concentrations. Therefore, it was concluded that leakage of radon through the adhesive and the adhesive-connections to both metal and AAC is negligible.

References

[1] Aldenkamp F.J., Stoop P., Sources and Transport of Indoor Radon - Measurements and mechanisms, Ph.D. thesis, University of Groningen, The Netherlands, 1994.

[2] Anonymous, Condensation and Energy: Catalogue of Material Properties, IEA Annex XIV volume 3, chapter 2, International Energy Agency (IEA), 1991.

[3] Anonymous, NVN 5699: Radioactivity measurements, Determination method of the rate of radon exhalation of stony building products, NEN, The Netherlands, 1999.

[4] Berentsen J., Radon Vessel Control System, TU/e report nr. 91, Eindhoven University of Technology, The Netherlands, 2002 (in Dutch).

[5] Bosmans G., Optionele maatregelen ter reductie van de stralings-eigenschappen van praktijkbeton, Intron report 96173, Intron, The Netherlands, 1997 (in Dutch).

[6] Cozmuta I., Radon generation and transport - a journey through matter, Ph.D. thesis, University of Groningen, The Netherlands, 2001.

[7] van der Graaf E.R., van der Spoel W.H., de Meijer R.J., Radon transport in building materials, KVI-report R-88, KVI, The Netherlands, 1995 (revised 1996).

[8] van der Graaf E.R., Cozmuta I., van der Pal M., Calibration of the NGD-KVI porosimeter and results of initial experiments on aerated concrete samples from TUE, KVI-report S-75, KVI, The Netherlands, 1996 (in Dutch).

[9] Put L.W., van der Graaf E.R., Invoerparameters voor radontransport-modellen: een literatuurstudie, KVI-report R-92, KVI, The Netherlands, 1996 (in Dutch).

[10] van der Spoel W.H., van der Graaf E.R., Enkele kanttekeningen bij de stralingsprestatienormering, *Bouwfysica*, 15(4):8-12, 2002.

List of symbols

symbol	unit	description
α		efficiency of the radon-release measurement
ε_a	m^3m^{-3}	air-filled porosity
η		emanation coefficient
λ_L	s^{-1}	leakage constant
λ_{Rn}	s^{-1}	radon decay constant
λ_V	s^{-1}	ventilation rate of the set-up
ρ	kg m^{-3}	bulk density of AAC
A_{Ra}	Bq	radium activity
C_0	Bq m^{-3}	radon concentration at time t = 0
C(t)	Bq m^{-3}	radon concentration at time t
C_{eq}	Bq m^{-3}	equilibrium radon concentration
E_m	Bq $kg^{-1}s^{-1}$	radon-release rate per unit of mass
N_{BG}	s^{-1}	background count rate
N_{bm}	s^{-1}	count rate due to radon release of the building material
N_{tot}		total count rate in the energy range between 52 keV and 680 keV
P_{eq}	Pa	pressure in both enclosures at the end of the experiment
P_1	Pa	pressure in enclosure 1 at the start of the experiment
P_2	Pa	pressure in enclosure 2 at the start of the experiment
R	Bq s^{-1}	radon-release rate
R_{setup}	Bq s^{-1}	contribution of components of the set-up
V_1	m^3	volume available for air in enclosure 1
V_1'	m^3	volume available for air in enclosure 1 with AAC sample present
V_2	m^3	volume available for air in enclosure 2
V_{setup}	m^3	volume available for air in set-up
V_{AAC}	m^3	bulk volume of the AAC sample
t	s	time
t_m	s	measuring time for gamma-ray spectrum
t_w	s	waiting time before measurement

4

Emanation and adsorption of radon

4.1 Introduction

In the previous chapter, a set-up and the general properties of autoclaved aerated concrete (AAC) have been presented. However, to describe the combined advective and diffusive transport of radon in a porous material using the model described in chapter 2, radon adsorption and emanation coefficient for AAC are required.

An emanation coefficient describes the potential release of radon from a material. To calculate an emanation coefficient, both the total amount of radon formed in the material and the amount available for transport out of the material need to be determined. The formation of radon depends on the radium activity concentration only, and can be determined using gamma spectroscopy. This common method has been presented in the previous chapter. To determine the amount of radon available for transport, various methods are available. For an accurate measurement, it is necessary to correct for the adsorption of radon in a material. A method combining the measurement of both emanation coefficient and adsorption coefficient will be presented in this chapter and the results will be discussed.

The next section gives an overview of the literature on the emanation-coefficient measurement in relation to material properties and measuring conditions. It also discusses the necessity to determine the adsorption coefficient. In section 4.3, the method for the combined measurement of emanation and adsorption coefficient is described. Measurement results are presented and discussed in section 4.4. The last section draws the conclusions from the measurements.

4.2 Emanation coefficient

4.2.1 Typical values

Table 4.1 gives an overview of typical values of emanation coefficients for building materials. From this table it can be seen that the emanation coefficient is not only dependent on the type of building material, but also that the emanation coefficient can vary up to a factor 50 within a type of building material (e.g. for brick). This means that the emanation coefficient of AAC cannot be accurately calculated from the values reported in literature. Therefore, it is necessary to measure the emanation coefficient of the AAC samples used in this study.

Table 4.1 Overview of typical emanation coefficients for Dutch building materials

Building material	emanation coefficient	reference
Autoclaved Aerated Concrete	0.09 – 0.42	[18,6]
Concrete	0.01 – 0.26	[18,1,13]
Brick	0.001 – 0.05	[6,1,13]
Gypsum (natural)	0.09 – 0.19	[6]
Phosphogypsum	0.03 – 0.13	[1]

4.2.2 Emanation and moisture content

Next to the medium, also the ambient conditions are known to influence the emanation coefficient. Almost without exception, starting from a dry material, an increase in emanation coefficient is found for increasing moisture contents [11,26,27,4,25]. Often a maximum value is found. Tanner [29] suggested the following explanation for this phenomena: a reasonable amount of the radon atoms that escape from a grain will bury themselves in another grain due to recoil. Because the recoil distance is considerably smaller for water (0.1μm) compared to air (63 μm), the probability of radon atoms burying themselves in other grains will be reduced when the grains are covered with a layer of water. Because the radon is considered emanated when it is present in either the air filled or water filled pore space, an increase in moisture content will result in an increased radon content in the water-filled pore space, leading to an increased emanation coefficient. A maximum emanation coefficient is reached when all radon atoms escaping the grain are prevented (by the presence of moisture) from entering other grains. This maximum has been reported by several authors. Modelling of the relation between emanation coefficient and moisture content showed a good correlation with measurements [17].

4.2.3 Emanation and temperature

The emanation coefficient is also found to be temperature dependent [10,11,26], although this influence was often smaller than the influence of changes in moisture content. Stranden [26] found an increase in emanation coefficient with increasing temperatures. Stranden suggested this effect could be due to adsorption of radon. Van der Waals adsorption (or physical adsorption) of gases is known to be temperature dependent [3], and an increase in temperature results in a decrease in adsorption coefficient, leading to an increased radon concentration in the air phase. Secondly, increased flows of air or water vapour out of the samples would result in increased radon emanation. However, in both mechanisms the radon is already available for transport and should, according to the definition used in this study, be considered emanated.

4.2.4 Adsorption

Adsorption of radon on the solid phase of porous materials may play an important role in the release of radon into the indoor and outdoor environment [10,23,24]. Besides that adsorption lowers the radon concentration in the pore space of the material, it is also known to retard diffusion and advection of radon [12,16,5,19,25]. Most experimental studies on the transport of radon in porous media concentrated on determining the diffusion coefficient (e.g. [28,20,21,9]), permeability and/or radon-production rate (e.g. [27,8,14,15]), sometimes as a function of temperature and moisture content. Since adsorption may affect these transport quantities, the effect of adsorption should implicitly be accounted for in these experiments. However, to avoid ambiguities of what is actually measured, the adsorption properties should preferably be measured separately. An additional advantage is that the simulation of radon transport can then be based on models that include adsorption explicitly.

Schery and Whittlestone [23] and Schery and Lopez [24] carried out extensive measurements of radon adsorption on a range of solid materials. Their results indicate that, for widely used building materials, such as fired brick and poured concrete, adsorption lowers diffusive transport by about a factor 2. Schery and Whittlestone used an experimental technique in which the gamma-ray activity of millilitre-size samples of porous media containing a high known radon concentration in the pore space is counted using a NaI well detector. The method described in this thesis has the advantage over the technique used by Schery and Whittlestone that standard radon-gas monitoring equipment can be used. In addition, larger samples are used. The use of larger samples lowers the variability between samples due to inhomogeneities and facilitates the determination of the open porosity for materials with negligible adsorption.

4.3 Experimental method

4.3.1 Mathematical formalism

To determine the emanation and adsorption coefficient, a radon-producing porous sample inside a leak-tight chamber filled with air at atmospheric pressure is considered. The radon activity in the chamber is divided in three phases: radon adsorbed to the solid surfaces of the porous sample, the radon in the water phase and radon in the air phase. The air-phase radon activity is denoted by A_{air} , the water-phase radon activity by A_{water} and the adsorbed-phase radon activity by A_{ads}. Radon that is contained in the solid matrix can be ignored because it does not contribute to the air-phase radon concentration, the measurable quantity in the experiments. The rate of change of total radon activity in the chamber $A_{air} + A_{water} + A_{ads}$ is determined by the radon-production rate S and rate of decay $\lambda(A_{air} + A_{water} + A_{ads})$:

$$\frac{d(A_{air} + A_{water} + A_{ads})}{dt} = S - \lambda(A_{air} + A_{water} + A_{ads}) , \qquad (4.1)$$

where:

S radon production (Bq s^{-1});

λ decay constant for radon ($2.1 \cdot 10^{-6} s^{-1}$).

With $A_{air} + A_{water} + A_{ads} = 0$ as initial condition, the solution of differential equation 4.1 is given by

$$(A_{air} + A_{water} + A_{ads})(t) = \frac{S}{\lambda}\left(1 - e^{-\lambda t}\right). \qquad (4.2)$$

The radon activity in the air phase can be written as $A_{air} = C_{air}\, V_{air}$, where C_{air} is the air-phase radon activity concentration (Bq m^{-3}) and V_{air} is the air volume in the chamber. We assume that, at any time, the adsorbed-phase activity is reversible and in equilibrium with the air-phase and the water-phase activity. Furthermore, we assume that the adsorbed activity and the water-phase activity are linearly dependent on the concentration in the air. This allows to write the adsorbed activity as:

$$A_{ads} = m_m k_{ads} C_{air}\,, \tag{4.3}$$

where m_m is the mass of the material sample and k_{ads} is the radon adsorption coefficient. The water-phase activity can be written as:

$$A_{water} = L V_{water} C_{air} \tag{4.4}$$

where L is the Ostwald coefficient and V_{water} the water volume. With these definitions and assumptions, equation 4.2 can be written as

$$C_{air}(t) = \frac{S}{\lambda(V_{air} + L V_{water} + m_m k_{ads})}\left(1 - e^{-\lambda t}\right). \tag{4.5}$$

In three consecutive experiments, the chamber contains 1) a sample of porous material and a radon source, 2) a sample of porous material and no radon source, 3) a radon source and no sample. The radon-production rate of the material sample and source is denoted as S_m and S_s, respectively. The air-phase radon concentration in these experiments is then given by equation 4.5 with $S_m + S_s$, S_m, and S_s substituted for S, respectively. As the volume of the material sample and the source cannot be neglected with respect to the air volume of the empty chamber V_{ch}, the term V_{air} will differ in each experiment. The volume occupied by the material and source is given by V_m (1-ε_a) and V_s, respectively, where V_m is the bulk volume of the sample and ε_a the air-filled porosity. The volume of the sample occupied by water, $V_{m,water}$ is equal to $\varepsilon_w V_m$ where ε_w equals the water-filled porosity. The radon concentration is reduced by absorption of radon in water-filled pores and adsorption to the solid phase. The air volume in the first experiment therefore equals $V_{m+s,air} = V_{ch} - V_m(1-\varepsilon_a) - V_s$, in the second experiment $V_{m,air} = V_{ch} - V_m(1-\varepsilon_a)$ and in the third experiment $V_{s,air} = V_{ch} - V_s$. The time dependence of the air-phase radon concentration in the first experiment is thus described by:

$$C_{air}(t) = C_{m+s}^{eq}\left(1 - e^{-\lambda t}\right), \tag{4.6}$$

where:

$$C_{m+s}^{eq} = \frac{S_m + S_s}{\lambda(V_{m+s,\,air} + L V_{m,\,water} + m_m k_{ads})} \tag{4.7}$$

and t the time since the closure of the chamber. The time dependence of the air-phase radon concentration of the second experiment is:

$$C_{air}(t) = C_{m}^{eq}\left(1 - e^{-\lambda t}\right), \tag{4.8}$$

where:

$$C_{m}^{eq} = \frac{S_m}{\lambda(V_{m,\,air} + L V_{m,\,water} + m_m k_{ads})}\,. \tag{4.9}$$

And in the third experiment:

$$C_{\text{air}}(t) = C_{\text{s}}^{\text{eq}}\left(1 - e^{-\lambda t}\right), \tag{4.10}$$

where:

$$C_{\text{s}}^{\text{eq}} = \frac{S_{\text{s}}}{\lambda(V_{\text{s, air}})}. \tag{4.11}$$

Combining equations 4.7, 4.9, and 4.11, k_{ads} can be written as

$$k_{\text{ads}} = \frac{C_{\text{m}}^{\text{eq}}\left(V_{\text{m, air}} + LV_{\text{m, water}}\right) + C_{\text{s}}^{\text{eq}}V_{\text{s, air}} - C_{\text{m+s}}^{\text{eq}}\left(V_{\text{m+s, air}} + LV_{\text{m, water}}\right)}{m_{\text{m}}(C_{\text{m+s}}^{\text{eq}} - C_{\text{m}}^{\text{eq}})}. \tag{4.12}$$

With k_{ads} known, the total amount of radon emanated to the air phase, the water phase and reversibly adsorbed to the pore surfaces can be calculated from the radon concentration in the air phase:

$$A_{\text{emanated}} = C_{\text{eq, m}}\left(V_{\text{m, air}} + LV_{\text{m, water}} + k_{\text{ads}}m_{\text{m}}\right). \tag{4.13}$$

Together with the total radon production of the sample, deducted from its mass and its radium content (see chapter 3 for measurement), the emanation coefficient may be calculated as:

$$\eta = \frac{A_{\text{emanated}}}{m_{\text{m}}C_{\text{Ra}}}. \tag{4.14}$$

4.3.2 Experimental set-up

Each experiment took place in a leak-tight cylindrical chamber (radius 10 cm, height 16 cm) with a stainless-steel wall and aluminium bottom and top flanges, schematically shown in *Figure 4.1*. The alpha activity is measured with a 5 cm diameter scintillation flask (length 15 cm) mounted on a 5 cm diameter circular opening in the cylindrical wall of the chamber. A glass fibre filter between the container and the flask prevents transport of radon progeny into the flask. The opposite side of the flask is closed with a transparent window and positioned in front of the photo-multiplier tube of a radiation monitor[1]. The alpha activity is measured by recording the number of pulses in consecutive intervals of two hours for at least three days. Given the radon concentration as a function of time and the relative efficiencies for radon and radon daughters, an expression for the time dependent count rate is obtained. Integration over two-hour periods gives an expression for the number of counts in each interval.

1 Pylon AB-5 Radiation Detector, Pylon, Electronics Inc., Ottawa, Canada.

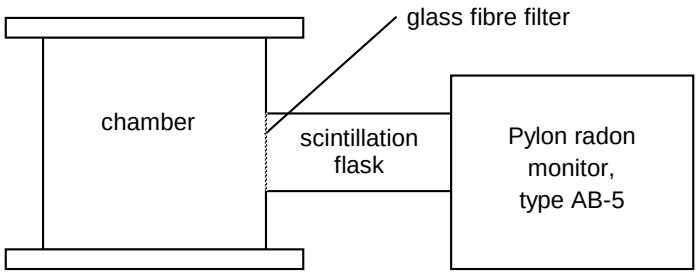

Figure 4.1: Schematic representation of experimental set-up.

The mathematical formalism to calculate the radon activity concentration from the counts is shown in *Intermezzo 4.1*. In addition, the efficiencies for the two alpha-emitting radon daughters, ^{218}Po and ^{214}Po, relative to the efficiency for ^{222}Rn were measured in a separate experiment [8]. The equilibrium concentrations C_{m+s}^{eq}, C_{m}^{eq} and C_{s}^{eq} may be obtained by fitting equation 4.16 to the data using equation 4.6, 4.8, and 4.10, respectively. A weighed fit was used with $\sigma_{N_j} = 1.5\sqrt{N_j}$ as a first-order approximation of the standard deviation of the counted pulses in each interval. The factor 1.5 arises from the correlated counting statistics of radon and its progeny.

Several sets of AAC cylinders with a radius of 60 mm and thickness of 45 mm were used as material sample. Each set consisted of three cylinders of which each sample is considerably smaller than its diffusion length for radon. In addition, the influence of variations between the samples is reduced. The samples are kept in a closed canister with a cup of saturated salt solution during at least three weeks before an experiment to equilibrate the moisture content. The created relative humidity in the canister depends on the salt dissolved[1]. A small fan is used to assure well mixing of air. The temperature of the cans is kept at 20.0 $\pm$ 0.5 ^{o}C by storing the cans in a temperature-controlled room. The bulk density and porosity of the AAC samples are taken from measurement results described in chapter 3.

As a radon source, either about 30 g of uranium tailings with a ^{226}Ra-activity of approximately 30 Bq or a Pylon model 2000A source with an ^{226}Ra-activity of 122 Bq was used. Since the source strength of the tailings is strongly dependent on the water content, these sources were conditioned simultaneously with the samples.

Before the start of an experiment, the chamber was flushed with radon-free air for at least 3 h. The relative humidity (*RH*) of the airflow was set to a value corresponding with the relative humidity in the storage can by directing part of the flow through a humidifier. The chamber also contained a cup with a volume of 50 cm^3 of the same saturated salt solution to maintain a constant relative humidity. Loss or gain of moisture in the sample was checked by weighing the samples before and after an experiment. Most radon-ingrowth experiments were stopped after about five days.

[1] For 0% relative humidity, 50g of P_2O_5 is used instead of a saturated salt solution.

The radon-adsorption coefficient of aerated concrete was measured for nine relative-humidity levels evenly distributed between *RH* = 0 and 0.97.

Intermezzo 4.1: From count-rates to radon concentrations

The count-rate measured with a scintillation flask depends on the alpha activity of ^{222}Rn and its progeny ^{218}Po and ^{214}Po. The concentrations of radon progeny ^{218}Po, ^{214}Pb and ^{214}Po, respectively denoted as $C_2(t)$, $C_3(t)$ and $C_4(t)$ (with corresponding decay constants λ_2 = 3.78·10^{-3} s^{-1}, λ_3 = 4.31·10^{-4} s^{-1} and λ_4 = 5.81·10^{-4} s^{-1}) are given by:

$$C_i(t) = e^{-\lambda_i t}\int_0^t e^{\lambda_i t}\lambda_i C_{i-1}(t)dt + C_i(t_0)e^{-\lambda_i t} \quad i = 2,3,4\,, \qquad (4.15)$$

where $C_i(t_0)$ (i = 2,3,4) is the ^{218}Po, ^{214}Pb and ^{214}Po concentration at t = 0, respectively. In the experiments, $C_1(t) = C_{air}(t)$, and $C_i(t_0) = 0$ (i = 1,2,3,4). The net number of counts N_j in time in j (from $t_{j-1} = j\text{-}1\Delta t$ to $t_j = j\Delta t$, j = 1,2,... where Δt is the time interval at which the number of pulses are registered) is obtained by integrating the alpha activity in the measuring volume V_f of the scintillation flask from time t_{j-1} to t_j:

$$N_j = V_f \int_{t_{j-1}}^{t_j} (\xi_1 C_1(t) + \xi_2 C_2(t) + \xi_4 C_4(t))dt\,, \qquad (4.16)$$

where ξ_1, ξ_2, and ξ_4 are the efficiencies for detecting an alpha particle emitted in the decay of ^{222}Rn, ^{218}Po and ^{214}Po, respectively. The detection efficiencies ξ_1, ξ_2, and ξ_4 were determined by introducing a high radon concentration in a scintillation flask (without radon initially) and registering the number of pulses in 10 min intervals during 3 h. A least squares fit to the data with ξ_2/ξ_1 and ξ_4/ξ_1 and the initial radon concentration as free parameters yielded ξ_2/ξ_1 = 1.15 ± 0.03 and ξ_4/ξ_1 = 1.333 ± 0.018. For the detection efficiency for radon, a value of ξ_1 = 0.622 ± 0.005 was found. This is however not a relevant parameter in the calculation of k_{ads} because it cancels in equation 4.12.

4.4 Results and discussion

4.4.1 Adsorption coefficient

An example of the radon ingrowth of three consecutive experiments at a *RH* = 0.29 is shown in *Figure 4.2*. The radon concentration $C_{m+s}(t)$ becomes higher than $C_s(t)$ because of extra radon produced by the material and the smaller air volume in the chamber. In this example, the radon concentration in the measurement with sample and source present should be (9.35 ± 0.17)% higher than with only the source present. This increase is caused by the contribution of the radon produced by the AAC sample of (2.88 ± 0.05)%, and the reduction in open-air volume of (6.47 ± 0.16)%. In *Figure 4.2,* it can be observed that $C_{m+s}(t)$ is (8.91 ± 0.13)% higher than $C_s(t)$. This indicates that (0.4 ± 0.2)% of the radon in the chamber is adsorbed.

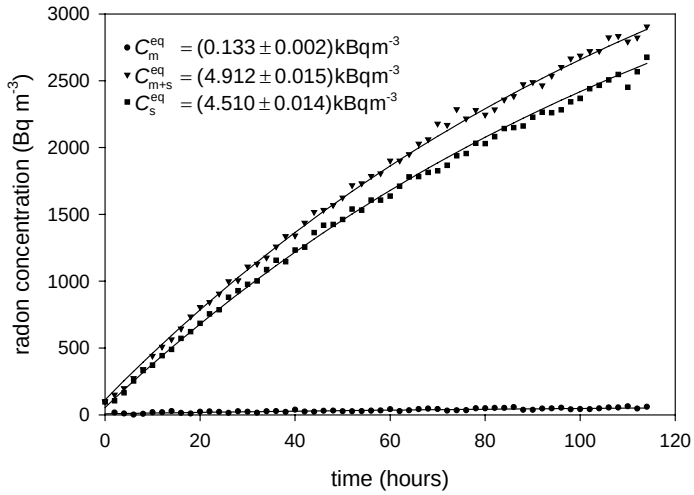

Figure 4.2: Radon ingrowth of the sample material (C_m), the source and sample material (C_{m+s}), and source (C_s) at RH = 0.29. Solid lines represent best-fitting curves

Table 4.2 shows the results of repeated measurements and the *a priori* calculated standard deviation (see *Intermezzo 4.2*). The variation of the measurements does not exceed the *a priori* calculated standard deviation. This indicates that the *a priori* calculation of the standard deviation gives a good estimate for the uncertainty in the adsorption coefficient.

Table 4.2 Results of repeated measurement of adsorption coefficient

RH	k_{ads} (10^{-4} m^{3}kg^{-1})	*a priori* calculated sd (10^{-4} m^{3}kg^{-1})
0	11.1	1.1
0	10.8	0.4
0	10.3	0.9
0.06	4.6	0.6
0.06	4.9	0.6

The measured adsorption coefficient of AAC as a function of the relative humidity and moisture content are shown in *Figure 4.3* and *Figure 4.4*, respectively. It is seen that adsorption decreases with increasing moisture contents between 0 and 0.01. This equals a relative humidity level of 0 to 0.33. From *Figure 4.4*, a linear relation between the moisture content and the adsorption coefficient can be observed for this interval. Hardly any adsorption is observed for higher relative humidity levels or moisture content. The decreasing trend at low moisture contents can be caused by water that increasingly blocks or occupies the radon adsorption sites. A adsorption sites for radon must be occupied by water for moisture contents > 0.01 or *RH* > 0.33. A similar trend was found by Schery and Whittlestone [23] for soils and by Schery and Lopez [24] for building materials. In contradiction to the results presented here,

they generally observed a decreasing adsorption coefficient in the *full* moisture content range of the materials. As the absolute value of the observed adsorption coefficient is concerned, the results presented here agree well with those found by Schery and Lopez [24] for poured concrete.

Intermezzo 4.2: Calculating the uncertainty in the adsorption coefficient

Equation 4.12 can be rearranged to:

$$k_{ads} = \frac{C_m^{eq}\left(V_{ch} - (1-\varepsilon_a - L\varepsilon_w)V_m\right) + C_s^{eq}\left(V_{ch} - V_s\right) - C_{m+s}^{eq}\left(V_{ch} - V_s - (1-\varepsilon_a - L\varepsilon_w)V_m\right)}{m_s(C_{m+s}^{eq} - C_s^{eq})}.$$

The variance in k_{ads}, $\sigma_{k_{ads}}^2$, is calculated using:

$$\begin{aligned}\sigma_{k_{ads}}^2 = {} & \sigma_{C_m^{eq}}^2\left(\frac{\partial k_{ads}}{\partial C_m^{eq}}\right)^2 + \sigma_{C_s^{eq}}^2\left(\frac{\partial k_{ads}}{\partial C_s^{eq}}\right)^2 + \sigma_{C_{m+s}^{eq}}^2\left(\frac{\partial k_{ads}}{\partial C_{m+s}^{eq}}\right)^2 + \\ & \sigma_{V_m}^2\left(\frac{\partial k_{ads}}{\partial V_m}\right)^2 + \sigma_{V_s}^2\left(\frac{\partial k_{ads}}{\partial V_s}\right)^2 + \sigma_{\varepsilon_w}^2\left(\frac{\partial k_{ads}}{\partial \varepsilon_w}\right)^2 + \\ & \sigma_{V_{ch}}^2\left(\frac{\partial k_{ads}}{\partial V_{ch}}\right)^2 + \sigma_{\varepsilon_a}^2\left(\frac{\partial k_{ads}}{\partial \varepsilon_a}\right)^2 + \sigma_{m_m}^2\left(\frac{\partial k_{ads}}{\partial m_m}\right)^2\end{aligned}$$

where: σ_j^2 the variance in component *j*. *Table 4.3* shows the contribution of the various components adding to uncertainties in the adsorption coefficient calculated of the experiment at *RH* = 0.29. It is seen that the uncertainty of the porosity and of the equilibrium radon concentrations C_{m+s}^{eq} and C_s^{eq} are the main contributors to the combined standard uncertainty in k_{ads}, $\sigma_{k_{ads}}^2$.

Table 4.3: Example of contributions of various components to the uncertainty in calculated adsorption coefficient

component *j*	value	σ_j	$\sigma_j^2\left(\frac{\partial k_{ads}}{\partial j}\right)^2$ (10^{-10} m^{6}kg^{-2})	relative contribution (%)
C^{eq}_{m+s}(kBq m^{-3})	4.912	0.015	3.0	29.0
C^{eq}_{m} (kBq m^{-3})	0.133	0.002	0.03	0.3
C^{eq}_{s} (kBq m^{-3})	4.510	0.014	2.8	27.3
ε_a	0.778	0.012	4.0	39.0
V_m (10^{-3} m^3)	1.55	0.03	0.4	4.2
V_{ch} (10^{-3} m^3)	5.41	0.03	0.03	0.2

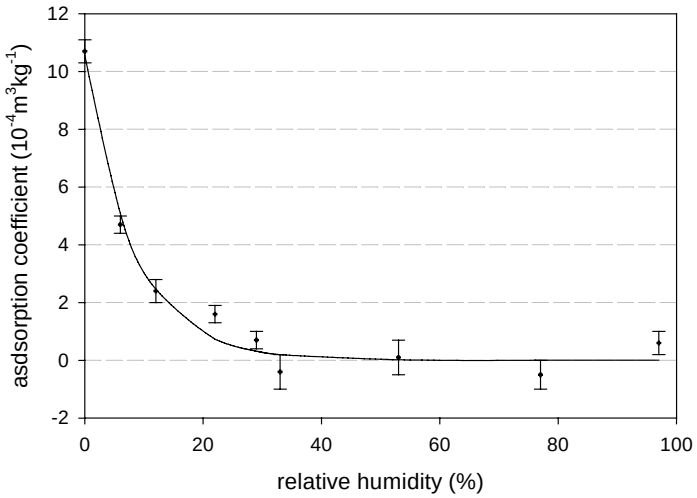

Figure 4.3 Radon adsorption coefficient as a function of the relative humidity. The uncertainties correspond to one standard deviation. The line equals the empirical relation: $k_{ads} = 0.001 \cdot e^{-12RH}$, where RH is the relative humidity.

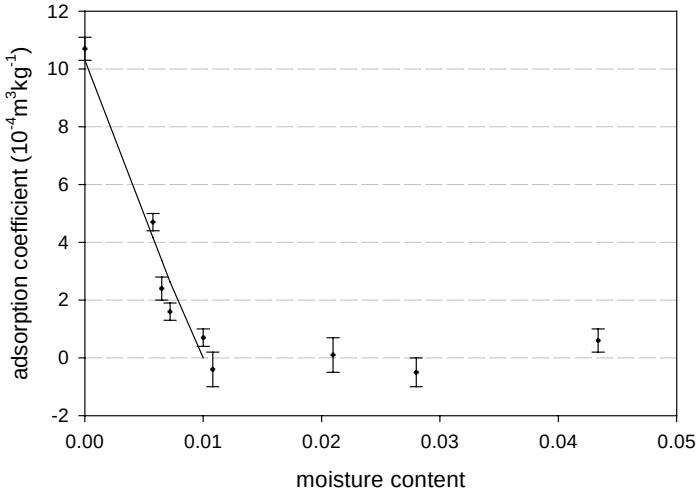

Figure 4.4 Radon adsorption coefficient as a function of the moisture content. The moisture content is given as fraction of the total sample volume. The uncertainties correspond to one standard deviation. The line equals the empirical relation: $k_{ads} = 0.001 - 0.1MC$, where MC is the fraction of the pore volume filled with moisture.

However, adsorption is considered a process due to interaction with the surface of the material rather than the volume of the sample. Therefore, it is interesting to examine how the adsorption coefficient relates to the (free) surface area of the

material. A simple method has been used to estimate the surface area of the AAC covered by moisture as a function of the relative humidity (see *Intermezzo 4.3*). *Figure 4.5* shows the relation between the adsorption coefficient and the estimated surface area filled with water. It can be observed that, similar to *Figure 4.4*, the adsorption is negligible when more than 0.17 km^2 of the pore-surface is covered with moisture. However, just before no adsorption is reached, the reduction in adsorption coefficient is found. A possible explanation for this effect is that the left-hand side of the curve describes the adsorption in the smallest pores and that either radon has to compete with other (gaseous) components for the adsorption sites or that the entry of those pores for radon is limited.

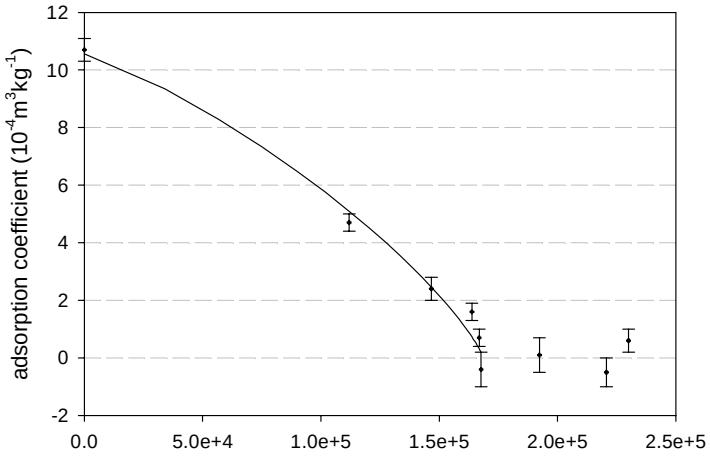

Figure 4.5 Radon adsorption coefficient as function of the surface area covered by water. The uncertainties correspond to one standard deviation. The line shows the calculated value (see also Intermezzo 4.3).

Intermezzo 4.3: Calculating the surface area occupied by water

To calculate the surface area occupied by water for each *RH*-level, the increase in moisture content for each step in *RH*-level together with the radius and the length of the pores that are filled with moisture in each step is required.

To calculate the increase in moisture content for each increase in *RH*-level, the empirical relations found between the relative humidity, moisture content and the emanation coefficient has been used. By substitution of the empirical relation between the emanation coefficient and the moisture content into the empirical relation between the emanation coefficient and the relative humidity, an expression for the moisture content as function of the *RH*-level is found.

To calculate the maximum pore size filled at a certain *RH*-level, we assume the Kelvin equation is valid for the whole *RH*-range:

$$r_i = \frac{-2\sigma V_L}{RT \ln RH_i}, \tag{4.17}$$

where:

r_i maximum pore radius filled with moisture for RH_i (m);
RH_i relative humidity;
σ surface tension water (N m^{-1});
R gas constant (J $mol^{-1}K^{-1}$);
T absolute temperature (K);
V_L molar volume of water (m^3mol^{-1}).

Note that applying the Kelvin equation to RH-levels smaller than approximately 40% [ref] is incorrect and a description using multi-layer effects, such as the BET-isotherm, would be better. However, lacking the experimental data for this isotherm, the Kelvin equation has been used for the complete *RH*-range.

The length of the pores that are filled with moisture due to the increase in moisture content, l_i (m), is given by:

$$l_i = \frac{V_m \Delta mc_i}{\pi r_i^2}, \tag{4.18}$$

where:

V_m volume of sample (m^3);
Δmc_i increase in moisture content for interval *i*.

The increase in surface area occupied by moisture, ΔS_i, is now given by:

$$\Delta S_i = 2\pi r_i l_i. \tag{4.19}$$

The total amount of surface area covered with water from interval *RH = 0* to RH_a, S_a, is gained via summation over the values for ΔS_i:

$$S_a = \sum_{i=1}^{a} \Delta S_i. \tag{4.20}$$

4.4.2 Emanation coefficient

Figures 4.6, 4.7 and *4.8* show the emanation coefficient as a function of the relative humidity, moisture content and the surface area of the AAC covered with moisture, respectively. The emanation coefficient increases almost linearly with the moisture contents. The increasing trend is comparable with results reported in the literature and can be explained by an increasing layer of water around the radon-emitting grains. Because radon trapped in the water layer can escape to the air-phase where radon trapped in the solid grains cannot escape before decaying, the emanation coefficient will increase with increased moisture content. Measurements show that the recoil-distance for radon in water is approximately 0.1 μm. The maximum radius of the pores filled with moisture at RH = 0.97 is 0.03 μm. This can explain the sharp increase in emanation coefficient for large surface areas covered with moisture: pores with a diameter of almost the recoil distance for water are filled up here. These pores will effectively stop the radon from re-entering the solid matrix after recoil. This effect results in an increased emanation coefficient.

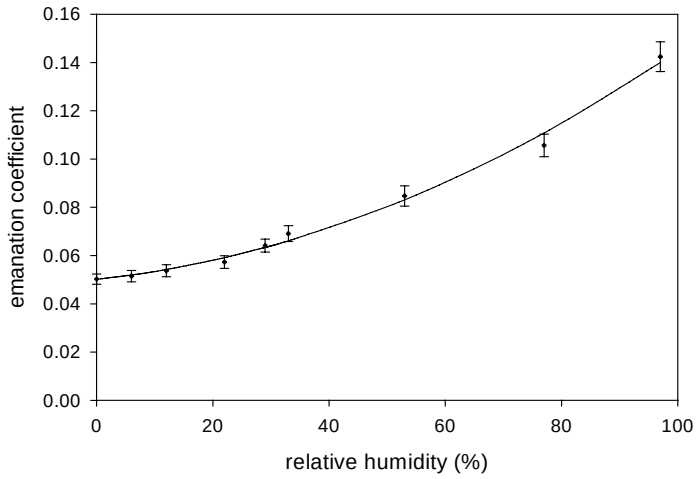

Figure 4.6 Emanation coefficient as a function of relative humidity. The uncertainties correspond to one standard deviation. The line equals the empirical relation: $\eta = 0.05 + 0.025RH + 0.07RH^2$, where RH is the relative humidity.

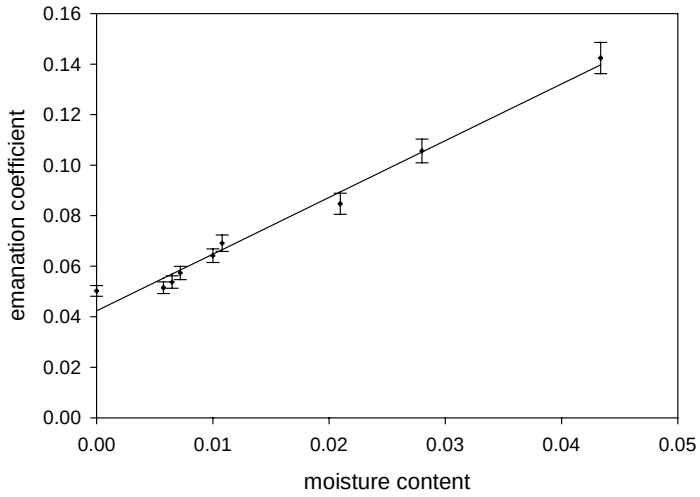

Figure 4.7 Emanation coefficient as a function of the moisture content. The moisture content is given as fraction of the total sample volume. The uncertainties correspond to one standard deviation. The line equals the empirical relation: $\eta = 0.042 + 2.25MC$, where MC is the fraction of the pore volume filled with moisture.

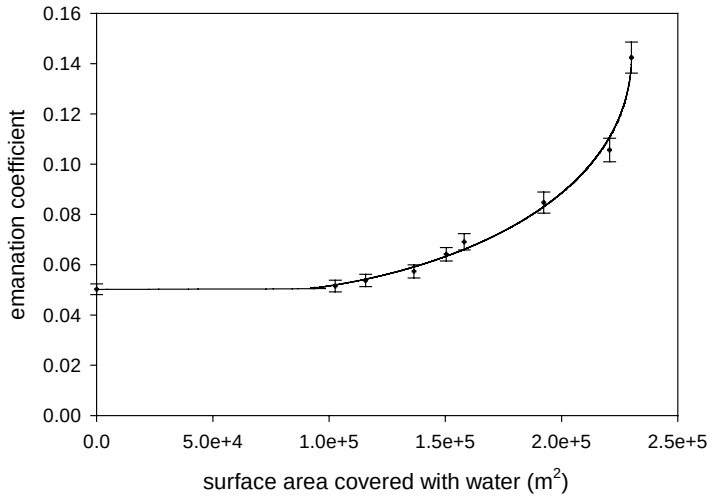

Figure 4.8 Emanation coefficient as a function of surface area covered by water. The uncertainties correspond to one standard deviation. The line shows the calculated value (see also Intermezzo 4.3).

4.4.3 Measurement accuracy

For the adsorption coefficient, the accuracy of the method is mainly determined by the uncertainty in the value of the porosity of the samples and the uncertainties of the fitted equilibrium radon concentrations C_{m+s}^{eq} and C_{s}^{eq}. The uncertainty in the porosity, determined with the gas-displacement method, can be caused by the a systematic

uncertainty caused by the used method and/or by the variance in the porosity of the samples, this would results in a statistical error. The latter is assumed for the calculations. Based on the quantities and standard uncertainties involved in the calculation of k_{ads} (see *Intermezzo 4.2*), a combined standard uncertainty for k_{ads} of approximately $0.5 \cdot 10^{-4}$ m^3kg^{-1} is calculated for a typical measurement period of 5 days.

Assuming no adsorption occurs at *RH* > 0.33, the scattering in the measured adsorption coefficients in this range must be due to random effects. The standard deviation of the four data points in this range is also $0.5 \cdot 10^{-4}$ m^3kg^{-1}. In addition, repeated measurements of k_{ads}, see *Table 4.2*, do not indicate a different value. It is therefore concluded that $0.5 \cdot 10^{-4}$ m^3kg^{-1} is a reasonable estimate of the experimental uncertainty. This uncertainty is of the same order of magnitude as obtained with the experimental procedure employed by Schery and Whittlestone [2]. Sensitivity analysis shows that the accuracy of the method can be improved by using larger samples. A lower porosity and/or higher density with respect to autoclaved aerated concrete, common for most other building materials, also positively affects the precision.

On average, the *a priori* calculated uncertainty in emanation coefficient is 0.005. The variance in the emanation coefficient was calculated using the same method as for the adsorption coefficient. These calculations showed that the main contributors to the variance in the emanation coefficient are the variance in the volume measurements of the chamber and sample, the variance in the radon equilibrium concentration and the variance in the radium content. The variance in radon concentration can be decreased by longer measuring times, more efficient and/or larger scintillation cells and higher volume sample/chamber ratios. Note that the latter measure results in a stronger dependence of the emanation coefficient on the adsorption coefficient as a larger fraction of the radon is adsorbed. This means that the uncertainty in the emanation coefficient will be more dependent on the uncertainty in the adsorption coefficient.

4.4.4 Effects of adsorption on radon transport

A commonly used quantity to describe the effect of adsorption on radon transport in a porous material is the retardment factor *R*:

$$R = 1 + \frac{\rho_m k_{ads}}{\varepsilon_a}, \tag{4.21}$$

where ρ_m is the bulk density of the porous material. For AAC, the maximum adsorption coefficient (at dry conditions) results in $R = 1.8$. This value will lower the radon diffusion length by a factor $\sqrt{R} = 1.3$.

4.4.5 Effects of moisture content

The effects of adsorption are limited to low relative humidity levels. Only for RH < 0.33 adsorption is observed. Retardment of radon can reduce the diffusion length with a factor 1.3. However, this will not play a role for most radon-exhalation measurement which are conducted at *RH* = 0.5.

The emanation coefficient, however, varies throughout the entire *RH*-range. A difference of a factor of more than 3 is found between the emanation coefficient at *RH* = 0 and 0.97. As only 5% of the pore-volume is occupied by water at *RH* = 0.97, and therefore 95% of the pore-volume does not efficiently stop the radon atoms from entering a neighbouring grain, a further increase in emanation coefficient with increasing moisture content can be expected.

The measurements show that emanation coefficients determined for *RH* = 0.50 only, provide limited information on this important material property. The emanation coefficient determined under these conditions can easily differ more than 25% from the value of the emanation coefficient under practical conditions.

4.5 Conclusions

A relatively simple experimental method has been used to measure the adsorption coefficient and emanation coefficient of porous materials. The adsorption coefficient can be measured with a precision of approximately $5 \cdot 10^{-5}$ $m^3 kg^{-1}$ provided the porosity is known with a similar accuracy as in the presented case. The uncertainty in emanation coefficient is approximately 0.005, largely depending on the uncertainty in the measured radon concentration, radium content and the volumes of chamber and sample. The value for the emanation coefficient at *RH* = 50% does not significantly differ from the values found in chapter 3.

A strong influence of the *RH*-level and the moisture content on the emanation coefficient and the adsorption coefficient is found. The reduced adsorption for larger RH-levels can be explained by occupation of the adsorption sites by the present moisture. This effect is strongest for the adsorption sites near the *RH*-levels where adsorption is negligible. This suggests that besides capillary condensation also mono and multi-layer adsorption of water plays an important role. For the emanation coefficient, an increased value is found for increasing RH-levels. The relation between the emanation coefficient and the moisture content is almost linear. A sharp increase in emanation coefficient is found for pores with a radius near the recoil distance for radon in water. This supports the theory that a layer of moisture reduces the recoil speed of radon and thereby increases the chance of radon being available for transport, i.e. reducing the chance, that radon re-enters the matrix.

So the measurement of the adsorption coefficient and emanation coefficient do not only provide the input parameters for the model calculations for the advective and diffusive transport, which will be presented in the next chapter, but also give insight in the processes taking place on a microscopic scale.

References

[1] Ackers J.G., Gemeten Radon Emanatiefactoren van Bouwmaterialen, RD-TNO Rapport RD-E/8901-271, TNO, The Netherlands, 1985 (in Dutch).

[2] Adan O.C.G., On the fungal defacement of interior finishes, Ph.D. thesis, Eindhoven University of Technology, The Netherlands, 1994.

[3] Atkins P .W., Physical Chemistry, 4th Edition, Oxford University Press, Oxford, United Kingdom, 1990.

[4] Cozmuta I., Radon Generation and Transport: a journey through matter, Ph.D. thesis, University of Groningen, The Netherlands, 2001.

[5] Chrysikopoulos C.V., Kitanidis P.K., Roberts P.V., Analysis of One-Dimensional Solute Transport Through Porous Media With Spatially Variable Retardation Factor, *Wat. Resour. Res.*, 26:437-446, 1990.

[6] Van Dijk W., De Jong P., Determining the ^{222}Rn Exhalation rate of Building Materials using Liquid Scintillation Counting, *Health Physics*, 61:501-509, 1991.

[7] Edwards J.C., Bates R.C., Theoretical evaluation of radon emanation under a variety of conditions, *Health Physics*, 39:263-274, 1980.

[8] Fleischer R.L., Moisture and ^{222}Rn emanation, *Health Physics*, 52:797-799, 1987.

[9] Gadd M.S., Borak T.B., In-situ determination of the diffusion coefficient of ^{222}Rn in concrete, *Health Physics*, 68:817-822, 1995.

[10] Gan T.H., Mason G.C., Wise K.N., Desorption of ^{222}Rn by Moisture and Heat, *Health Physics*, 50:407-410, 1986.

[11] Goh T.B., Oscarson D.W., Cheslock M., Shaykewich C., Fluence rate of radon from soil: effect of sorption barriers, moisture content, and temperature, *Health Physics*, 61:359-365, 1991.

[12] Hirst W., Harrison G.E., The diffusion of radon gas mixtures, *Proc. Roy. Soc. London*, A169:573-586, 1939.

[13] Van der Lugt G., Stralingshygienische aspecten van het Stoken van Steenkool en het gebruik van vliegas, *Energiespectrum*, 8:270-283, 1984 (in Dutch).

[14] Markkanen M., Arvela H., Radon emanation from soils, *Rad. Prot. Dos.*, 45:268-272, 1992.

[15] Menetrez M.Y., Mosley R.B., Snoddy R.S., Brubaker S.A., Evaluation of radon emanation from soil with varying moisture content in a soil chamber, *Environment Int.*, 22:S447-S453, 1996.

[16] Nazaroff W.W., Moed B.A., Sextro R.G., Soil as a Source of Indoor Radon: Generation, Migration, and Entry. In: Nazaroff W.W., Nero A.V., editors, Radon and its Decay Products in Indoor Air, John Wiley & Sons, 1988.

[17] Plantinga S.D., Radon emanation: its dependence on moisture content and grain size, KVI-report R-94, KVI, The Netherlands, 1996.

[18] Roelofs L.M.M., Scholten L.C., The effect of Aging, Humidity, and Fly-ash, Additive on the Radon Exhalation from Concrete, *Health Physics*, 67:266-271, 1994.

[19] Rogers V.C., Nielson K.K., Multiphase radon generation and transport in porous materials, *Health Physics*, 60:807-815, 1991.

[20] Rogers V.C., Nielson K.K., Correlations for predicting air permeabilities and ^{222}Rn diffusion coefficients of soils, *Health Physics*, 61:225-230, 1991.

[21] Rogers V.C., Nielson K.K., Holt R.B., Snoddy R., Radon diffusion coefficients for residential concretes, *Health Physics*, 67:261-265, 1994.

[22] Rutherford P.M., Dudas M.J., Arocena J.M., Radon emanation coefficients for phosphogypsum, *Health Physics*, 69:513-520, 1995.

[23] Schery S.D., Whittlestone S., Desorption of Radon at Earth's Surface, *J. Geophys. Res.*, 94(D15):18297-18303, 1989.

[24] Schery S.D., Lopez T.L., Sorption of Radon on Porous Materials and the Importance of Controlling Radon in the Indoor Environment. In: Kay J.G., Keller G.E., Miller J.J., editors, Indoor air pollution: radon, bio aerosols and VOC's, Lewis Publishers, Chelsea, United Kingdom, 1991.

[25] Van der Spoel W.H., Radon transport in sand: a laboratory study, Ph.D. thesis, Eindhoven University of Technology, Eindhoven, The Netherlands, 1998.

[26] Stranden E., Kolstad A.K., Lind B., The influence of moisture and temperature on radon exhalation, *Radiat. Prot. Dosim.*, 7:55-58, 1984.

[27] Strong K.P., Levins D.M., Effect of moisture content on radon emanation from uranium ore and tailings, *Health Physics*, 42:27-32, 1982.

[28] Søgaard-Hansen J, Damkjær A, Determining ^{222}Rn diffusion lengths in soils and sediments, *Health Physics*, 53:455-459, 1987.

[29] Tanner A.B., Radon Migration in the Ground: A Review, In: Adams J.A.S., Lowder W.M., editors, The natural Radiation Environment, University of Chicago Press, Chicago, USA, 161-190, 1964.

List of symbols

symbol	description
Δt	time interval at which the number of pulses are registered (s)
ε_a	air-filled pore space of porous sample (m^3m^{-3})
ε_w	water-filled pore-space of porous sample (m^3m^{-3})
η	emanation coefficient
λ	decay constant of radon ($2.098\ 10^{-6}\ s^{-1}$)
λ_2	decay constant of ^{218}Po ($3.78\ 10^{-3}\ s^{-1}$)
λ_3	decay constant of ^{214}Pb ($4.31\ 10^{-4}\ s^{-1}$)
λ_4	decay constant of ^{214}Po ($5.81\ 10^{-4}\ s^{-1}$)
ρ_m	bulk density of the material (kg m^{-3})
σ_j^2	variance in quantity *j*
ξ_1	efficiency for detecting an α-particle emitted in the decay of ^{222}Rn (Bq^{-1})
ξ_2	efficiency for detecting an α-particle emitted in the decay of ^{218}Po (Bq^{-1})
ξ_4	efficiency for detecting an α-particle emitted in the decay of ^{214}Po (Bq^{-1})
A_{ads}	radon adsorbed-phase activity (Bq)
A_{air}	radon air-phase activity (Bq)
$A_{emanated}$	total amount of radon emanated from sample (Bq)
A_{water}	radon water-phase activity (Bq)
$C_1(t)$	concentration of ^{222}Rn (Bq m^{-3})

List of symbols (continued)

symbol	description
$C_2(t)$	concentration of ^{218}Po (Bq m^{-3})
$C_3(t)$	concentration of ^{214}Pb (Bq m^{-3})
$C_4(t)$	concentration of ^{214}Po (Bq m^{-3})
C_{air}	air-phase radon concentration (Bq m^{-3})
C_{m+s}^{eq}	air-phase equilibrium radon concentration of measurement with material sample and radon source (Bq m^{-3})
C_{m}^{eq}	air-phase equilibrium radon concentration of measurement with material sample (Bq m^{-3})
C_{s}^{eq}	air-phase equilibrium radon concentration of measurement with radon source (Bq m^{-3})
$C_i(t=0)$	i = 2,3,4 The ^{218}Po, ^{214}Pb and ^{214}Po concentration at t = 0 (Bq m^{-3})
C_{Ra}	radium content (Bq kg^{-1})
k_{ads}	adsorption coefficient (m^{3}kg^{-1})
L	Ostwald coefficient (0.26 at T = 293 K)
m_m	mass of porous material sample (kg)
S	radon production rate (Bq s^{-1})
R	retardment factor
S_m	radon production rate material sample (Bq s^{-1})
S_s	radon production rate radon source (Bq s^{-1})
t	time (s)
V_{air}	air volume in the chamber (m^3)
V_{ch}	air volume of the empty chamber (m^3)
V_f	measuring volume of scintillation flask (m^3)
V_m	bulk volume of porous sample (m^3)
$V_{m,air}$	air volume of porous sample (m^3)
$V_{m+s,air}$	air volume of porous sample and radon source (m^3)
$V_{m,water}$	water-filled volume of porous sample (m^3)
V_s	volume of radon source (m^3)
$V_{s,air}$	air volume of measurement with radon source (m^3)
V_{water}	water-filled volume (m^3)

5

Radon transport measurements

5.1 Introduction

In the preceding chapters, measurements of various material properties necessary to model the generation, adsorption and transport of radon in autoclaved aerated concrete (AAC) have been presented. The present chapter presents the radon-transport measurements and compares them with model calculations. Both advective and diffusive transport of radon in AAC is considered. To be able to treat the two mechanisms independently, a measurement of the diffusion coefficient is required. A new method has been developed for this purpose. The method and its results are presented in section 5.2. The method for measuring combined advective and diffusive transport and its results are described in section 5.3. Section 5.4 gives an overview of the model calculations to describe the measurement results. The chapter ends with a section discussing the results and drawing conclusions considering the transport of radon.

5.2 Independent measurement of D_e

5.2.1 Introduction

Several techniques are available for determining the effective diffusion coefficient, D_e of radon in porous materials. A common approach is to position a porous material between two compartments. In one of the compartments, which we will call the source chamber, a known high radon-activity concentration is introduced while the radon concentration in, or flux into, the other (ventilated) compartment, which we will call the detection chamber, is measured under steady-state conditions. This technique concerns a direct measurement of the diffusion coefficient for steady-state conditions in case radon decay in the sample can be ignored. However, when the radon decay in the sample cannot be ignored, the partition-corrected porosity of the sample has to be known. In the previous chapter, a method is presented to determine this parameter.

Alternatively, the diffusion coefficient can be determined by measuring the change in radon concentration or flux as a function of time. Such a time-dependent method was introduced by Nielson et al. [8] and Zapalac [12]. In the experiments of Nielson et al., a known high radon-activity concentration is introduced in the source chamber, while the radon concentration in the detection chamber, is monitored continuously using a scintillation cell. Zapalac measured the steady-state flux of activity in a similar experiment. The advantage of time-dependent methods is that they are considerably faster than steady-state methods. Three important difficulties are faced when determining the diffusion coefficient using a time-dependent method. First of all, radon can leak, often undetected, from the set-up. Such leakage can, depending on the chamber where the leakage occurs, lead to an overestimation or underestimation of the diffusion coefficient. Note that this problem also occurs in the steady-state measurements. This problem may be circumvented by measuring the total amount of radon produced in the set-up, i.e. the radon concentration in both chambers. A second problem is radon leakage from the source chamber to the detection chamber

along the sides of the sample. This would result in an overestimation of the diffusion coefficient. Measurements at the KVI [7,2] show that it is difficult to detect and/or prevent leakage of radon alongside the sample. A method to detect such leakage is described in chapter 3 and consists of repeated radon ingrowth measurements using the same sample with a various layers and kinds of adhesives. When no leakage takes place along these sealants, the measurements will, within their uncertainty levels, yield the same results. A third problem, more specific for time-dependent methods, occurs when fitting the *diffusion-advection model* to the measured data using a weighted least-squares fit. For a correct fit, the weight factor must be related to the uncertainty in the data. The commonly used algorithm of Aldenkamp and Stoop [1] for calculating the uncertainty in radon concentrations from quasi-continuous radon measurements corrects for the correlation between radon and its short-lived, alpha-emitting progeny but assumes that the consecutive radon concentrations are not correlated. For diffusion measurements, however, the consecutive radon concentrations are highly correlated and the measurements are conducted continuously rather than quasi-continuously. Therefore, this algorithm cannot be used to calculate the uncertainties in the measured count rates. A new algorithm that corrects for this correlation is presented here.

In this section, two methods for determining the diffusion coefficient are presented. The first method, the ingrowth method, measures the ingrowth of radon in both chambers as a function of time. The second method, the ventilation method, is also time-dependent but uses a larger concentration gradient, created by ventilation of the detection chamber. The latter method yields a quicker measurement. This section is finished with a comparison of the two methods. The same set-up and sample has been used for both measurements.

5.2.2 Experimental set-up

Set-up: The experimental set-up is schematically shown in *Figure 5.1*. It consists of a leak-tight stainless-steel cylindrical canister (height 160 mm, diameter 200 mm) with a removable flange at the upper side. The flat topside of a porous cylindrical sample of AAC (height h = 104 mm, inner radius r_1 = 25.5 mm, outer radius r_2 = 90 mm) is glued against the bottom side of the flange while the flat bottom side of the sample is glued against a thin cylindrical stainless steel disc (180 mm diameter). In the middle of the flange, a scintillation cell is mounted to a photo-multiplier tube (PMT1). The steel tube leading to the scintillation cell has a length of 100 mm; the scintillation cell itself has a length of 150 mm. The inner diameter of the scintillation cell and the steel tube is about 50 mm. The second scintillation cell (PMT2) is similarly mounted to the cylinder wall of the canister. The scintillation cells are separated from the volumes with a glass-fibre filter to prevent transport of radon daughters while the opposite sides of the cells are closed with a transparent window and positioned in front of a photo-multiplier tube. A calibrated radon source[1] is placed in the inner compartment to create a radon concentration gradient over the sample. The total volume of the inner and outer compartments are V_1 = 0.704 ± 0.018 L and V_2 = 2.77 ± 0.02 L,

[1] Pylon certified radon source type 2000A with an activity for radium of 127 Bq (± 4%).

respectively. The radii and height of both the sample and the inner volume (V_1) are measured using a sliding calliper and a ruler. The total volume of the setup (i.e. the combined volume of the compartments and the sample) is determined by a water-volume measurement. For this measurement, the compartments, including the scintillation cells (without the scintillation paper present), are filled with water and from the increase in mass of the setup and the density of the water (derived from the temperature of the water), the volume of the total setup is calculated.

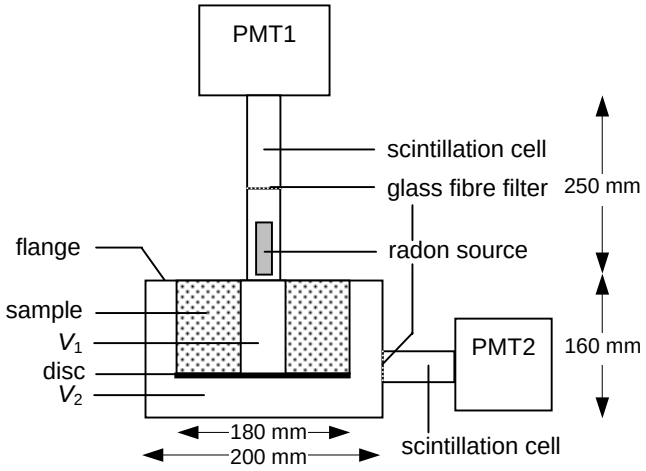

Figure 5.1 Schematic representation of the set-up for measuring the radon diffusion coefficient.

Detection efficiencies: The detection efficiencies, η_2 and η_4, of the short-lived, alpha-emitting progeny, respectively ^{218}Po and ^{214}Po, relative to the detection efficiency for radon, η_1, have been determined in an earlier experiment [9]. In this measurement a high radon concentration is introduced in a scintillation cell and registering the number of pulses in 10-minute intervals during 3 h. A least-squares fit to the data yields a value of 1.15 ± 0.03 and 1.333 ± 0.018 for respectively η_2/η_1 and η_4/η_1. The detection efficiency for radon, η_1 has been determined by measuring the ingrowth of radon during several weeks in a closed chamber with a known volume containing a radon source with a known activity. This yields a detection efficiency for radon of 0.493 ± 0.006 for the scintillation cell in the inner compartment. The detection efficiency for radon of the scintillation cell in the outer compartment compared to the cell in the inner compartment is 0.947 ± 0.016 (i.e. the absolute detection efficiency for radon in the outer compartment is 0.456 ± 0.005). Note that the given uncertainty includes only the standard deviation due to counting statistics. Uncertainties due to systematic uncertainties are not included in this value.

Table 5.1 Overview of the set-up parameters

parameter	value
V_1	$(0.704 \pm 0.018) \cdot 10^{-3}$ m^3
V_2	$(2.77 \pm 0.02) \cdot 10^{-3}$ m^3
h	0.104 ± 0.005 m
r_1	0.0255 ± 0.005 m
r_2	0.090 ± 0.005 m
S_1	$(2.67 \pm 0.11) \cdot 10^{-4}$ Bq s^{-1}
PMT1: η_1	0.493 ± 0.006 counts Bq^{-1}
η_2	0.567 ± 0.016 counts Bq^{-1}
η_4	0.657 ± 0.011 counts Bq^{-1}
PMT2: η_1	0.456 ± 0.005 counts Bq^{-1}
η_2	0.524 ± 0.016 counts Bq^{-1}
η_4	0.607 ± 0.010 counts Bq^{-1}

5.2.3 Ingrowth method

Measurement: An ingrowth measurement consists of a measurement of the radon ingrowth in both compartments, which are not ventilated. Before the start of the measurement, radon is removed from the set-up by ventilating it with radon-free air with a relative humidity (*RH*) of 50% at a rate of at least 10 h^{-1} for at least 8 hours. The airflow is introduced in the outer compartment and led out of the set-up via the inner compartment, thereby forcing it through the porous sample to include removal of radon present in the sample. After stopping the flow, the alpha-activity in both compartments is monitored by registering the total number of pulses in consecutive time intervals, Δt, of 30 minutes. After three weeks, the steady-state concentrations are reached and the measurement is stopped.

Mathematical description: Consider a hollow cylindrical sample with inner radius r_1 and outer radius r_2. A radon source with source-strength S_1 (in Bq) is placed in the inner compartment. Ignoring the radon generation in the sample, which generates about a 100 times less radon than the radon source S_1, and assuming the sample is homogeneous and isotropic so that the radon concentration, *C,* only changes in the radial direction, the macroscopic radon transport equation can be written in polar coordinates:

$$\frac{\partial C}{\partial t} = D_e \frac{\partial^2 C}{\partial r^2} + \frac{D_e}{r}\frac{\partial C}{\partial r} - \lambda C \,, \tag{5.1}$$

where:

t	time (s);
C	radon concentration (Bq m^{-3});
r	polar coordinate (m);
λ	decay constant for radon (s^{-1});
D_e	effective diffusion coefficient (m^{2}s^{-1}).

The bulk diffusion coefficient, D_b, is related to the effective diffusion coefficient using the partition corrected porosity β:

$$D_b = \beta D_e \,, \tag{5.2}$$

where

D_b bulk diffusion coefficient ($m^2 s^{-1}$);
β partition-corrected porosity.

Assuming a well-mixed, leak-tight compartment, the boundary condition at $r = r_1$ is:

$$V_1 \frac{\partial C}{\partial t} = 2\pi r_1 h D_b \frac{\partial C}{\partial r} - \lambda V_1 C + S_1 \,, \quad r = r_1;\ t \geq 0, \tag{5.3}$$

where V_1 is the volume of the inner compartment and h the height of the sample. The terms at the right-hand side account for a diffusive flux through the inner surface, radon decay and production, respectively. Similarly, the boundary condition at $r = r_2$ is written as:

$$V_2 \frac{\partial C}{\partial t} = -2\pi r_2 h D_b \frac{\partial C}{\partial r} - \lambda V_2 C \,, \quad r = r_2;\ t \geq 0, \tag{5.4}$$

where V_2 is the volume of the outer compartment. The initial condition of the ingrowth method is:

$$C = 0,\ t = 0. \tag{5.5}$$

Solving the differential equation 5.1 with the appropriate boundary and initial conditions yields an expression for the radon concentration in each of the compartments that basically can be written as:

$$C(t) = b_0 + \sum_{i=1}^{\infty} b_i \exp(a_i t) \tag{5.6}$$

To comply with the boundary condition, $C(r, t=0) = 0$, $\sum_{i=1}^{\infty} b_i = -b_0$.

In the experiment, however, it is not the radon concentration but the count rate that is measured. The count rate includes the counts from radon activity as well as its alpha emitting daughters, ^{218}Po and ^{214}Po. The procedure to calculate the radon concentration and its variance from the count rates is given in Appendix B. Note that the values for *a* and *b* are set by the boundary conditions.

Fitting procedure: With the radon concentrations and their variance, the diffusion coefficient can be calculated. To determine the diffusion coefficient, two least-squares fits have been conducted. In the first fit, only the diffusion coefficient is used

as a fit parameter. In the second fit, the diffusion coefficient, the radon source term and the relative efficiency of the scintillation cells (η_{PMT1}/η_{PMT2}) are the fitted parameters. The advantage of the second fit is that it is not influenced by systematic deviations in the relative efficiency and the radon-source strength.

Fitting three parameters, rather than one, can sometimes allows a large range of parameter values. To determine this effect for this fit, simulations have been conducted with several sets of generated data. The parameters values and their uncertainties have been calculated from these sets using the three parameter fit. These simulations [10] show this fit yields accurate values for the diffusion coefficient.

Measurement results: *Figure 5.2* shows the radon concentrations in the inner and outer compartment as a function of time obtained from the ingrowth method where a radon source is placed in the inner compartment and no ventilation took place. The fitted line shows the fit (768 data points) with only the diffusion coefficient as free parameter. This fit yields a value of $(5.20 \pm 0.06)\cdot10^{-7}$ m^2s^{-1} for D_e with a χ^2_{red} of 1.46. Note that the uncertainty reported here only includes the uncertainties in the measured counts. From the figure, it can be seen that the fit overestimate the measured count rates in the source chamber for large t. For the detection chamber, this effect seems not present. An overestimation of the detection efficiencies or an underestimation of the radon-source strength would result in such an overestimation. Fitting the radon-source term, however, does not yield a significant smaller value for radon-source strength. This effect can also be caused by changes in measurement conditions: increase or decrease in ambient temperatures will affect the radon emanation and the detection sensitivity of the scintillation cells. Repeated measurements may show whether the shown effect is due to (random) variations in measurement conditions. Another striking aspect is that the value for χ^2_{red} exceeds the expected value of 1.00 significantly. This can caused an underestimation of the uncertainties in count rates, by an incorrect model description or systematical errors in the model parameters. Because the calculation of the uncertainty in count rates has proven to yield accurate results in other measurements, this is not considered the cause of the deviation. The description of the model only includes the diffusive transport. However, small variations in temperature will result in advective transport of radon through the AAC. Furthermore, systematical errors in the model parameters can greatly influence the transport description (see section ***Sensitivity Analysis***).

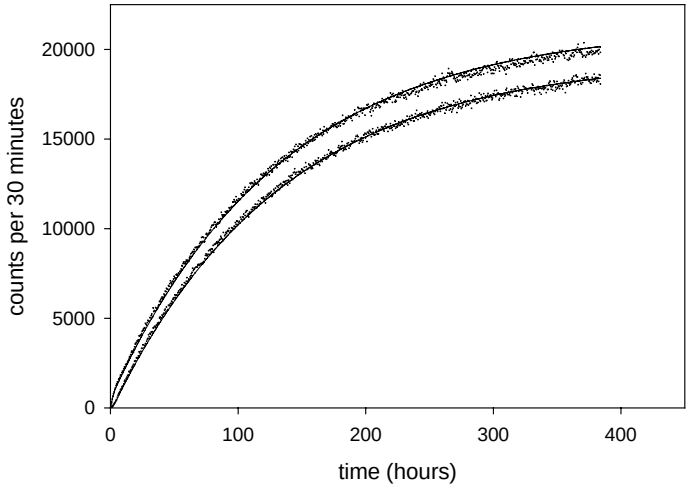

Figure 5.2 Count rates of the scintillations cells in the inner and outer compartment as a function of time for the ingrowth method. The upper line is the fitted curve for the inner compartment where the lower line is the fitted curve for the outer compartment. The dots represent the measured counts per 30 minutes intervals.

Fitting the model to the data using the relative efficiency, the source term and the diffusion coefficients as fit parameters yields a value for the diffusion coefficient of $(5.30 \pm 0.13) \cdot 10^{-7}$ $m^2 s^{-1}$ with a χ^2_{red} of 1.17. The ratio in net count rates of the scintillation cells as a function of time is shown in *Figure 5.3*. The value for the χ^2_{red} of this fit is better than in the previous fit. This suggests a systematic uncertainty in the relative efficiency and the radon-source term, have a large influence on the calculated diffusion coefficient. To further invest this phenomena, a sensitivity analysis has been conducted.

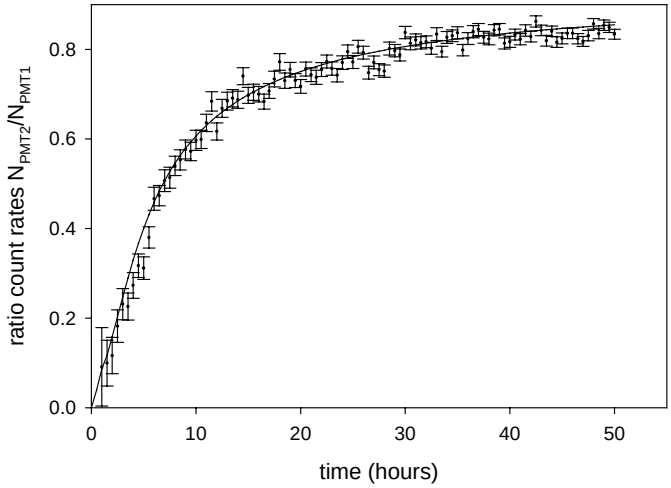

Figure 5.3 Ratio of net count rates of the scintillations cells in the inner and outer compartment as a function of time for the ingrowth method with the relative efficiency as free parameter. The line is the fitted curve where the dots with the error bars represent the measured ratio in counts per 30 minutes intervals. The error bars represent ± 1 standard deviation.

Sensitivity Analysis: The influence of the model-parameters has been analysed by varying the input parameters according to their uncertainties. This showed a large sensitivity for uncertainties in the relative efficiencies between the scintillation cells. *Figure 5.4* shows the effect of the relative efficiency on the calculated diffusion coefficient. A 0.5% change in relative efficiency results in a 20% change in the calculated diffusion coefficient. The large sensitivity for the relative efficiency can be reduced by changing the dimensions of sample or set-up. A reduced height, smaller inner radius and/or larger outer radius of the sample would lead to an increased concentration gradient over the sample and thereby to a decreased sensitivity for uncertainties in the relative efficiency. Furthermore, an increase in the volume of the outer compartment leads to reduced sensitivity for the uncertainties in the relative efficiencies. However, no leak-tight measurements could be obtained from a set-up with a larger outer volume and therefore the results could not be used for calculating the diffusion coefficient.

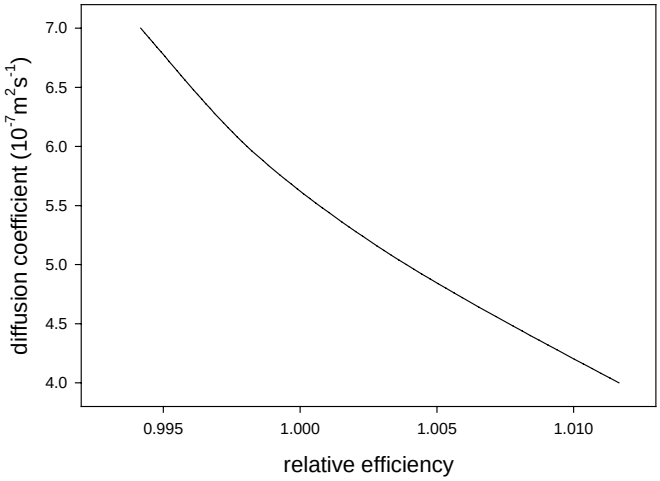

Figure 5.4 The calculated diffusion coefficient as a function of the relative efficiency of the two scintillation cells when using the ingrowth method.

5.2.4 Ventilation method

Mathematical description: The second method is similar to the ingrowth method except that the outer compartment is ventilated with radon-free air at a ventilation rate λ_v of 5 L min^{-1}, controlled by a Brooks mass flow controller. This means that the boundary condition for the inner compartment (equation 5.3) and the initial condition (equation 5.5) are the same for this method. The boundary condition for the outer compartment (equation 5.4) is now replaced by:

$$V_2 \frac{\partial C}{\partial t} = 2\pi r_2 h D_b \frac{\partial C}{\partial r} - (\lambda + \lambda_v) V_2 C \,, \; r = r_2; \; t \geq 0. \tag{5.7}$$

where:

λ_v ventilation rate in the outer compartment (s^{-1}).

For the measurement conducted here, the ventilation rate strongly reduces the radon concentration in the outer compartment. For simplicity, the boundary condition in the outer compartment is therefore replaced by:

$$C(r) = 0 \,, \; r = r_2. \tag{5.8}$$

This boundary condition has been used for solving the transport equations and was validated in the measurement. A least-squares fit is conducted with the diffusion coefficient as the only free parameter.

Measurement results: The results of ventilation method are shown in *Figure 5.5*. The least-squares fit yields an effective diffusion coefficient of (5.861 ± 0.014)·10^{-7} m^{2}s^{-1} with χ^2_{red} of 1.09. The value for χ^2_{red} of 1.09 suggests a good correlation between model description and measured count rates. The effect of the uncertainty in

the absolute efficiency of the scintillation cell is limited: a 1% change in absolute efficiency results in an approximately 1% change in value for the fitted diffusion coefficient.

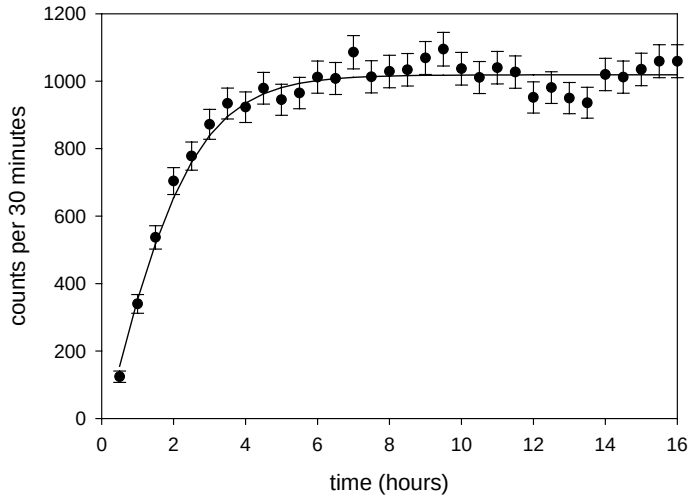

Figure 5.5 Net count rate in the inner compartment as a function of time. A radon source is placed in the inner compartment while the outer compartment is ventilated. The dots represent the measured counts per 30 minutes intervals and the solid line is the fitted curve. The error bars represent ± 1 standard deviation.

5.2.5 Discussion and conclusions

Both methods fit the measured data well. The values, however, vary from $(5.20 \pm 0.06)\cdot10^{-7}$ m^2s^{-1} and $(5.30 \pm 0.13)\cdot10^{-7}$ m^2s^{-1} for the ingrowth method to $(5.861 \pm 0.014)\cdot10^{-7}$ m^2s^{-1} for the ventilation method. The difference in calculated diffusion coefficient is significant, however, the given uncertainties only include the effects on counting statistics. These differences can be explained by the used measurement and calculation methods.

Sensitivity analysis shows that the value of the diffusion coefficient obtained by the 1-parameter fit of the ingrowth measurement is largely dependent on the efficiencies of the scintillation cells. A variation of 1% can already result in difference of 20% in the calculated diffusion coefficient. Although this could explain the difference in results between the 1-parameter fit of the ingrowth method and the ventilation method, it does not explain the results of the 3-parameter fit. A possible way to eliminate the influence of systematic uncertainties in the relative efficiency is to repeat the ingrowth measurement with the scintillation cell of the detection chamber on the source chamber and vice versa.

To reduce the effect of the sensitivity for the relative efficiency, the relative concentration gradient over the sample should be increased. This can be done by

using a larger detection chamber or a sample with a smaller height or larger outer radius. Using a stronger radon source would not suffice as it does not result in a relatively larger concentration gradient.

In the three-parameter fit of the ingrowth method the result is not influenced by the systematical errors in the relative efficiency and also this fit generates a diffusion coefficient that is significantly smaller than the ventilation method. Another possible cause for the found differences between the ingrowth method and the ventilation method is additional mixing taking place in the ventilation method due to advective transport induced by small pressure differences that arises from ventilating the outer compartment. This would result in an apparent larger diffusion coefficient. Therefore, the diffusion coefficient obtained by the three parameter fit of the ingrowth measurement will be used for the measurements presented in the next section, because it is not influenced by systematic errors in relative efficiencies or by the ventilation of the outer compartment and the thereby introduced pressure-differences over the sample.

To investigate the effect of ventilating the detection chamber, measurements with a range of ventilation rates should be conducted. It can be expected that advective transport will increase with increasing ventilation rates. Alternatively, measurements with samples of different sizes or permeabilities will give insight in the effect of ventilation on the diffusive transport and the quality of the method.

5.3 Combined diffusive and advective transport

5.3.1 Introduction

This section deals with the measurement of the combined diffusive and advective transport of radon in AAC. For this measurement, the set-up described in chapter 3 is used. In short, this set-up consists of a cylindrical stainless steel vessel containing a hollow cylinder of AAC. The AAC cylinder is closed on top and bottom to create two compartments on each side of the cylinder. The conditions in these compartments are measured and controlled. These conditions include the airflow through the set-up, which can be (partly) led through the AAC cylinder and thereby create an advective flow. A radon source can be used to create large concentration gradients.

5.3.2 Measurement conditions

The flow scheme for the measurement of combined diffusive and advective transport of radon is schematically shown in *Figure 5.6*. Air with a relative humidity of 50% is introduced in the outer compartment of the set-up (Q_{IN}) and leaves the set-up via the inner and/or outer compartment by Q^1_{OUT} and Q^2_{OUT} respectively. These three flows are controlled by a series of mass-flow controllers (MFC's). Because a fraction Q^1_{OUT} of the Q_{IN} leaves the set-up from the inner compartment, an airflow through the aerated concrete is induced, resulting in the advective transport of radon. The air flow is considered to be quasi-stationary during the measurement.

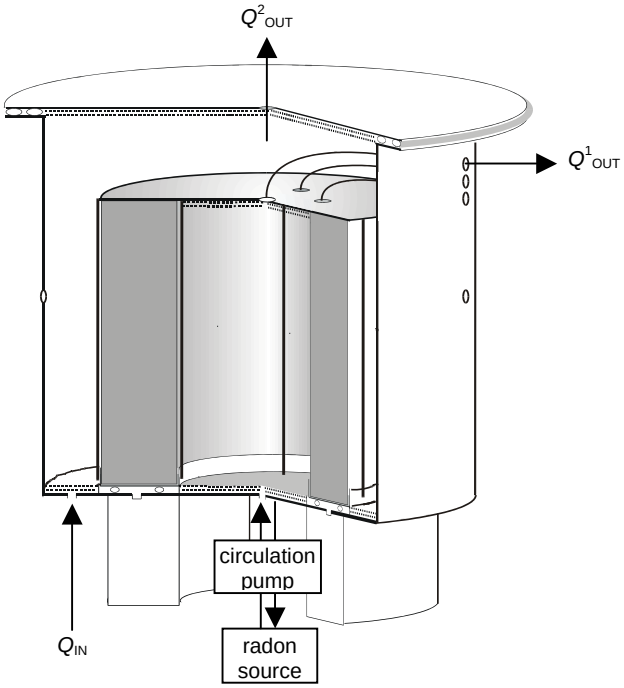

Figure 5.6 Configuration of the radon vessel for measuring combined diffusive and advective transport of radon in Autoclaved Aerated Concrete.

To create a radon concentration gradient over the AAC cylinder, a Pylon type 2000A radon source with a nominal activity of 22.2 kBq ^{226}Ra is placed in a five-litre stainless steel container. This container is connected to the inner compartment of the set-up by a circulation system. The air in the source container is recycled at a rate of 2 litres per minute via a continuous operating pump to provide good mixing of the generated radon throughout the inner compartment. This way a relative high radon concentration is maintained in the inner compartment.

The measurement starts with a Q_{IN} of 3 L min^{-1} and is increased in steps of 3 L min^{-1} up to a flow of 15 L min^{-1} every five days. The fraction of Q_{IN} leaving the set-up via the inner compartment (Q^1_{OUT}) is increased from 0 to 0.8 in steps of 0.2, each lasting 24 hours. The flow out of the outer compartment, Q^2_{OUT} is used to maintain a constant pressure in the set-up. This implies that in the first step only diffusive transport occurs while the other four steps combine diffusive with advective transport. The experiment takes 25 days to complete. The ambient temperature is set at 20.5 ^{o}C, and controlled by an air-conditioning unit. During the measurement, the airflows, the temperature, the pressure, the pressure-difference over the AAC cylinder, the relative humidity and the radon concentrations in both compartments were monitored.

5.3.3 Results

Airflows: *Figure 5.7* shows the flows in and out of the set-up as a function of time. The 24-hours time intervals can easily be recognized. The flows follow the set conditions. There is, however, a small difference between the flow into the set-up, Q_{IN} and the flow out of the set-up, $Q^1_{OUT} + Q^2_{OUT}$. Although leakage of air from the set-up would be a straightforward explanation, this is not likely the case as the apparent loss of air increase with the flow velocities. Due to the constant pressure in the vessel, leakage of air should be independent of the flows in and out of the set-up. More likely, the differences are caused by the uncertainties in the value given by the mass-flow controllers. The uncertainty in the readings of the mass-flow controllers, derived from the specifications of the manufacturer[2], yields an uncertainty in Q_{IN} and Q^2_{OUT} of respectively 0.11 L min^{-1} and 0.16 L min for $Q_{IN} = Q^2_{OUT}$ = 15 L min^{-1}. This results in a combined uncertainty of 0.2 L min^{-1}. The difference between the Q_{IN} and Q^2_{OUT} is, however, approximately 0.4 L min^{-1} and thus exceeds the given uncertainty level by a factor two. However, considering that the uncertainties given by the manufacturer are for optimal measurement conditions, i.e. dry air, constant pressure gradient and temperature, it is likely that for the uncertainty in the mass-flow measurements is actually larger than 0.2 L min^{-1} and probably render the differences insignificant. The relative uncertainties can possibly reduced by a calibration where the MFC's are connected in serial.

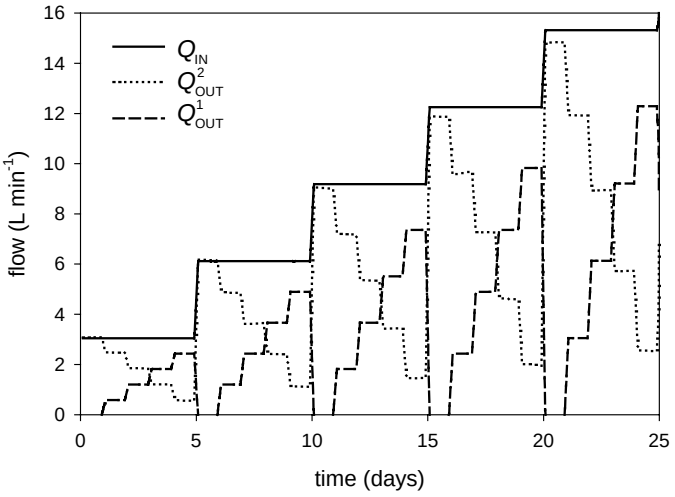

Figure 5.7 Flows in and out of the set-up as a function of time.

Pressure difference: In *Figure 5.8* the airflow through the AAC cylinder is given as a function of the pressure difference between the inner and outer compartment. The flow through the AAC has been calculated as the outgoing air of the inner compartment (this value is shown in the figure) as well as the difference between the ingoing and outgoing flow of the outer compartment ($Q_{IN} - Q^2_{OUT}$). The difference

[2] Bronkhorst Hi-Tec, Ruurlo, The Netherlands.

between both values, however, was within measurement uncertainties. *Figure 5.8* shows that the relation between pressure difference and flow is not entirely linear. A least-squares fit of the data (χ^2_{red} = 1.30) to the Darcy-Forchheimer relation yields a permeability K of (5.22 ± 0.08)·10^{-12} m^2 and a Forchheimer coefficient of (1.94 ± 0.05)·10^{10}. The non-linearity implies that (locally) the Reynolds number must be about a factor 100 larger than estimated in chapter 2.

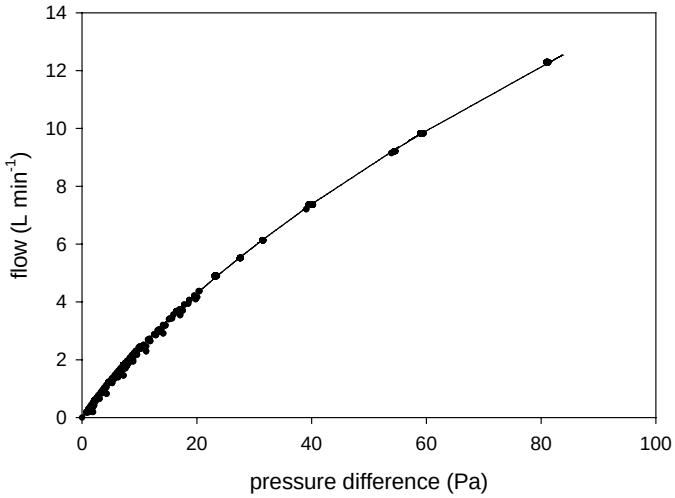

Figure 5.8 The airflow through the AAC cylinder as a function of the pressure difference over the AAC. The line represents the results from the Darcy-Forchheimer equation.

Temperature: The temperature of the air in the set-up varies between 20.2 °C and 21.2 °C during the measurement period. The temperature is about 0.2 °C higher in top of the set-up compared to the bottom of the set-up and it varies with time more in the outer compartment than in the inner compartment. The latter is due to the larger contact area of the outer compartment with the surrounding air. Nevertheless, the difference between minimum and maximum recorded temperatures did not exceed 1 °C. The temperature difference between the compartments did not exceed 0.3 °C and were on average less than 0.1 °C. Such steady temperatures and small temperature differences between the compartments are required as a temperature difference of 1 °C over the cylinder already results in a pressure difference of 4 Pa. These pressure differences will result in advective transport and thereby in additional mixing of radon. These effects can be considered negligible in the measurement presented here.

Radon concentrations: *Figure 5.9* and *Figure 5.10* show the measured radon concentrations in respectively the inner and outer compartment as a function of time. The radon concentrations have been calculated from the counts in 30-minute intervals using the algorithm of Aldenkamp and Stoop [1] for quasi-continuous radon measurements. The “peaks” in the radon concentration of the inner compartment

indicate the intervals with diffusion only (Q^2_{OUT} = 0) and the change in Q_{IN}. The height of these peaks only slightly decreases with the increasing ventilation in the outer compartment. This is conform expectations as the radon concentrations in the outer compartment are small and therefore enhanced ventilation will hardly increase the radon gradient. Such an increase is required to increase transport out of the inner compartment and reducing the peak height.

In addition, the 24-hours intervals with combined diffusive and advective transport can be distinguished. The pattern meets expectations: high radon concentrations in the inner compartment for diffusive transport only and decreasing concentrations with higher ventilation rates and combined advective and diffusive transport of radon. It can be observed that for airflows out of the inner compartment larger than 1.2 L min^{-1} the steady-state radon concentration is reached in the 24-hours interval.

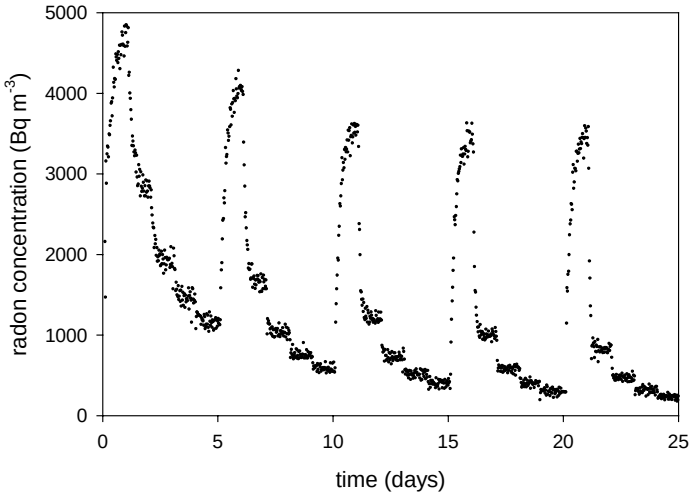

Figure 5.9 Measured radon concentrations in the inner compartment as a function of time. The peaks are the intervals without advective transport.

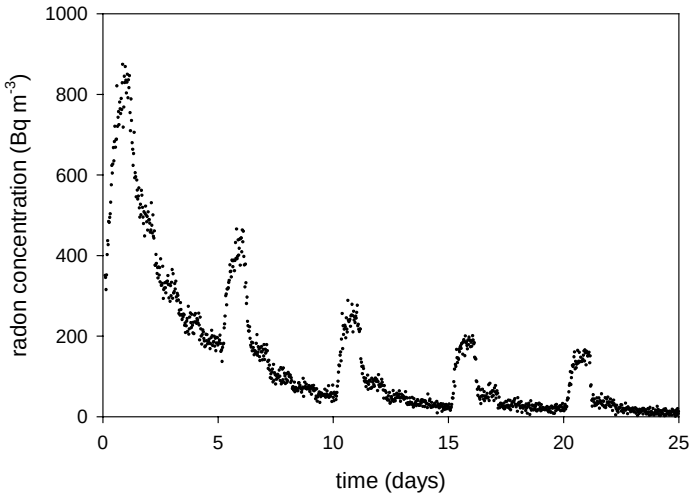

Figure 5.10 Measured radon concentrations in the outer compartment as a function of time. The peaks are the intervals without advective transport.

5.4 Modelling

5.4.1 Introduction

Three models are used to describe the measurement data: the *diffusion-advection model,* that assumes a homogeneous medium and a constant value for the diffusion coefficient, the *flow-dependent diffusion model* that derives possible extra flow-dependent effects and the *parallel-media model*, which corrects for inhomogeneity. After describing the model and discussing the results of each model, the three models will be compared and the results discussed.

5.4.2 Diffusion-advection model

Description: The *diffusion-advection model* considers AAC as a homogeneous material with a constant permeability and diffusivity throughout the entire sample. This model proved to accurately describe the combined diffusive and advective transport of radon in a column of sand [9].

Calculation method: The time-dependent combined diffusive and advective transport of radon in the air-filled pores of a porous medium is given by [9]:

$$\beta \frac{\partial C_a}{\partial t} = \nabla\left(\beta D_e \nabla C_a\right) + \frac{K}{\mu}\nabla P \nabla C_a - \beta\lambda C_a + \eta\rho C_{Ra}\,, \tag{5.9}$$

where:

β partition-corrected porosity;
C_a radon concentration in the air-filled pores (Bq m^{-3});
D_e effective diffusion coefficient ($m^2 s^{-1}$);
K permeability (m^2);

μ dynamic viscosity of air ($1.83 \cdot 10^{-5}$ Pa s, at T = 293K);
P pressure (Pa);
λ radon decay constant ($2.1 \cdot 10^{-6}$ s^{-1});
C_{Ra} radium concentration AAC (Bq kg^{-1});
ρ bulk density of AAC (kg m^{-3});
η emanation coefficient.

For the experiment described here, the boundary condition for the inner compartment is given by:

$$V_1 \frac{\partial C}{\partial t} = A_1 \beta D_e \frac{dC}{dr} - (\lambda + \lambda_1) V_1 C + Q_{OUT}^1 C + S_1, \; r = r_1, \tag{5.10}$$

where:
V_1 volume of the inner compartment (m^3);
A_1 surface area of the inner side of the AAC cylinder (m^2);
Q_{OUT}^1 airflow through the AAC cylinder (and out of the inner compartment) ($m^3 s^{-1}$);
λ_1 ventilation rate in the inner compartment (s^{-1});
S_1 radon production of the radon source in the inner compartment (Bq s^{-1}).

The boundary condition for the outer compartment is given by:

$$V_2 \frac{\partial C}{\partial t} = -A_2 \beta D_e \frac{dC}{dr} - (\lambda + \lambda_2) V_2 C - Q_{OUT}^1 C, \; r = r_2 \tag{5.11}$$

where:
V_2 volume of the outer compartment (m^3);
A_2 surface area of the outer side of the AAC cylinder (m^2);
λ_2 ventilation rate in the outer compartment (s^{-1});

The initial condition is C(t=0) = 0. The ventilation rates in the inner and outer compartment are calculated from the measured flow rates and the volumes of the inner and outer compartment. An overview of the input parameters is given in *Table 5.2*. These parameters are measured in the previous sections and chapters of this thesis.

Table 5.2 Values of the input parameters for the diffusion-advection model.

parameter	value	described in:
V_1	0.224 ± 0.003 m^3	Chapter 3
V_2	0.483 ± 0.006 m^3	Chapter 3
r_1	0.303 ± 0.002 m	Chapter 3
r_2	0.399 ± 0.002 m	Chapter 3
h	0.743 ± 0.002 m	Chapter 3
A_2	1.862 ± 0.005 m^2	Chapter 3
A_1	1.414 ± 0.005 m^2	Chapter 3
D_e	(5.30 ± 0.13)·10^{-6} m^2s^{-1}	Section 5.2
S_1	0.0466 ± 0.019 Bq s^{-1}	This section
C_{Ra}	11.5 ± 0.4 Bq kg^{-1}	Chapter 3
ε_a	0.768 ± 0.014	Chapter 3
ε_w	0.020 ± 0.002	Chapter 3
k_{ads} (at 50% *RH*)	0	Chapter 4
η	0.084 ± 0.004	Chapter 4
β	0.773 ± 0.015	Chapter 4
ρ	560 ± 6 kg m^{-3}	Chapter 3

Results: Radon concentrations calculated using the *diffusion-advection model* and measured radon concentrations are shown in *Figure 5.11*. This figure shows clearly that the calculated radon concentrations in the outer compartment using the *diffusion-advection model* are considerably lower than the measured concentrations for combined diffusive and advective transport. The differences exceed the uncertainty in measured radon concentrations and model parameters and are thus significant. The lower calculated concentrations indicate that diffusive transport is less influenced by the advective transport than expected for a homogeneous medium. This influence could be caused by dispersion effects or by inhomogeneity of the sample. Both options will be discussed in the next subsections.

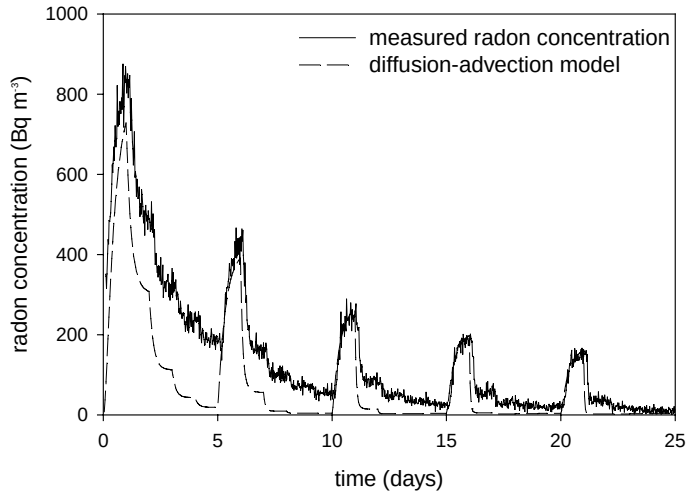

Figure 5.11 Radon concentrations in the outer compartment as a function of time: measured and modelled values.

5.4.3 Flow-dependent diffusion

Description: This approach assumes AAC is a homogeneous material but that the effective diffusion coefficient is flow-dependent and sets the value of the effective diffusion coefficient such that the data is described. A least-squares fit has been used to find the optimal diffusion coefficients for each time interval.

Calculation method: The *flow-dependent diffusion approach* uses the same equations to describe the time-dependent combined advective and diffusive transport of radon in a porous medium as the diffusion-advection model, except that the diffusion coefficient is a free parameter. The diffusion coefficient is calculated for each time-interval of 24 hours using a least-squares regression fit.

Results: The measured and modelled radon concentrations in the outer compartment as a function of time are presented in *Figure 5.12*. The good correlation between measurements and calculations was the criteria for changing the diffusion coefficient and therefore the good correlation between measurements and model does not permit any conclusions towards the quality of the *flow-dependent diffusion approach*. It does, however, show that it is possible to obtain a correct description by adapting the diffusion coefficient.

Of greater importance is the relation between the optimised diffusion coefficient and the flow rate, which is shown in *Figure 5.13*. The results show an almost linear relation between the flow rate and the effective diffusion coefficient. A linear fit yields an effective diffusion coefficient of $(8.0 \pm 0.8) \cdot 10^{-7} m^2 s^{-1}$ for $Q = 0$. This value is larger than any of the values measured on the small sized samples in section 5.2.

The magnitude of the effect of the flow on the diffusion coefficient is much larger than would be expected from the Peclet and Reynolds numbers (see chapter 2). Even when assuming that large pores are connected with each other via small pores creating high air velocities in the small pores, resulting in larger Peclet and Reynolds numbers than estimated for pores with a constant radius, the effect can not be explained by hydrodynamic dispersion. Local variations in air flow velocities due to variations in flow paths can have resulted in mechanical dispersion effects. This effect, however, would exceed values report in the literature [11,13,5,3,4].

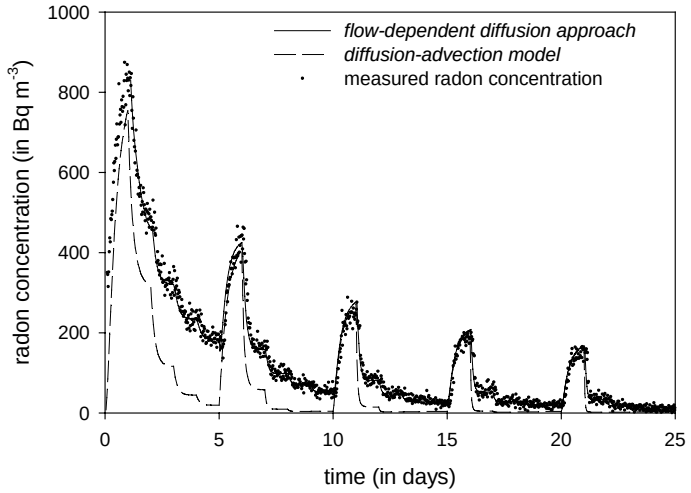

Figure 5.12 Radon concentrations in the outer compartment, measured and calculated using the flow-dependent diffusion model as a function of time.

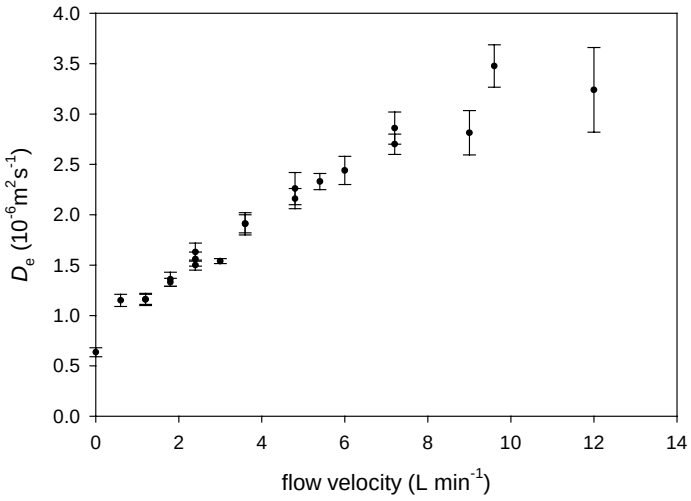

Figure 5.13 Effective diffusion coefficient as a function of the velocity of the airflow through the AAC. The error bars represent ± 1 standard deviation.

Furthermore, the consistency of the results of the empirical data can be tested by comparing the desired diffusion coefficients at equal airflow velocities but at different concentration gradients, which can be seen in *Figure 5.13* as the multiple points at the same flow velocities. It can be observed that the desired diffusion coefficients at same airflow velocities do not differ significantly. This means that the flow-dependent diffusion coefficient is not concentration dependent, as can be expected for the radon concentrations that are extremely low in terms of molar concentrations.

The fact that there is such a simple relation between the effective diffusion coefficient and the flow rate in our assumption of a homogeneous medium and that conditions are likely not corresponding to dispersion effect, may be considered an indication for a too simple model. As a logical next step we therefore investigate the possibility that we have a material composed of two homogeneous components differing in permeability only.

5.4.4 Parallel-media model

Description: The *diffusion-advection model* showed a poor correlation, which could only be improved by adjusting the diffusion coefficient to very high values. A possible explanation is that the media description has been incorrect and needs to be adapted. In the *parallel-media model*, radon is assumed to be transported from the outer to the inner compartment via two parallel connected media, i.e. it is assumed the AAC is not a homogeneous material. A schematically representation of this model is given in *Figure 5.14*. Each medium has its own permeability, diffusion coefficient and volume. Furthermore, it is assumed that there is no exchange of radon between the two media. Although this model is clearly an oversimplification of the real situation, it is intended as a first step in explaining the data and towards an improved description of the transport of radon in porous building materials.

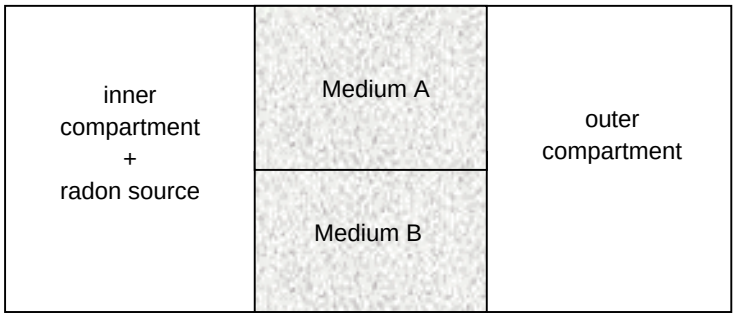

Figure 5.14 Schematic representation of parallel-media model.

Calculation method: In the *parallel-media model*, each medium has three unknown parameters: volume, permeability and diffusion coefficient. For simplicity, we assume the diffusion coefficient in both media is equal to the diffusion coefficient measured in section 5.2. Reason for this choice is that the diffusive transport is, contrary to the advective transport, not dependent on the pore radius. This leaves 4 unknown model

parameters. The number of degrees of freedom is less. The first restriction is that the sum of the volumes of the compartments must equal the total volume of the AAC. The second restriction is that the sum of the flows through the two media must equal the airflow through the AAC cylinder. These constraints reduce the number of degrees of freedom of this model to two: the ratio of the volume and the ratio of the permeability of both media. The results of this model were compared with steady-state concentrations as they would be found with the *flow-dependent diffusion approach*. A comparison with the (time-dependent) measurements was not possible since steady-state conditions were not attained in each 24 hours interval. A least-square fit was conducted to determine the values for the ratios in volume and permeability.

Results: In *Figure 5.15*, the equilibrium radon concentrations, as found by extrapolation of measured data using the *flow-dependent diffusion approach*, and the radon concentrations modelled by the *parallel-media model* are shown. The values for the ratio in volume and permeability of the two media obtained from the least-square fit (χ^2_{red} = 1.09) are presented in *Table 5.3*. The permeability has been calculated using the value for *K* found in the fit of the Darcy-Forchheimer equation, surface areas of both media and the ratio in permeabilities. The results indicate one relative large medium with a relative small permeability together with a small medium with a relative high permeability. According to this model, approximately 90% of the airflow passes through approximately 8% of the volume of the AAC cylinder.

Table 5.3 Calculated ratios in volume and permeability of the two media assumed in the parallel-media model.

parameter	ratio	medium A	medium B
volume	0.08 ± 0.03	0.146 m^3	0.012 m^3
permeability	153 ± 40	$(4.3 \pm 1.7)\cdot10^{-13}$ m^2	$(5.7 \pm 1.6)\cdot10^{-11}$ m^2

The *parallel-media model* describes the data as good as the *flow-dependent diffusion model*. Unlike the *flow-dependent diffusion approach*, a characteristic of this model is a large flow in one of the media combined with a small volume, indicating preferential flow paths. Such paths can be created by (micro)cracks or inhomogeneity in the AAC cylinder. The differences in flow rates can result in different Reynolds numbers and thereby higher Reynolds numbers might be created in the preferential flow path than for one, homogeneous medium. This could explain the measured non-linearity between flow and pressure-difference, especially as the flow rates increase considerably for larger pores and cracks. For a further validation of this model, the transport parameters such as permeability and diffusion coefficients of these paths should be measured independently.

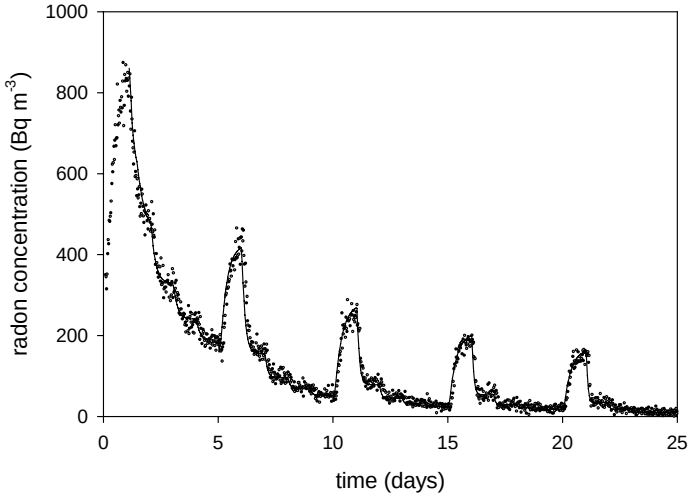

Figure 5.15 Radon concentrations in the outer compartment, measured and calculated using the flow-dependent diffusion model as a function of time.

5.4.5 Discussion and conclusions

Three approaches have been used to correlate the measured radon concentration to radon concentrations calculated using measured material parameters such as the air-filled porosity, adsorption coefficient and diffusion coefficient and the initial and boundary conditions. The *diffusion-advection model* that showed a good correlation between radon concentrations calculated from these parameters and the measured radon concentrations for sand, was insufficient to describe the transport of radon in AAC correctly. It can therefore be concluded that the *diffusion-advection model* does not suffice for describing the combined advective and diffusive transport of radon through the examined AAC cylinder. A better description is found when assuming either a flow-dependent diffusion coefficient (*flow-dependent diffusion approach*) or inhomogeneity (*parallel-media model*). The flow-dependency of the diffusion coefficient, however, is considerably larger than expected from theoretical models for dispersion and other flow-dependent effects (see chapter 2). Therefore, the results of the *flow-dependent diffusion approach* are not satisfying nor do they yield a physical explanation for the found results.

The *parallel-media model* fits the complete measurement well with only two additional parameters. These parameters, the ratios in volume and permeability, indicate that about 90% of the air flows through about 7% of the sample volume. Such preferential flows can be caused by connectivity of large pores and by (micro) cracks. This means that we not only have a model that describes the data correctly, but that there is also a physical explanation available that supports the *parallel-media model*.

The presence of the preferential flows means that the model calculations for the transport of air, radon and moisture through AAC where AAC is assumed a

homogeneous material is incorrect, even though the influence of the preferential flows does not always will be as large as presented here.

Although the *parallel-media model* has parameters that can be physically explained, its parameters have not been determined independently. Independent measurement would be a great step forward in the validation of the model. Some methods that can help to determine these parameters are presented and discussed in the next chapter.

References

[1] Aldenkamp F.J., Stoop P., Sources and Transport of indoor radon, Ph.D. thesis, University of Groningen, The Netherlands, 1994.

[2] Cozmuta I., Radon generation and transport - a journey through matter, Ph.D. thesis, University of Groningen, The Netherlands, 2001.

[3] Dullien F.A.L., Porous media: fluid transport and pore structure, Academic Press, New York, 1979.

[4] Greenkorn R.A., Flow Phenomena in Porous Media: fundamentals and applications in petroleum, water, and food production, Marcel Dekker INC., New York, 1983.

[5] Han N.W., Bhakta J., Carbonell R.G., Longitudinal and lateral dispersion in packed beds: effect of column length and particle size distribution, *A.I.Ch.E. Journal*, 31(2):277-288, 1985.

[6] Inkret W.C., Borak T.B., Boes D.C., Estimating the Mean and Variance of Measurements from Serial Radioactive Decay Schemer with Emphasis on ^{222}Rn and its Short-Lived Progeny, *Rad. Prot. Dos.*, 32(1):45-55, 1990.

[7] Koopmans M., de Meijer R.J., Radondoorlaatbaarheid van bouwmaterialen, KVI-report R-46, KVI, The Netherlands, 1993 (in Dutch).

[8] Nielson K.K., Rich D.C., Rogers V.C. and Kalkwarf D.R., U.S. Nuclear Regulatory Commission; Report NUREG/CR-2875, 1982.

[9] van der Spoel W.H., Radon transport in sand: a laboratory study, Ph.D. thesis, Eindhoven University of Technology, The Netherlands, 1998.

[10] van der Spoel W.H., van der Pal M., Sensitivity analysis of an improved method for measuring the radon diffusion coefficient of porous materials, Proc. NRE-VII, Greece, 2002.

[11] Verlaan M.L., Dispersion in heterogeneous media, Ph.D. thesis, Delft University of Technology, The Netherlands, 2001.

[12] Zapalac G.H., A time-dependent method for characterizing the diffusion of ^{222}Rn in concrete, *Health Physics*, 45(2):377-383, 1983.

[13] Saffman P.G., Dispersion in flow through a network of capillaries, *Chemical Engineering Science*, 11:125-129, 1959.

List of symbols

symbol	description
β	partition-corrected porosity
ε_a	air-filled porosity
ε_w	water-filled porosity
η	emanation coefficient
η_1	counting efficiency of scintillation cell for ^{222}Rn
η_2	counting efficiency of scintillation cell for ^{118}Po
η_4	counting efficiency of scintillation cell for ^{114}Po
λ	decay constant of radon ($2.1 \cdot 10^{-6} s^{-1}$)
λ_1	ventilation rate inner compartment (s^{-1})
λ_2	ventilation rate outer compartment (s^{-1})
μ	dynamic viscosity (Pa s)
ρ	density of AAC (kg m^{-3})
A_1	inner surface area of AAC cylinder (m^2)
A_2	outer surface area of AAC cylinder (m^2)
C	radon concentration (Bq m^{-3})
C_{Ra}	radium concentration (Bq kg^{-1})
D_b	bulk diffusion coefficient ($m^2 s^{-1}$)
D_e	effective diffusion coefficient ($m^2 s^{-1}$)
K	permeability (m^2)
P	pressure (Pa)
Q_{IN}	flow into the outer compartment (L min^{-1})
Q^1_{OUT}	flow out of the inner compartment (L min^{-1})
Q^2_{OUT}	flow out of the outer compartment (L min^{-1})
S_1	radon production (Bq s^{-1})
V_1	volume inner compartment (m^3)
V_2	volume outer compartment (m^3)
h	height of AAC cylinder (m)
k_{ads}	adsorption coefficient ($m^3 kg^{-1}$)
r	radius (m)
r_1	inner radius AAC cylinder (m)
r_2	outer radius AAC cylinder (m)
t	time (s)

6

General discussion and conclusions

6.1 Introduction

In the preceding chapters, we have measured model parameters and compared calculations of the combined diffusive and advective transport of radon based on these model parameters with measurements. From this comparison, it became clear that a diffusion-advection model assuming homogeneity, which was adequate to describe the transport of radon in sand, does not suffice for the transport of radon in autoclaved aerated concrete. A better description is obtained when assuming heterogeneity, represented by the *parallel-media model*. This indicates that AAC, and probably also other building materials, should be treated as a heterogeneous material rather than a homogeneous. To support this hypothesis, some initial measurements have been conducted. The first results of these measurements will be presented and discussed in the next section. The third section will discuss the possible effects of heterogeneous building materials on the indoor radon concentration. The last section will give a future outlook.

6.2 Heterogeneity assessment

After the measurement the AAC cylinder was visually inspected. To conduct this inspection, it was required to take the cylinder out of the set-up for examination. Because of the possibility of introducing leaks and damaging the cylinder, this procedure was not conducted until the last experiment was completed. This inspection showed large cracks near the bottom of the AAC cylinder (see *Figure 6.1).* Although those cracks were not (visually) present when the cylinder was placed in the set-up, it is possible they were present at time of the measurements presented in the previous chapter. These cracks largely influence the advective transport if they serve as the preferential flow paths. Such flow paths were suggested by the results of the *parallel-media model*. However, the surface area calculated by the *parallel-media model* is considerably larger than the surface-area of the cracks in the AAC cylinder. This means that either the flow of air and radon through the cracks has a large interaction with the surrounding bulk material or that other (non visible) flow paths are present.

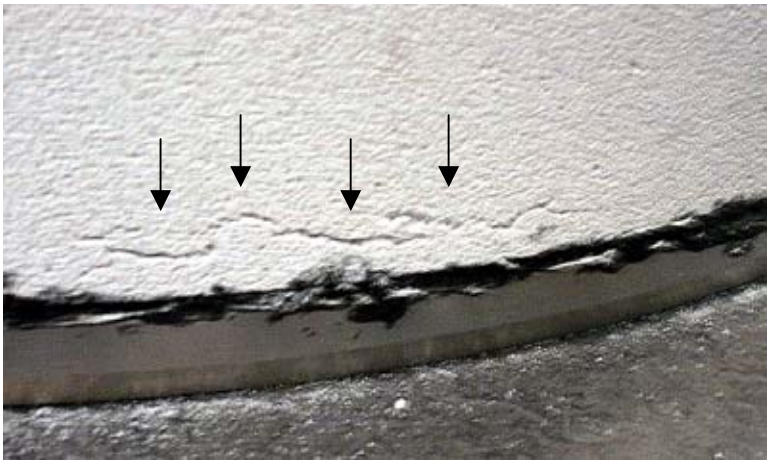

Figure 6.1 Detail of the cylinder of AAC, the adhesive and the bottom ring after the combined advective and diffusive transport measurements. The arrows show the visible cracks.

One of the main effects of the cracks is an increased permeability. To determine the fraction of airflow through the cracks in the AAC, the permeability of AAC samples with and without visible cracks was measured. These samples were taken from an AAC cube from the same batch as the cube used for the AAC cylinder. The direction of the applied airflow was in the same plane as the airflow in the AAC cylinder. The measurement consisted of measuring the flow rate as a function of the pressure difference for a range of pressure-differences. This measurement was conducted at the Department of Civil Engineering of the Catholic University of Leuven (KUL). The results are shown in *Figure 6.2* and *6.3*. It can be observed that the flow velocity in the visually cracked samples is about a factor 50 higher than in the visually uncracked sample. Furthermore, extrapolation suggests an offset in either the flow velocity or the pressure difference. For the fits, however, it is assumed that the flow velocity is zero when there is no pressure difference.

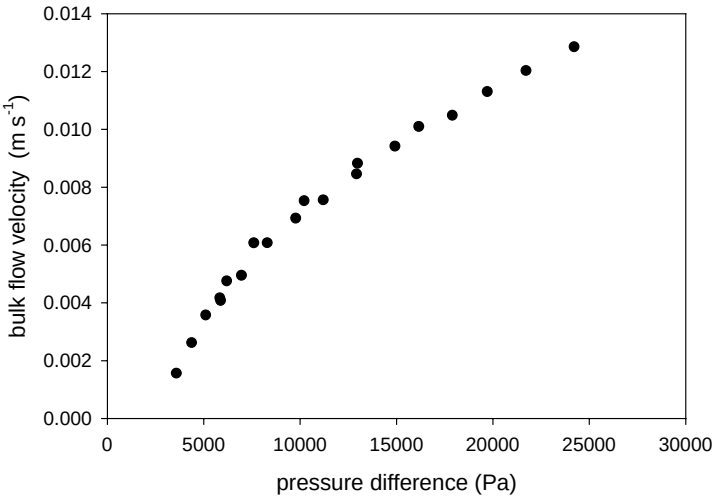

Figure 6.2 Relation between bulk flow velocity (m s^{-1}) and the pressure difference (Pa), measured on a sample of AAC without visible cracks.

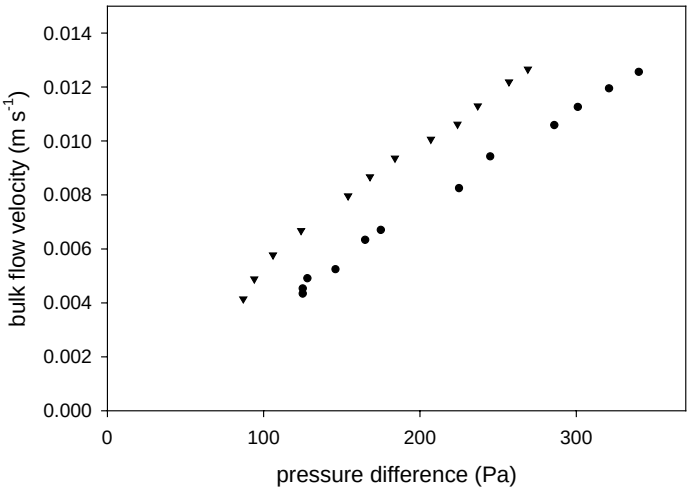

Figure 6.3 Relation between flow velocity (m s^{-1}) and the pressure difference (Pa), measured on two samples of AAC containing visible cracks.

Table 6.1 Permeability and Forchheimer coefficient from a least-squares fit of the data.

sample	K (m^2)	Forchheimer
uncracked	$(1.72 \pm 0.17)\cdot10^{-12}$	$(5.3 \pm 0.7)\cdot10^{8}$
cracked # 1	$(1.08 \pm 0.03)\cdot10^{-10}$	$(2.8 \pm 0.4)\cdot10^{6}$
cracked # 2	$(6.83 \pm 0.13)\cdot10^{-11}$	0*

* a 2-parameter fit yielded a negative value for the Forchheimer coefficient.

Table 6.1 shows the values of the Darcy-Forchheimer relation, which was applied to describe the relation between pressure-gradient and flow-velocity in the cracked and the visually uncracked samples. The permeability of the visually uncracked sample is about three times smaller than the permeability of the AAC cylinder used for the combined advective and diffusive transport measurements. With the relation between the pressure difference and the flow of the uncracked sample, the fraction of air flowing through the visually uncracked part of the AAC cylinder can be calculated:

$$f_{UC}(\Delta P) = \frac{\vec{q}_{UC}(\Delta P)}{\vec{q}_{measured}(\Delta P)}, \qquad (6.1)$$

where:

f_{UC} fraction of the air flowing through the visually uncracked AAC;

$\vec{q}_{UC}$ flow through the uncracked AAC as a function of the pressure gradient, extrapolated from the measurements on the visually uncracked samples using the Darcy-Forchheimer equation (m s^{-1});

$\vec{q}_{measured}$ the flow through the AAC cylinder measured as a function of the pressure gradient during the combined advective and diffusive transport measurements (m s^{-1}).

This fraction is shown in *Figure 6.4*.

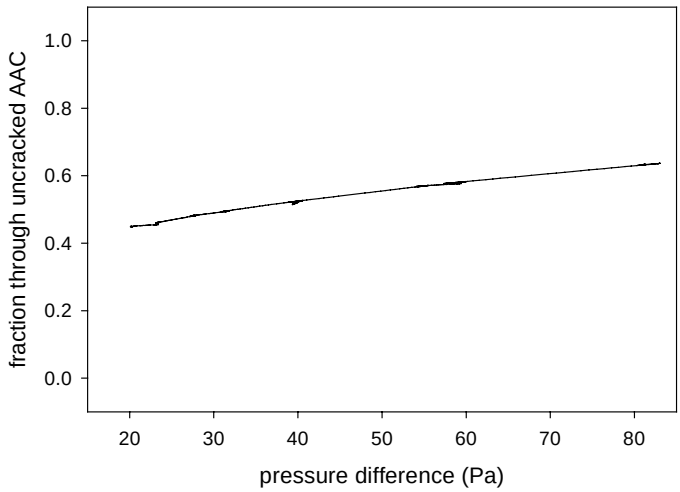

Figure 6.4 Fraction of the airflow passing through the visually uncracked part of the AAC cylinder as a function of pressure difference.

From *Figure 6.4* it can be observed that 40% to 60% of the air flows through the visually uncracked part of the AAC cylinder. A similar fraction of air flows through the cracks in the AAC cylinder. The fraction passing through the cracks, however, is significantly lower than the fraction found with the *parallel-media model*. The fraction of air through visually uncracked material increases with the pressure difference. This

is probably caused by a (more) turbulent flow through the cracks compared to the flow through the bulk material.

From these results, it can be concluded that visible cracks have a major influence on the combined advective and diffusive transport of radon in AAC but can only partly explain the results of the *parallel-media model*, where 90% of the air flows through preferential flow paths. To fully explain this result, the representation of the uncracked AAC as a homogeneous material where no dispersion occurs cannot be correct.

To examine structure of the visually uncracked AAC, another experiment was conducted. A sample of uncracked AAC was placed in a PVC cylinder and subsequently the air was evacuated from the sample and the sample filled with water. Subsequently a layer of an aqueous solution containing the dye *brilliant blue* was homogeneously spread over the surface of the sample. The solution was led through the AAC sample using gravity by adding water on top and removing water from the bottom of the sample. After adding a volume of water that approximately equalled 5% of the sample volume, the sample was dried in an oven at 105 ^{o}C for 24 hours and cut in two to determine the distribution of the brilliant blue throughout the sample. The procedure is schematically shown in *Figure 6.5.*

The resulting slice is shown in *Figure 6.6*. It can be observed that the dye is not homogeneously distributed over the pores but that only some pores are dyed, even much further than expected from the applied flow rate. This means that a solution containing brilliant blue is not transported homogeneously through uncracked AAC. If the transport of air is comparable with the transport of the brilliant blue, this means that the air does not flow homogeneously through visually uncracked AAC.

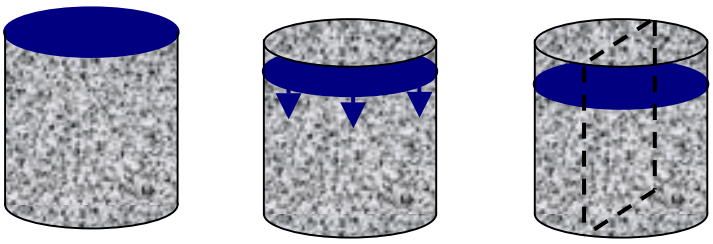

Figure 6.5 Dyeing experiment: on the left the solution containing the dye brilliant blue is spread over the surface of the cylinder, the middle shows the solution transported through the AAC sample and on the right the dashed line show how the sample is cut.

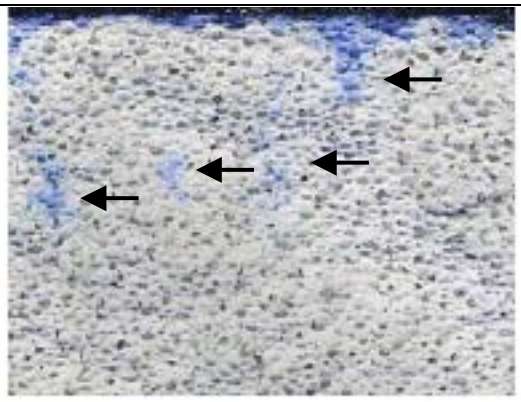

Figure 6.6 Cross-section of AAC after drying, the arrows indicate the traces of brilliant blue.

The permeability measurements presented in this section show that relatively large and visual present cracks influence the combined diffusive and advective transport of radon through AAC but that this only partly explains the results of the *parallel-media model*. The measurements with the dye *brilliant blue,* indicates that also in visually uncracked AAC preferential flows occur. These flows also add to the preferential flow found in *parallel-media model*. Based on these results, we can conclude that heterogeneity, due to both flows through visually present cracks as well as preferential flow paths in visually uncracked AAC, plays an important role in the combined diffusive and advective transport of radon through building materials.

6.3 Consequences of inhomogeneity

The measurements on AAC have shown a large influence of volume-wise small inhomogeneities on the transport of radon. This raises the question whether this effect plays an important role for other porous building materials and what the magnitude of this effect can be. We will try to answer these questions for concrete because concrete is a well-studied material, widely applied and exhales considerable amounts of radon.

Concrete is known to contain cracks and in addition, this fraction increases in time, due to curing of the concrete. It is therefore reasonable to assume that the inhomogeneity effects found for AAC also play a role in the transport of radon through concrete and increase in time. This means that measurements results from fresh, uncracked concrete sample-cubes do not only include the effects of the regular cracks and also lacks to effects of aging. The static radon exhalation rates of concrete is known to change considerably: even for well-conditioned samples an increase in radon exhalation rate of 50% is observed for the first 6-12 months, followed by a decrease in the next 7 years [4]. The increase can be caused by opening of cracks. The decrease is assumed to be due to release of moisture from the concrete.

One of the effects of the inhomogeneity is a considerable overestimation of the diffusion length for radon in the bulk material when this is determined with the common method of a radon gradient over a sample concrete and measurement of the resulting radon flux. If we assume that the diffusion coefficient in the cracks is of the same order of magnitude as for air, the cracks occupy 0.1% of the volume and run through the entire sample, this would already result in a measured diffusion length of approximately 0.05 m compared to measured diffusion lengths of 0.03 to 0.26 m for (uncracked) concrete [3]. This implies that the radon-exhalation rate can] depend more on the surface area rather than on the volume of the concrete then assumed from the measured diffusion length. Two other effects occur: the surface area of the cracks will contribute to the total exhalation rate of the concrete which means with increasing number of cracks in time, increased radon exhalation rates. The second effect is that the exchange of air on both sides of the concrete due to pressure differences will be considerable quicker then when assuming a homogeneous flow through the concrete.

The next step is to see how inhomogeneity affects the transport of radon in a dwelling and whether this can explain the discrepancy between the measured radon concentrations in dwellings and model calculations based on the measured radon exhalation rates and the measured ventilation rates in the second Dutch survey.

The pressure in the average Dutch dwelling is lower than the ambient pressure due to heating and wind effects. Air leaves the dwelling via the chimney or ventilation shaft. The underpressure will result in entry of air into the dwelling via crawl space and cavity walls. As a result, radon in the crawl space and cavity walls will enter the dwelling and contribute to the indoor radon concentration. This contribution will exceed the expected levels based on diffusion-driven radon-exhalation rates. When pressurising the dwelling, these effects will be strongly reduced. Such an effect was indeed observed in the measurements of Aldenkamp and Stoop [1]. It requires more detailed measurements to relate the observed effect quantitatively to the presence of preferential flows in cracks.

6.4 Future development

This thesis shows that inhomogeneity can play an important role in the transport of radon in porous building materials. Future research should therefore focus on quantifying this effect and finding methods to determine the required model parameters independently from the measurements. Such a method could include an improved version of the brilliant blue measurement. The improvements include a solid validation and calibration of the method. Image analysis can prove a useful tool in this process.

Another possible approach is the multi-scale modelling as conducted by the Catholic University of Leuven [2]. The cracks and the AAC matrix can be described at a macroscopic level. A possible method for determining the presence of cracks is X-ray measurements. At a meso-scale the transport of moisture, air and radon in the artificial air pores and the capillary pores are described and scaled up to the macro-

description. Such an approach would yield better insight in the transport of radon related to the presence of cracks and surface-related effects compared to the *parallel-media model*. Alternatively, the effect of mechanical dispersion can be investigated using a ‘random walk’-model.

Another aspect that should be further examined is the effect of inhomogeneity on the transport of radon in a dwelling. An interesting experiment would be putting a dwelling on overpressure rather than underpressure and see how this affects the radon concentration and whether this is in line with expectations. In addition to the experiments in the test house in Roden, where this already has been conducted, also the radon generation and transport properties of all the present building material and the underlying soil should be measured. It should also include an analysis of the effects of such a ventilation regime on other building aspects such as energy consumption, moisture transport and comfort. If a test-house will be build for this purpose, it is recommended to include a system to control the entry of radon from the soil and monitor the conditions of the soil, e.g. pressure and moisture content.

If the conclusions of this work are valid for dwellings the model behind the calculation of the radon performance index (RPI) has to be strongly modified. Applying the proposed RPI-model will lead to values that have no bearing with reality.

References

[1] Aldenkamp F.J., Stoop P., Sources and Transport of indoor radon, Ph.D. thesis, University of Groningen, The Netherlands, 1994.

[2] Carmeliet J., A multiscale network model for simulating moisture transfer properties of porous media, *Transport in porous media*, 35(1):67-88, 1999.

[3] Put L.W., van der Graaf E.R., Invoerparameters voor radontransportmodellen: een literatuurstudie, KVI-report R-92, KVI, The Netherlands, 1996 (in Dutch).

[4] Roelofs L.M.M., Scholten L.C., The effect of aging, humidity and fly-ash additive on the radon exhalation from concrete, *Health Physics*, 67(3):206-271, 1994.

Appendix A: Sensitivity Analysis Gas-displacement method

The relative uncertainty in the porosity ($\Delta\varepsilon/\varepsilon$) was calculated by propagation of uncertainties as a function of three parameters P_1, V_1, V_2 (see *Figures A.1*, *A.2* and *A.3*). In this estimate, the uncertainties in the volume and pressure determinations were set at 0.05% and 0.15%, respectively. The uncertainties in the volumes are based on the estimated accuracy of a volume-determination where the enclosures are filled with water and weighed. The uncertainty in the pressures relates to the specifications of the available pressure transducers.

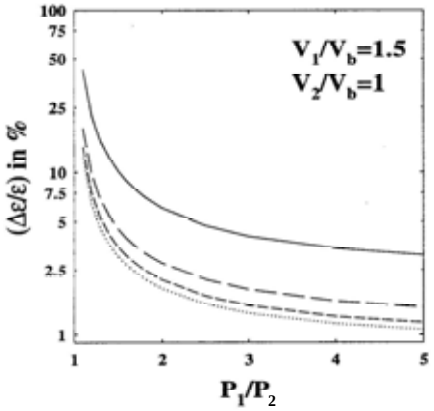

Figure A.1 Relative uncertainty in the porosity as function of P_1/P_2 at fixed values of V_1/V_b and V_2/V_b for ε_{air} = 0.1 (solid line), 0.3 (large dashed line), 0.5 (small dashed line) and 0.8 (dotted line).

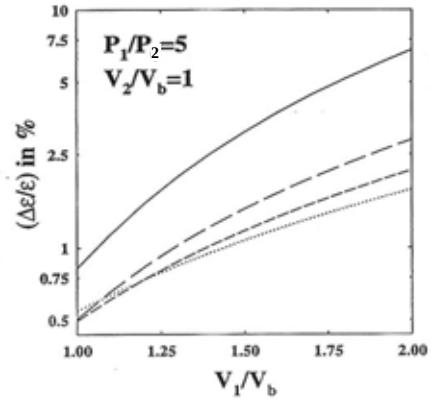

Figure A.2 Relative uncertainty in the porosity as function of V_1/V_b at fixed values of P_1/P_2 and V_2/V_b for ε_{air} = 0.1 (solid line), 0.3 (large dashed line), 0.5 (small dashed line) and 0.8 (dotted line).

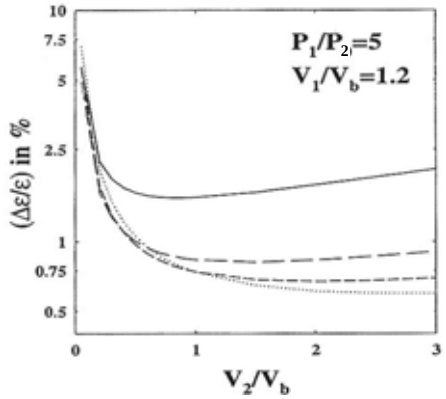

Figure A.3 Relative uncertainty in the porosity as function of V_2/V_b at fixed values of P_1/P_2 and V_1/V_b for ε_{air} = 0.1 (solid line), 0.3 (large dashed line), 0.5 (small dashed line) and 0.8 (dotted line).

The sensitivity analysis shows that the method is most sensitive for large P_1 compared to P_2, the volume around the sample in volume V_1 is as small as possible and if the volume of V_2 is about the size of the bulk volume of the sample. The first condition was met by setting P_1 to the maximum value of the range of the pressure transducer (0.5 MPa). The second condition was met by reducing the volume V_1 via filling the free space around the sample with metal pieces such as plates, spheres and blocks depending on the used sample. The last condition was met in the design of the set-up by making the enclosure V_2 half the volume of enclosure V_1. The used volumes were 6 and 12 litres respectively.

To calibrate the set-up, the volumes of the enclosures were determined with the gas-displacement method using samples with a known volume and via filling the enclosures with water and weighing. The volumes of both enclosures were measured by filling them with water of a known temperature and subsequently weighing them. Using the density for water at the measured temperature, the volumes of the enclosures were calculated. The volume of enclosure V_1 was measured with the gas-displacement method while containing respectively 0, 50, 100, 150 and 199 metal balls with a known volume. Comparing the volume given by the weight measurements and the gas-displacement method, the accuracy of the set-up and its volumes was determined. The results of this calibration are shown in *Figure A.4*. It shows that the volumes measured with the gas-displacement method match the volumes calculated from volumes of the balls and the water-weigh method within 1% (95% uncertainty interval).

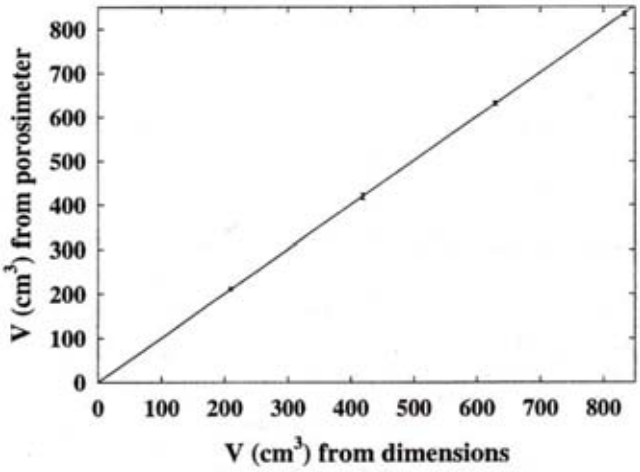

Figure A.4 Volumes measured by the porosimeter as function of the volumes measured via filling with water and weighing. Deviations between the measured volumes are within 1%.

Appendix B: Calculation of radon concentration and variance

Part 1: Solution for ingrowth method

The solution of equation 5.1 and boundary conditions 5.3, 5.4 and 5.5 consists of the sum of the steady-state and time-dependent part. For the steady-state part, i.e. $\frac{\partial C}{\partial t} = 0$, the solution of equation 5.1 is given by a linear combination of the modified Bessel functions of the first and second kind of order zero:

$$C(r) = A_0^{(1)} I_0\left(l^{-1} r\right) + B_0^{(1)} K_0\left(l^{-1} r\right), \tag{B.1}$$

where l is the radon diffusion length:

$$l = \sqrt{\frac{D_e}{\lambda}}. \tag{B.2}$$

The coefficients $A_0^{(1)}$ and $B_0^{(1)}$ follow from substition of B.1 in the boundary conditions 5.3 and 5.4:

$$A_0^{(1)} = \frac{-S_1 \lambda E_{2,0}}{V_1 g_0^{(1)}} \qquad B_0^{(1)} = \frac{S_1 \lambda E_{4,0}}{V_1 g_0^{(1)}}, \tag{B.3}$$

where

$$g_0^{(1)} = E_{1,0} E_{2,0} - E_{3,0} E_{4,0}, \tag{B.4}$$

and

$$\begin{aligned} E_{1,0} &= \; l^{-1} k_1 I_1\left(l^{-1} r_1\right) - \lambda I_0\left(l^{-1} r_1\right) \\ E_{2,0} &= \; l^{-1} k_1' K_1\left(l^{-1} r_2\right) - \lambda K_0\left(l^{-1} r_2\right) \\ E_{3,0} &= -l^{-1} k_1 K_1\left(l^{-1} r_1\right) - \lambda K_0\left(l^{-1} r_1\right) \\ E_{4,0} &= -l^{-1} k_1' I_1\left(l^{-1} r_2\right) - \lambda I_0\left(l^{-1} r_2\right) \end{aligned}. \tag{B.5}$$

The time-dependent part is found by Laplace transformation. The Laplace transform $\bar{C}(s) = \mathrm{L}(C(t))$ of equations 5.1, 5.3 and 5.4 using 5.5 are respectively

$$D_e \frac{\partial^2 \bar{C}}{\partial r^2} + \frac{D_e}{r} \frac{\partial \bar{C}}{\partial r} + q^2 \bar{C} = 0, \tag{B.6}$$

$$k_1 \frac{\partial \bar{C}}{\partial r} - (s + \lambda)\bar{C} + \frac{S_1 \lambda}{V_1 s} = 0 \qquad r = r_1, \tag{B.7}$$

$$-k_1' \frac{\partial \bar{C}}{\partial r} - (s + \lambda)\bar{C} = 0 \qquad r = r_2, \tag{B.8}$$

with

$$q^2 = \frac{-(s+\lambda)}{D_e}, \tag{B.9}$$

$$k_1 = \frac{2\pi r_1 hD}{V_1}, \tag{B.10}$$

$$k_1' = \frac{2\pi r_2 hD}{V_2}. \tag{B.11}$$

The solution of B.6 is given by a linear combination of the Bessel functions of the first and second kind of order zero:

$$\bar{C}(r) = A^{(1)} J_0(qr) + B^{(1)} Y_0(qr). \tag{B.12}$$

The coefficients $A^{(1)}$ and $B^{(1)}$ follow from substition of B.12 in the boundary conditions B.7 and B.8:

$$A^{(1)} = \frac{-S_1 \lambda E_2}{V_1 s g^{(1)}(s)} \qquad B^{(1)} = \frac{S_1 \lambda E_4}{V_1 s g^{(1)}(s)}, \tag{B.13}$$

where

$$g^{(1)}(s) = E_1 E_2 - E_3 E_4, \tag{B.14}$$

and

$$\begin{aligned} E_1 &= -qk_1 J_1(qr_1) - (s+\lambda) J_0(qr_1) \\ E_2 &= \quad qk_1' Y_1(qr_2) - (s+\lambda) Y_0(qr_2) \\ E_3 &= -qk_1 Y_1(qr_1) - (s+\lambda) Y_0(qr_1) \\ E_4 &= \quad qk_1' J_1(qr_2) - (s+\lambda) J_0(qr_2) \end{aligned}. \tag{B.15}$$

The reverse transform can be found using the theorem that if a transform $\bar{y}$ has the form:

$$\bar{y} = \frac{f(s)}{h(s)}. \tag{B.16}$$

where $f(s)$ and $h(s)$ are polynomials in s which have no common factor, the degree of $f(s)$ being lower than that of $h(s)$, and if

$$h(s) = (s-a_1)(s-a_2)\ldots(s-a_m), \tag{B.17}$$

where $a_1, a_2, \ldots a_m$ are constants which may be real or complex but must all be different, then the function $y(t)$ is given by:

$$y(t) = \sum_{r=1}^{m} f(a_r) \left(\left. \frac{dh(s)}{ds} \right|_{s=a_r} \right)^{-1} \exp(a_r t), \tag{B.18}$$

which still holds for $m = \infty$.

The coefficients B.13 have poles for s = 0 and when $g^{(1)}(s) = 0$. The equilibrium solution B.1 follows from the pole s = 0. The 'first' root of $g^{(1)}(s)$ is $s = a_1^{(1)} = -\lambda$ (i.e. when q = 0), for which the solution in the time domain is

$$C(t) = \frac{-2D_e S_1 k_1^{'} \exp(-\lambda t)}{V_1 r_2 \left[k_1 k_1^{'} \left(\frac{r_2}{r_1} - \frac{r_1}{r_2} \right) + 2D_e \left(\frac{k_1^{'}}{r_2} + \frac{k_1}{r_1} \right) \right]} \tag{B.19}$$

The other roots $s = a_i^{(1)}$, *i=2,3,...* of $g^{(1)}(s)$ are smaller than $-\lambda$ (i.e. $q > 0$) and have to be found numerically. The solution in the time domain for these poles is

$$C(r,t) = \frac{\lambda S_1}{V_1} \sum_{i=2}^{\infty} (-E_2 J_0(q_i^{(1)} r) + E_4 Y_0(q_i^{(1)} r)) \left(a_i^{(1)} \frac{dg^{(1)}(s)}{ds} \bigg|_{s=a_i^{(1)}} \right)^{-1} \exp(a_i^{(1)} t) , \tag{B.20}$$

where

$$\frac{dg(s)}{ds} \bigg|_{s=a_i} = E_{1,A} E_2 + E_{2,A} E_1 - E_{3,A} E_4 - E_{4,A} E_3 , \tag{B.21}$$

and

$$\begin{aligned}
E_{1,A} &= \left(\frac{k_1 r_1}{2D_e} - 1 \right) J_0(q_i r_1) + \frac{q_i r_1}{2} J_1(q_i r_1) \\
E_{2,A} &= \left(\frac{-k_1^{'} r_2}{2D_e} - 1 \right) Y_0(q_i r_2) + \frac{q_i r_2}{2} Y_1(q_i r_2) \\
E_{3,A} &= \left(\frac{k_1 r_1}{2D_e} - 1 \right) Y_0(q_i r_1) + \frac{q_i r_1}{2} Y_1(q_i r_1) \\
E_{4,A} &= \left(\frac{-k_1^{'} r_2}{2D_e} - 1 \right) J_0(q_i r_2) + \frac{q_i r_2}{2} J_1(q_i r_2)
\end{aligned} \quad . \tag{B.22}$$

The complete solution is given by the sum of equations B.1, B.19 and B.20.

Part 2: Solution for ventilation method

The boundary condition for $r = r_2$ $t \geq 0$ is given by:

$$\bar{C} = 0 \quad r = r_2, t \geq 0 . \tag{B.23}$$

For the steady-state part, i.e. $\frac{\partial C}{\partial t} = 0$, the solution of equation 5.1 is given by a linear combination of the modified Bessel functions of the first and second kind of order zero:

$$C(r) = A_0^{(1')} I_0\left(l^{-1} r\right) + B_0^{(1')} K_0\left(l^{-1} r\right). \tag{B.24}$$

The boundary conditions are given by:

$$A_0^{(1')}\left[k_1 I_1\left(\frac{r_1}{l^2}\right) - k_2 I_0\left(\frac{r_1}{l}\right)\right] + B_0^{(1')}\left[-k_1 K_1\left(\frac{r_1}{l^2}\right) - k_2 K_0\left(\frac{r_1}{l}\right)\right] + k_3 = 0 , \tag{B.25}$$

and

$$A_0^{(1')} I_0\left(\frac{r_2}{l}\right) + B_0^{(1')} K_0\left(\frac{r_2}{l}\right) = 0 . \tag{B.26}$$

This yields:

$$A_0^{(1')} = \frac{-k_3 F_{2,0}}{h_0} \qquad B_0^{(1')} = \frac{k_3 F_{4,0}}{h_0}, \tag{B.27}$$

where:

$$h_0 = F_{1,0} F_{2,0} - F_{3,0} F_{4,0} , \tag{B.28}$$

and:

$$\begin{aligned} F_{1,0} &= E_{1,0} \\ F_{1,0} &= K_0\left(\frac{r_2}{l}\right) \\ F_{1,0} &= E_{3,0} \\ F_{4,0} &= I_0\left(\frac{r_2}{l}\right) \end{aligned} . \tag{B.29}$$

To find the poles for $q > 0$ and $p < -\lambda$, the derivative $\left.\frac{d(ph)}{dp}\right|_{p=p_n}$ is required:

$$\frac{dh}{dp} = F_{1A} F_2 + F_{2A} F_1 - F_{3A} F_4 - F_{4A} F_3 , \tag{B.30}$$

where:

$$
\begin{aligned}
F_{1A} &= E_{1A} \\
F_{2A} &= \frac{r_2}{2qD_e} Y_1(qr_2) \\
F_{3A} &= E_{3A} \\
F_{4A} &= \frac{r_2}{2qD_e} J_1(qr_2)
\end{aligned}
\quad . \tag{B.31}
$$

Nederlandse samenvatting

Radon, een radioactief edelgas, wordt gezien als één van de grootste bedreigingen van de gezondheid in het Nederlandse binnenmilieu. Naar schatting van de Wereld Gezondheids Raad (WHO) veroorzaakt de radon aanwezig in Nederlandse woningen zo'n 800 gevallen van longkanker per jaar. Hiermee overschrijdt radon de door de overheid gestelde maximale risico voor één enkele bron.

Om inzicht te verkrijgen in de bron van de radon in Nederlandse woningen zijn diverse onderzoeksprojecten uitgevoerd. Volgens het laatste nationale onderzoek waarbij radon concentraties en ventilatiestromen in diverse delen van de woning zijn gemeten, vormen bouwmaterialen de belangrijkste bron van radon. Deze conclusie staat echter haaks op metingen van de radon exhalatiesnelheid, de hoeveelheid radon uitgestoten per tijdseenheid, van bouwmaterialen.

Het doel van dit promotie-onderzoek is om inzicht te krijgen in de processen die een rol spelen bij de productie en transport van radon in bouwmaterialen. Hiertoe is een opstelling gebouwd waarin de productie en transport van radon in bouwmaterialen nauwgezet kan worden gemeten en gestuurd. Door vergelijking van deze metingen met modelberekeningen kunnen de huidige fysische modellen worden getoetst op hun geldigheid.

Voor de modelberekeningen zijn invoerparameters nodig die het hier onderzochte bouwmateriaal, cellenbeton, beschrijven. De porositeit, diffusie coëfficiënt, de adsorptie coëfficiënt en de emanatie coëfficiënt behoren tot de belangrijkste modelparameters. Voor sommige van deze parameters zijn standaard meetmethoden beschikbaar, terwijl voor andere parameters nieuwe methoden zijn ontwikkeld.

Voor de bepaling van de adsorptie coëfficiënt en de emanatie coëfficiënt is een nieuwe meetmethode ontwikkeld. De nieuwe meetmethode meet de ingroei van radon onder drie condities waaruit de beide parameters worden berekend. Het voordeel van deze methode ten opzichte van de bestaande methoden is dat er gebruik gemaakt kan worden van standaard meetapparatuur en relatief grote proefstukken. Metingen en berekeningen op basis van de onzekerheden in meetopstelling en proefstukken komen goed overeen en laten zien dat zowel de adsorptie coëfficiënt alswel de emanatie coëfficiënt met een hoge nauwkeurigheid kunnen worden bepaald.

De diffusie coëfficiënt is bepaald via twee verschillende methoden. De eerste methode, de zogenaamde ingroeimethode, wordt de ingroei van radon in twee, door cellenbeton van elkaar gescheiden, compartimenten gemeten waarbij in één van de compartimenten een radonbron is geplaatst. Deze methode blijkt zeer gevoelig te zijn voor onzekerheden in onderlinge meetefficiencies van de radondetectoren. Bij de tweede methode, de ventilatiemethode, wordt één van de compartimenten geventileerd waardoor een grotere radongradiënt ontstaat. Hierdoor wordt de invloed

van de onzekerheid in de efficiency verminderd. Nadeel van deze methode is echter dat de ventilatie van het compartiment leidt tot de stroming van lucht door het cellenbeton, hetgeen leidt tot een overschatting van de diffusie coëfficiënt. De waarde voor de diffusie coëfficiënt ligt bij de ventilatiemethode ongeveer 10% hoger dan bij de ingroeimethode. Nader onderzoek is noodzakelijk om de precieze oorsprong van de verschillen vast te stellen.

De bepaling van het transport van radon in cellenbeton bestaat uit een meting waarbij een hoge radon concentratie in het binnencompartiment van de opstelling wordt gecreëerd door middel van een radonbron terwijl het buitencompartiment wordt geventileerd met radonvrije lucht. Hierdoor ontstaat er een concentratieverschil over het tussengelegen cellenbeton. Hierdoor vindt er diffusief transport van radon van het binnencompartiment naar het buitencompartiment plaats. Naast het diffusief transport vindt er ook advectief transport van radon plaatst door lucht van het buitencompartiment naar het buitencompartiment te laten stromen.

Vergelijking van meting met modelberekeningen laat een grote discrepantie zien wanneer wordt aangenomen dat cellenbeton een homogeen materiaal is. Aanmerkelijk betere overeenkomsten tussen modelberekeningen en meting worden gevonden wanneer het cellenbeton wordt voorgesteld als een materiaal dat bestaat uit twee, parallel geschakelde compartimenten met allebei een eigen permeabiliteit en volume. Een soortgelijk resultaat wordt gevonden wanneer de diffusie coëfficiënt afhankelijk wordt gemaakt van de luchtdoorstroomsnelheid. Hoewel het laatste bekend is als dispersie, zijn de effecten vele malen groter dan verwacht voor de toegepaste doorstroomsnelheden.

Metingen van de permeabiliteit van cellenbeton en een visuele inspectie van de cilinder van cellenbeton, waaraan de experimenten zijn verricht, laten zien dat er zichtbare scheuren in de cilinder aanwezig zijn en dat deze een grote invloed op het transport hebben gehad. Desondanks dient er ook een deel van het schijnbaar ongescheurde cellenbeton preferentiële doorstroom kanalen te bevatten.

Gezien het feit dat vrijwel elk bouwmateriaal (micro)scheuren bevat, kan worden geconcludeerd dat de huidige modellen voor het beschrijven van radon transport in bouwmaterialen onvolledig zijn. Vervolgonderzoek zal zich dan ook moeten richten op het komen een betere beschrijving van het poreuze medium voor het transport van radon. Alleen op basis van dergelijke gegevens kan men komen tot een model dat het transport van radon in woningen fysisch correct kan beschrijven.

Curriculum Vitae

Michel van der Pal werd geboren op 30 december 1973 te Hoorn. Hij volgde van 1986 tot en met 1992 de opleiding VWO aan de Regionale Scholengemeenschap Enkhuizen te Enkhuizen.

In 1992 werd de opleiding Scheikunde aan de Universiteit Utrecht aangevangen. Deze studie werd in 1997 *met genoegen* afgesloten bij de capaciteitsgroep Grensvlakken en Thermodynamica. Het afstudeeronderzoek betrof een onderzoek naar de desorptiekinetiek van organische contaminanten in sediment, dat werd uitgevoerd bij het Rijksinstituut voor Zoetwaterbeheer en Afvalwaterverwerking (RIZA). Daarnaast was hij werkzaam voor de Chemiewinkel, onder andere op het gebied van bodemverontreiningen.

De opleiding tot doctor werd in 1998 aangevangen. Dit onderzoek naar “de ontwikkeling van radonarme bouwmaterialen” werd uitgevoerd bij de faculteit Bouwkunde aan de Technische Universiteit Eindhoven in samenwerking met de faculteit Natuurkunde en het Kernfysisch Versneller Instituut (KVI) in Groningen. De eerste twee jaar van het onderzoek werden voltijds uitgevoerd, vervolgens in deeltijd (0,8 fte). Het proefschrift dat voortkwam uit dit onderzoek zal op 7 januari 2004 met succes worden verdedigd.

Dankwoord

Aan alles komt een einde, zo ook aan dit proefschrift. Ik wil van dit moment dan ook gebruik maken om een aantal mensen te bedanken die op één of andere wijze hebben bijgedragen aan de totstandkoming van dit proefschrift.

Ten eerste wil ik mijn promotoren, Nico Hendriks en Rob de Meijer, en mijn copromotor, Wim van der Spoel, bedanken voor jullie opbouwende kritiek en de vele discussies die we aan dit onderwerp hebben gewijd. Ik hoop dan ook dat het radonderzoek een passend vervolg krijgt.

Zonder metingen was er van dit proefschrift niet veel terechtgekomen. Ik ben dan ook veel dank verschuldigd aan de technici van FAGO die mij met de diverse opstellingen en metingen hebben geholpen. Harry Smulders: jij loste, vaak schijnbaar ongestructureerd, maar altijd succesvol de computerproblemen op waar ik zelf niet meer uitkwam. Ook is er nog steeds ontzag voor het werk van Guus Theuws. Er ligt, naar het schijnt, in de W-hal nog steeds een laag stof van een blok cellenbeton dat door jou tot een cilinder werd omgetoverd. Maar ook jouw connecties met de nukkige GTD kwamen vaak goed van pas.

Ook mag ik de bijdrage van Emiel van der Graaf, voor de inhoudelijke ondersteuning, en Ron ten Have, voor de technische ondersteuning, van het KVI niet onvermeld laten: in de eerste week van mijn promotieonderzoek wist ik vrijwel alle radonmeters om zeep te helpen maar desondanks bleven jullie (terecht) vertrouwen houden in een goede afloop.

Daarnaast heb ik nog enkele studenten weten te strikken om een bijdrage te leveren aan mijn onderzoek: Marieke Nijland, Marieke Krijnen, Dionne Neilen en Siemon Bierma, jullie deden in het kader van Materiaalkunde 4 een eerste poging om de adsorptie coëfficiënt van cellenbeton te bepalen. Hoewel dit niet altijd even succesvol was, leverde het wel voldoende kennis en ervaring op waarmee Bjorn van Munster, in het kader van een P8-project, een mooie serie meetresultaten kon neerzetten. Tenslotte is er nog mijn dank voor de bijdrage van Jelle Berentsen. Jij hebt in het kader van je afstuderen bij de Fontys Hogeschool de besturingssoftware voor de complexe radon meetopstelling aanzienlijk verbeterd en uitgebreid. Hierbij stond de gebruikersvriendelijkheid voorop. Het eindresultaat mag er wezen. Het is nu alleen nog wachten op die vriendelijke gebruikers…

Naast de technische en inhoudelijke ondersteuning van mijn onderzoek ben ik ook een aantal mensen dankbaar die hebben gezorgd voor de broodnodige afleiding van het onderzoek. Ten eerste wil ik mijn paranimfen, Nico Weel en Pascal de Haan, bedanken voor hun ondersteuning, mede toen ik in de Thaise put zat... Ik kijk alweer uit naar onze volgende vakantie samen! Ook mijn huisgenoten mag ik niet vergeten. Met name met Jelle Berentsen en Arjan Zoet heb ik met plezier menig biertje mogen drinken. Verder wil ik Gerben van der Wel bedanken als collega en vriend voor de

gezellige tijd op de TU/e. Iedere keer was het weer een genoegen om met jou over de meest uiteenlopende onderwerpen te discussiëren. Misschien dat we die discussies in de toekomst maar in Zuid-Amerika moeten voeren? Daarnaast mag ik natuurlijk mijn andere (ex)collega's niet vergeten: Fabien van Mook voor de discussies over onder andere (de tekortkomingen van) ons staatsbestel, Dionne Neilen, voor de wekelijkse uitnodigingen voor de AIO-koffie en Myriam Ariës voor het organiseren van ons wekelijks uurtje volleybal en de nodige flauwe grappen.

Dan is er natuurlijk de RISK-bende: Alex van der Linde, Gerard Cornelissen, Hilde Ketelaar en Knesseth Hassell. Altijd was het weer een onmogelijkheid om een datum te vinden waarop we allemaal beschikbaar waren. Als het dan zover was dan was het toch altijd weer feest. Elke keer probeerde ik jullie toch altijd weer met plezier van het bord te vegen, het liefst vanuit een schijnbaar hopeloze positie. Helaas lieten jullie dat niet al te vaak toe. In die gevallen maakten de woordgrapjes veel goed. Mooi man!

Ook dank aan Marc Londo, die tegenwoordig met beide voeten op de grond staat. Misschien dat we nu eens niet die ene regenachtige dag in augustus weten uit te kiezen voor onze buitenlucht activiteit? Alhoewel, Faust in de stromende regen was toch onovertroffen. De sfeer hangt nog steeds in het gebouw...

Tenslotte nog een bekentenis: Nico Haselager heeft mij weten te verslaan met schaken. Of dit een positieve bijdrage heeft geleverd aan dit werk, laat ik hier maar even buiten beschouwing maar de gezellige avonden met Poolse graswodka en de bijbehorende goede maaltijden waren dat in ieder geval wel!

Als allerlaatste maar niet als allerminste wil ik mijn vriendin bedanken: Anna, tack själv för den åren tillsammans och så pass där vilja följa många mer!

Puss och kram,
Michel.

BOUWSTENEN is een publicatiereeks
van de Faculteit Bouwkunde,
Technische Universiteit Eindhoven.
Zij presenteert resultaten van
onderzoek en andere activiteiten op
het vakgebied der Bouwkunde,
uitgevoerd in het kader van deze
Faculteit.

BOUWSTENEN zijn verkrijgbaar bij:

Publicatiewinkel 'Legenda'
Gebouw Vertigo
Faculteit Bouwkunde
Technische Universiteit Eindhoven
Postbus 513
5600 MB Eindhoven

of telefonisch te bestellen:
040 - 2472293
040 - 2472529

Reeds verschenen in de serie BOUWSTENEN:

nr 1
Elan, a computermodel for building energy design, theory and validation
M.H. de Wit
H.H. Driessen
R.M.M. van der Velden

nr 2
Kwaliteit, keuzevrijheid en kosten Evaluatie van experiment Klarendal, Arnhem
drs J. Smeets
C. le Nobel, arch. HBO
M. Broos
J. Frenken
A. v.d. Sanden

nr 3
Crooswijk van 'bijzonder' naar 'gewoon'
drs V. Smit
ir K. Noort

nr 4
Staal in de woningbouw
ir E.J.F. Delsing

nr 5
Mathematical theory of stressed skin action in profiled sheeting with various edge conditions
ir A.W.A.M.J. v.d. Bogaard

nr 6
Hoe berekenbaar en betrouwbaar is de coëfficiënt k in x - ko en x - ks?
ir K.B. Lub
drs A.J. Bosch

nr 7
Het typologisch gereedschap Een verkennende studie omtrent typologie en omtrent de aanpak typologisch onderzoek
J.H. Luiten arch. HBO

nr 8
Informatievoorziening en beheerprocessen
ir A. Nauta / drs J. Smeets (red.)
Prof. H. Fassbinder (projectleider)
ir A. Proveniers
drs J.v.d. Moosdijk

nr 9
Strukturering en verwerking van tijdgegevens voor de uitvoering van bouwwerken
ir W.F. Schaefer
ir P.A. Erkelens

nr 10
Stedebouw en de vorming van een speciale wetenschap
K. Doevendans

nr 11
Informatica en ondersteuning van ruimtelijke besluitvorming
dr G.G. van der Meulen

nr 12
Staal in de woningbouw, korrosiebescherming van de begane grondvloer
ir E.J.F. Delsing

nr 13
Een thermisch model voor de berekening van staalplaatbeton-vloeren onder brandomstandigheden
ir A.F. Hamerlinck

nr 14
De wijkgedachte in Nederland Gemeenschapsstreven in een stedebouwkundige context
dr ir K. Doevendans
dr R. Stolzenburg

nr 15
Diaphragm effect of trapezoidally profiled steel sheets. Experimental research into the influence of force application
ir A.W.A.M.W. v.d. Bogaard

nr 16
Versterken met spuit-ferrocement. Het mechanische gedrag van met spuit-ferrocement versterkte gewapende betonbalken
ir K.B. Lub
ir M.C.G. van Wanroy

nr 17
De tractaten van Jean Nicolas Louis Durand
ir G. van Zeyl

nr 18
Wonen onder een plat dak. Drie opstellen over enkele vooronderstellingen van de stedebouw
dr ir K. Doevendans

nr 19
Supporting decision making processes
A graphical and interactive analysis of multivariate data
drs W. Adams

nr 20
Self-help building productivity
A method for improving house building by low-income groups applied to Kenya 1990-2000
ir P. A. Erkelens

nr 21
De verdeling van woningen: een kwestie van onderhandelen
drs V. Smit

nr 22
Flexibiliteit en kosten in het ontwerpproces Een besluitvormingondersteunend model
ir M. Prins

nr 23
Spontane nederzettingen begeleid Voorwaarden en criteria in Sri Lanka
ir P.H. Thung

nr 24
Fundamentals of the design of bamboo structures
O. Arce-Villalobos

nr 25
Concepten van de bouwkunde
Prof.dr ir M.F.Th. Bax (red.)
dr ir H.M.G.J. Trum (red.)

nr 26
Meaning of the site
Xiaodong Li

nr 27
Het woonmilieu op begrip gebracht
Jaap Ketelaar

nr 28
Urban environment in developing countries
editors: dr ir Peter A. Erkelens
dr George G. van der Meulen

nr 29
Stategische plannen voor de stad Onderzoek en planning in drie steden
Prof. dr H. Fassbinder (red.)
ir H. Rikhof (red.)

nr 30
Stedebouwkunde en stadsbestuur
ir Piet Beekman

nr 31
De architectuur van Djenné
Een onderzoek naar de historische stad
P.C.M. Maas

nr 32
Conjoint experiments and retail planning
Harmen Oppewal

nr 33
Strukturformen Indonesischer Bautechnik Entwicklung methodischer Grundlagen für eine 'konstruktive pattern language' in Indonesien
Heinz Frick

nr 34
Styles of architectural designing Empirical research on working styles and personality dispositions
Anton P.M. van Bakel

nr 35
Conjoint choice models for urban tourism planning and marketing
Benedict Dellaert

nr 36
Stedelijke Planvorming als co-produktie
Prof. dr H. Fassbinder (red.)

nr 37
Design Research in the Netherlands
editors: Prof. dr R.M.Oxman,
Prof. dr ir. M.F.Th. Bax,
Ir H.H. Achten

nr 38
Communication in the Building Industry
Bauke de Vries

nr 39
Optimaal dimensioneren van gelaste plaatliggers

nr 40
Huisvesting en overwinning van armoede
dr.ir. P.H. Thung en dr.ir. P. Beekman (red.)

nr 41
Urban Habitat: The environment of tomorrow
George G. van der Meulen,
Peter A. Erkelens

nr 42
A typology of joints
John C.M. Olie

nr 43
Modeling constraints-based choices for leisure mobility planning
Marcus P. Stemerding

nr 44
Activity-based travel demand modeling
D. Ettema

nr 45
Wind-induced pressure fluctuations on building facades
Chris Geurts

nr 46
Generic Representations
Henri Achten

nr 47
Johann Santini Aichel
Dirk De Meyer

nr 48
Concrete behaviour in multiaxial compression
Erik van Geel

nr 49
Modelling site selection
Frank Witlox

nr 50
Ecolemma model
Ferdinand Beetstra

nr 51
Conjoint approaches to developing activity-based models
Donggen Wang

nr 52
On the effectiveness of ventilation
Ad Roos

nr 53
Conjoint modeling approaches for residential group preverences
Eric Molin

nr 54
Modelling architectural design information by features
Jos van Leeuwen

nr 55
A spatial decision support system for the planning of retail and service facilities
Theo Arentze

nr 56
Integrated lighting system assistant
Ellie de Groot

nr 57
Ontwerpend leren, leren ontwerpen
dr.ir. J.T. Boekholt

nr 58
Temporal aspects of theme park choice behavoir
Astrid Kemperman

nr 59
Ontwerp van een geïndustrialiseerde funderingswijze
Faas Moonen

nr 60
Merlin: A decision support system for outdoor leisure planning
Manon van Middelkoop

nr 61
The aura of modernity
Jos Bosman

nr 62
Urban Form and Activity-Travel Patterns
Daniëlle Snellen

nr 63
Design Research in the Netherlands 2000
Henri Achten

nr 64
Computer Aided Dimensional Control in Building Construction
Rui Wu

nr 65
Beyond Sustainable Building
editors: Peter A. Erkelens
Sander de Jonge
August A.M. van Vliet
co-editor: Ruth J.G. Verhagen

nr 66
Das globalrecyclingfähige Haus
Hans Löfflad

nr 67
Cool Schools For Hot Suburbs
René J. Dierkx

nr 68
A Bamboo Building Design Decision Support Tool
Fitri Mardjono

nr 69
Driving rain on building envelopes
Fabien van Mook

nr 70
Heating Monumental Churches
Henk Schellen

nr 71
Van Woningverhuurder naar Aanbieder van Woongenot
Patrick Dogge

nr 72
Moisture transfer properties of coated gypsum
Emile Goossens

nr 73
Plybamboo wall-panels for housing
Mr. Gonzales Beltran

nr 74
Proceedings of the 20th International Symposium on Automation and Robotics in Construction
Editors: Ger J. Maas & Frans J.M. van Gassel